

## DYSON-SCHWINGER EQUATIONS: A TOOL FOR HADRON PHYSICS

PIETER MARIS

*Department of Physics, North Carolina State University  
Raleigh, NC 27695-8202, USA*

and

CRAIG D. ROBERTS

*Physics Division, Argonne National Laboratory  
Argonne, IL 60439-4843, USA*

Received (received date)

Revised (revised date)

Dyson-Schwinger equations furnish a Poincaré covariant framework within which to study hadrons. A particular feature is the existence of a nonperturbative, symmetry preserving truncation that enables the proof of exact results. The gap equation reveals that dynamical chiral symmetry breaking is tied to the long-range behaviour of the strong interaction, which is thereby constrained by observables, and the pion is precisely understood, and seen to exist simultaneously as a Goldstone mode and a bound state of strongly dressed quarks. The systematic error associated with the simplest truncation has been quantified, and it underpins a one-parameter model efficacious in describing an extensive body of mesonic phenomena. Incipient applications to baryons have brought successes and encountered challenges familiar from early studies of mesons, and promise a covariant field theory upon which to base an understanding of contemporary large momentum transfer data.

*Keywords:* Bethe-Salpeter Equation, Confinement; Dynamical Chiral Symmetry Breaking; Dyson-Schwinger Equations; Electroweak and Strong Form Factors; Faddeev Equation; Hadron Physics; QCD Modelling

*PACS numbers:* 12.38.Aw, 12.38.Lg, 13.60.-r 13.75.-n 14.20.-c, 14.40.-n, 14.65.-q, 24.85.+p

### Contents

1. Introduction .....	2
2. Dyson-Schwinger Equations .....	3
3. Foundation for a Description of Mesons .....	19
4. <i>Ab Initio</i> Calculation of Meson Properties .....	33
5. On Baryons .....	49
6. Epilogue .....	61
References .....	62

## 1. Introduction

A central goal of contemporary nuclear physics is to understand the properties of hadrons in terms of the elementary excitations in quantum chromodynamics (QCD): quarks, gluons and ghosts, because this is a crucial step in validating the theory. Here “elementary excitations” means those quantum fields in terms of which QCD’s Lagrangian is naturally expressed; for example, the analogues in quantum electrodynamics (QED) are the electron and photon. Just as positronium does not appear in the QED Lagrangian but is understood as a relativistic bound state in the theory, hadrons do not appear in QCD’s Lagrangian: they are supposed to be bound states of quarks and gluons. It is an observational fact that hitherto only colourless hadrons have been observed and that hadrons cannot be “ionised;” i.e., unlike positronium, for which the addition of a few ( $\sim 7$ ) electron-volts will separate the electron and positron, no amount of energy available presently is sufficient to break a hadron into separated coloured constituents. To understand this unique feature of confinement is one of the most significant challenges in physics.

The defining problems of hadron physics can now be stated: specify and solve the quantum field theoretical bound state problem whose solution is the hadron spectrum; calculate the interactions of these hadrons between themselves and with electroweak probes; and use these interactions as incisive tools with which to identify the origins of confinement and elucidate its effects on, and expression in, observables. These problems are essentially nonperturbative.

In considering hadron physics it is natural to think of numerical simulations of lattice-QCD, which over the last thirty years has become an independent branch of high-energy physics with numerous large-scale collaborations. An essential aspect of lattice-QCD is the enumerable, finite grid used to represent the spacetime continuum, which means that a comparison between simulations and experiment necessarily involves extrapolations. In modern studies the extrapolation to the continuum limit; i.e., to small spacing between the lattice sites, is reliably handled. However, that is not true of the extrapolation to infinite volume. Furthermore, most simulations continue to employ the so-called quenched approximation, which introduces an *a priori* unquantifiable systematic error. Significant resources are being expended to overcome these difficulties, by developing improved algorithms, and by the obvious expedient of acquiring faster computers with more memory. Lattice-QCD’s current status can be appraised from the proceedings of any of the major lattice conferences, e.g., Refs. [1]. There are naturally successes and problems, and we leave their description to practitioners, e.g., Ref. [2].

In describing many aspects of hadron physics, light-front concepts and techniques are useful, as may be seen, e.g., from Ref. [3]. The application, exploration and improvement of these methods, too, forms an identifiable subfield but one that is not insular: much is being gained by capitalising on the opportunities that exist to inform other nonperturbative approaches and models, and the feedback that

brings. This framework has seen numerous recent successes, e.g., a renormalisation group approach to the light-front Hamiltonian,<sup>4</sup> applications<sup>5</sup> of light-front Hamiltonian techniques to the transverse lattice formulation of QCD, and refinements of discretised light-front quantisation.<sup>6</sup> A perspective on the approach's status and future is presented in Ref. [7].

Reviewing this material it is readily apparent that drawing a connection between QCD and hadron observables is difficult, and that is why modelling remains a keystone of hadron physics. Constituent-quark-like models currently provide a peerless description of the baryon spectrum and baryon decays,<sup>8,9</sup> correlating a wealth of data via few parameters. Furthermore, while such models do not simultaneously give a satisfactory description of low-lying light-quark mesons, for which an accurate representation of dynamical chiral symmetry breaking (DCSB) is essential, they can be adapted and applied to guide the search for exotic and hybrid hadrons<sup>a</sup> and glueballs.<sup>10,11,12</sup> When focusing on properties of the baryon octet and decuplet, such as elastic and transition form factors at small to moderate momentum transfer, mean field models of baryon structure ameliorate some of the deficiencies of constituent-quark models and provide additional insights.<sup>13,14,15,16</sup> At higher momentum transfers a proper expression of Poincaré covariance becomes important in models of such processes.<sup>9,17</sup>

Contemporary Dyson-Schwinger equation (DSE) studies complement these approaches. Modern comparisons with and predictions of experimental data can properly be said to rest on model assumptions but they can be tested within the framework and also via comparison with lattice-QCD simulations, and the predictions are very good. Furthermore, progress in understanding the intimate connection between symmetries and truncation schemes has enabled the proof of exact results. Herein we review recent phenomenological applications and the foundation of their success. There are naturally challenges, which we shall also highlight.

## 2. Dyson-Schwinger Equations

The best known DSE is the simplest: the *Dyson* or *gap* equation, which describes how the propagation of a fermion is modified by its interactions with the medium being traversed. In QCD that equation is:<sup>b</sup>

$$S^{-1}(p) = Z_2 (i\gamma \cdot p + m_{\text{bare}}) + Z_1 \int_q^\Lambda g^2 D_{\mu\nu}(p-q) \frac{\lambda^a}{2} \gamma_\mu S(q) \Gamma_\nu^a(q;p); \quad (2.1)$$

i.e., the renormalised DSE for the dressed-quark propagator. In Eq. (2.1),  $D_{\mu\nu}(k)$  is the renormalised dressed-gluon propagator,  $\Gamma_\nu^a(q;p)$  is the renormalised dressed-quark-gluon vertex,  $m_{\text{bare}}$  is the  $\Lambda$ -dependent current-quark bare mass that appears in the Lagrangian and  $\int_q^\Lambda := \int^\Lambda d^4q/(2\pi)^4$  represents a *translationally-invariant*

<sup>a</sup>In fact, these quantum mechanical models must be adapted because exotic hadrons are, by definition, those states which cannot be constructed in the simplest versions of the model, with only constituent-quark degrees of freedom.

<sup>b</sup>We employ a Euclidean metric throughout, with:  $\{\gamma_\mu, \gamma_\nu\} = 2\delta_{\mu\nu}$ ;  $\gamma_\mu^\dagger = \gamma_\mu$ ; and  $a \cdot b = \sum_{i=1}^4 a_i b_i$ .

regularisation of the integral, with  $\Lambda$  the regularisation mass-scale.<sup>c</sup> In addition,  $Z_1(\zeta^2, \Lambda^2)$  and  $Z_2(\zeta^2, \Lambda^2)$  are the quark-gluon-vertex and quark wave function renormalisation constants, which depend on the renormalisation point,  $\zeta$ , and the regularisation mass-scale, as does the mass renormalisation constant

$$Z_m(\zeta^2, \Lambda^2) = Z_4(\zeta^2, \Lambda^2)/Z_2(\zeta^2, \Lambda^2). \quad (2.2)$$

The renormalised mass is  $m(\zeta) := m_{\text{bare}}(\Lambda)/Z_m(\zeta^2, \Lambda^2)$ . When  $\zeta$  is very large the right-hand-side (r.h.s.) can be evaluated in perturbation theory whereby one finds

$$m(\zeta) = \frac{\hat{m}}{(\ln \zeta/\Lambda_{\text{QCD}})^{\gamma_m}}, \quad (2.3)$$

with  $\gamma_m = 12/(33 - 2N_f)$ , where  $N_f$  is the number of current-quark flavours that contribute actively to the running coupling, and  $\Lambda_{\text{QCD}}$  and  $\hat{m}$  are renormalisation group invariants:  $\hat{m}$  is the renormalisation-group-invariant current-quark mass.

The solution of Eq. (2.1) is the dressed-quark propagator, which takes the form

$$S^{-1}(p) = i\gamma \cdot p A(p^2, \zeta^2) + B(p^2, \zeta^2) = \frac{1}{Z(p^2, \zeta^2)} [i\gamma \cdot p + M(p^2)] \quad (2.4)$$

and is obtained by solving the gap equation subject to the renormalisation condition that at some large spacelike  $\zeta^2$

$$S^{-1}(p)|_{p^2=\zeta^2} = i\gamma \cdot p + m(\zeta). \quad (2.5)$$

The gap equation illustrates the features and flaws of each DSE. It is a non-linear integral equation for  $S(p)$  and hence can yield much-needed nonperturbative information. However, the kernel involves the two-point function  $D_{\mu\nu}(k)$  and the three-point function  $\Gamma_\nu^a(q; p)$ . The equation is therefore coupled to the DSEs these functions satisfy. Those equations in turn involve higher  $n$ -point functions and hence the DSEs are a tower of coupled integral equations with a tractable problem obtained only once a truncation scheme is specified. It is unsurprising that the best known truncation scheme is the weak coupling expansion, which reproduces every diagram in perturbation theory. This scheme is systematic and valuable in the analysis of large momentum transfer phenomena because QCD is asymptotically free but it precludes any possibility of obtaining nonperturbative information, which we identified as a key feature of the DSEs.

In spite of the problem with truncation, gap equations have long been used effectively in obtaining nonperturbative information about many-body systems as, e.g., in the Nambu-Gorkov formalism for superconductivity.<sup>18</sup> The positive outcomes have been achieved through a simple expedient of employing the most rudimentary truncation, e.g., Hartree or Hartree-Fock, and comparing the results with observations. Naturally, agreement under these circumstances is not an unambiguous

<sup>c</sup>It is only with a translationally invariant regularisation scheme that Ward-Takahashi identities can be preserved, something that is crucial to ensuring vector and axial-vector current conservation. The final stage of any calculation is to take the limit  $\Lambda \rightarrow \infty$ .

indication that the contributions omitted are small nor that the model expressed in the truncation is sound. However, it does justify further study, and an accumulation of good results is grounds for a concerted attempt to substantiate a reinterpretation of the truncation as the first term in a systematic and reliable approximation.

### 2.1. Nonperturbative truncation

To explain why Eq. (2.1) is called a gap equation we consider the chiral limit, which is readily defined<sup>19</sup> because QCD exhibits asymptotic freedom and implemented by employing<sup>20</sup>

$$Z_2(\zeta^2, \Lambda^2) m_{\text{bare}}(\Lambda) \equiv 0, \quad \Lambda \gg \zeta. \quad (2.6)$$

An equivalent statement is that one obtains the chiral limit when the renormalisation-point-invariant current-quark mass vanishes; i.e.,  $\hat{m} = 0$ . In this case the theory is chirally symmetric, and a perturbative evaluation of the dressed-quark propagator from Eq. (2.1) gives

$$B_{\text{pert}}^0(p^2) = m \left( 1 - \frac{\alpha}{\pi} \ln \left[ \frac{p^2}{m^2} \right] + \dots \right) \stackrel{m \rightarrow 0}{\equiv} 0; \quad (2.7)$$

viz., the perturbative mass function is identically zero in the chiral limit. It follows that there is no gap between the top level in the quark's filled negative-energy Dirac sea and the lowest positive energy level.

However, suppose that one had at hand a truncation scheme other than perturbation theory and that subject to this scheme Eq. (2.1) possessed a chiral limit solution  $B^0(p^2) \neq 0$ . Then interactions between the quark and the virtual quanta populating the ground state would have nonperturbatively generated a mass gap. The appearance of such a gap breaks the theory's chiral symmetry. This shows that the gap equation can be an important tool for studying DCSB, and it has long been used to explore this phenomenon in both QED and QCD.<sup>21</sup>

The gap equation's kernel is formed from a product of the dressed-gluon propagator and dressed-quark-gluon vertex. However, in proposing and developing a truncation scheme it is insufficient to focus only on this kernel. We have observed that the gap equation can be a tool for studying DCSB but it is only useful if the truncation itself does not destroy the chiral symmetry.

Chiral symmetry is expressed via the axial-vector Ward-Takahashi identity:

$$P_\mu \Gamma_{5\mu}(k; P) = S^{-1}(k_+) i\gamma_5 + i\gamma_5 S^{-1}(k_-), \quad k_\pm = k \pm P/2, \quad (2.8)$$

wherein  $\Gamma_{5\mu}(k; P)$  is the dressed axial-vector vertex. This three-point function satisfies an inhomogeneous Bethe-Salpeter equation (BSE):

$$[\Gamma_{5\mu}(k; P)]_{tu} = Z_2 [\gamma_5 \gamma_\mu]_{tu} + \int_q^\Lambda [S(q_+) \Gamma_{5\mu}(q; P) S(q_-)]_{sr} K_{tu}^{rs}(q, k; P), \quad (2.9)$$

in which  $K(q, k; P)$  is the fully-amputated quark-antiquark scattering kernel, and the colour-, Dirac- and flavour-matrix structure of the elements in the equation is

denoted by the indices  $r, s, t, u$ . The Ward-Takahashi identity, Eq. (2.8), entails that an intimate relation exists between the kernel in the gap equation and that in the BSE. (This is another example of the coupling between DSEs.) Therefore an understanding of chiral symmetry and its dynamical breaking can only be obtained with a truncation scheme that preserves this relation, and hence guarantees Eq. (2.8) without a *fine-tuning* of model-dependent parameters.

### 2.1.1. Rainbow-ladder truncation

At least one such scheme exists.<sup>22</sup> Its leading-order term is the so-called renormalisation-group-improved rainbow-ladder truncation, whose analogue in the many body problem is an Hartree-Fock truncation of the one-body (Dyson) equation combined with a consistent ladder-truncation of the related two-body (Bethe-Salpeter) equation. To understand the origin of this leading-order term observe that the dressed-ladder truncation of the quark-antiquark scattering kernel is expressed in Eq. (2.9) via

$$\begin{aligned} [L(q, k; P)]_{tu}^{t'u'} [\Gamma_{5\mu}(q; P)]_{u't'} &:= [S(q_+) \Gamma_{5\mu}(q; P) S(q_-)]_{sr} K_{tu}^{rs}(q, k; P) \\ &= -g^2(\zeta^2) D_{\rho\sigma}(k - q) [\Gamma_{\rho}^a(k_+, q_+) S(q_+)]_{tt'} [S(q_-) \Gamma_{\sigma}^a(q_-, k_-)]_{u'u} [\Gamma_{5\mu}(q; P)]_{t'u'} \end{aligned} \quad (2.10)$$

wherein we have only made explicit the renormalisation point dependence of the coupling. One can exploit multiplicative renormalisability and asymptotic freedom to establish that on the kinematic domain for which  $Q^2 := (k - q)^2 \sim k^2 \sim q^2$  is large and spacelike

$$[L(q, k; P)]_{tu}^{t'u'} = -4\pi\alpha(Q^2) D_{\rho\sigma}^{\text{free}}(Q) \left[ \frac{\lambda^a}{2} \gamma_{\rho} S^{\text{free}}(q_+) \right]_{tt'} \left[ S^{\text{free}}(q_-) \frac{\lambda^a}{2} \gamma_{\sigma} \right]_{u'u}, \quad (2.11)$$

where  $\alpha(Q^2)$  is the strong running coupling and, e.g.,  $S^{\text{free}}$  is the free quark propagator. It follows that on this kinematic domain the r.h.s. of Eq. (2.11) describes the leading contribution to the complete quark-antiquark scattering kernel,  $K_{tu}^{rs}(q, k; P)$ , with all other contributions suppressed by at least one additional power of  $1/Q^2$ .

The renormalisation-group-improved ladder-truncation supposes that

$$K_{tu}^{rs}(q, k; P) = -4\pi\alpha(Q^2) D_{\rho\sigma}^{\text{free}}(Q) \left[ \frac{\lambda^a}{2} \gamma_{\rho} \right]_{ts} \left[ \frac{\lambda^a}{2} \gamma_{\sigma} \right]_{ru} \quad (2.12)$$

is also a good approximation on the infrared domain and is thus an assumption about the long-range ( $Q^2 \lesssim 1 \text{ GeV}^2$ ) behaviour of the interaction. Combining Eq. (2.12) with the requirement that Eq. (2.8) be automatically satisfied leads to the renormalisation-group-improved rainbow-truncation of the gap equation:

$$S^{-1}(p) = Z_2 (i\gamma \cdot p + m_{\text{bare}}) + \int_q^{\Lambda} 4\pi\alpha(Q^2) D_{\mu\nu}^{\text{free}}(p - q) \frac{\lambda^a}{2} \gamma_{\mu} S(q) \frac{\lambda^a}{2} \gamma_{\nu}^a. \quad (2.13)$$

As will become apparent, the rainbow-ladder truncation provides the foundation for an explanation of a wide range of hadronic phenomena. There are some notable

exceptions; e.g., the description of the scalar meson sector is unconvincing, and it is natural to seek the reason. The recognition that this truncation is the first term in a systematic procedure has provided an answer.<sup>22</sup>

## 2.2. Systematic procedure

The truncation scheme of Ref. [22] is a dressed-loop expansion of the dressed-quark-gluon vertices that appear in the half-amputated dressed-quark-antiquark scattering matrix:  $S^2K$ , a renormalisation-group invariant.<sup>23</sup> All  $n$ -point functions involved thereafter in connecting two particular quark-gluon vertices are *fully dressed*. The effect of this truncation in the gap equation, Eq. (2.1), is realised through the following representation of the dressed-quark-gluon vertex,  $i\Gamma_\mu^a = \frac{i}{2}\lambda^a \Gamma_\mu = l^a \Gamma_\mu$ :

$$\begin{aligned} Z_1\Gamma_\mu(k,p) &= \gamma_\mu + \frac{1}{2N_c} \int_\ell^\Lambda g^2 D_{\rho\sigma}(p-\ell) \gamma_\rho S(\ell+k-p) \gamma_\mu S(\ell) \gamma_\sigma \\ &+ \frac{N_c}{2} \int_\ell^\Lambda g^2 D_{\sigma'\sigma}(\ell) D_{\tau'\tau}(\ell+k-p) \gamma_{\tau'} S(p-\ell) \gamma_{\sigma'} \Gamma_{\sigma\tau\mu}^{3g}(\ell, -k, k-p) + [\dots]. \end{aligned} \quad (2.14)$$

Here  $\Gamma^{3g}$  is the dressed-three-gluon vertex and it is readily apparent that the lowest order contribution to each term written explicitly is  $O(g^2)$ . The ellipsis represents terms whose leading contribution is  $O(g^4)$ ; viz., the crossed-box and two-rung dressed-gluon ladder diagrams, and also terms of higher leading-order.

This expansion of  $S^2K$ , with its implications for other  $n$ -point functions, yields an ordered truncation of the DSEs that guarantees, term-by-term, the preservation of vector and axial-vector Ward-Takahashi identities, a feature that has been exploited<sup>19,24,25</sup> to prove Goldstone's theorem and other exact results in QCD. It is readily seen that inserting Eq. (2.14) into Eq. (2.1) provides the rule by which the rainbow-ladder truncation can be systematically improved.

### 2.2.1. Planar vertex

The effect of the complete vertex in Eq. (2.14) on the solutions of the gap equation is unknown. However, insights have been drawn from a study<sup>23</sup> of a more modest problem obtained by retaining only the sum of dressed-gluon ladders; i.e., the vertex depicted in Fig. 2.1. The elucidation is particularly transparent when one employs the following choice for the dressed-gluon line in the figure:<sup>26</sup>

$$\mathcal{D}_{\mu\nu}(k) := g^2 D_{\mu\nu}(k) = \left( \delta_{\mu\nu} - \frac{k_\mu k_\nu}{k^2} \right) (2\pi)^4 \mathcal{G}^2 \delta^4(k), \quad (2.15)$$

which defines an ultraviolet finite model so that the regularisation mass-scale can be removed to infinity and the renormalisation constants set equal to one.<sup>d</sup> This

<sup>d</sup>The constant  $\mathcal{G}$  sets the model's mass-scale and using  $\mathcal{G} = 1$  simply means that all mass-dimensioned quantities are measured in units of  $\mathcal{G}$ .

Fig. 2.1. Integral equation for a planar dressed-quark-gluon vertex obtained by neglecting contributions associated with explicit gluon self-interactions. Solid circles indicate fully dressed propagators. The vertices are not dressed. (Adapted from Ref. [23].)

model has many positive features in common with the class of renormalisation-group-improved rainbow-ladder models and its particular momentum-dependence works to advantage in reducing integral equations to algebraic equations with similar qualitative features. There is naturally a drawback: the simple momentum dependence also leads to some model-dependent artefacts, but they are easily identified and hence not cause for concern.

The general form of the dressed-quark gluon vertex involves twelve distinct scalar form factors but using Eq. (2.15) only  $\Gamma_\mu(p) := \Gamma_\mu(p, p)$  contributes to the gap equation. This considerably simplifies the analysis since, in general,

$$\Gamma_\mu(p) = \alpha_1(p^2) \gamma_\mu + \alpha_2(p^2) \gamma \cdot p p_\mu - \alpha_3(p^2) i p_\mu + \alpha_4(p^2) i \gamma_\mu \gamma \cdot p. \quad (2.16)$$

The summation depicted in Fig. 2.1 is expressed via

$$\Gamma_\mu(p) = \gamma_\mu + \frac{1}{8} \gamma_\rho S(p) \Gamma_\mu(p) S(p) \gamma_\rho, \quad (2.17)$$

and inserting Eq. (2.16) into Eq. (2.17) one finds  $\alpha_4 \equiv 0$ , and hence the solution simplifies:

$$\Gamma_\mu(p) = \alpha_1(p^2) \gamma_\mu + \alpha_2(p^2) \gamma \cdot p p_\mu - \alpha_3(p^2) i p_\mu. \quad (2.18)$$

The three surviving functions are those which are most important in the dressed-quark-photon vertex.<sup>27</sup>

One can re-express this vertex as

$$\Gamma_\mu(p) = \sum_{i=0}^{\infty} \Gamma_\mu^i(p) = \sum_{i=0}^{\infty} [\alpha_1^i(p^2) \gamma_\mu + \alpha_2^i(p^2) \gamma \cdot p p_\mu - \alpha_3^i(p^2) i p_\mu], \quad (2.19)$$

where the superscript enumerates the order of the iterate:  $\Gamma_\mu^{i=0}$  is the bare vertex,

$$\alpha_1^0 = 1, \quad \alpha_2^0 = 0 = \alpha_3^0; \quad (2.20)$$

$\Gamma_\mu^{i=1}$  is the result of inserting this into the r.h.s. of Eq (2.17) to obtain the one-rung dressed-gluon correction;  $\Gamma_\mu^{i=2}$  is the result of inserting  $\Gamma_\mu^{i=1}$ , and is therefore the two-rung dressed-gluon correction; etc. A key observation<sup>23</sup> is that each iterate is

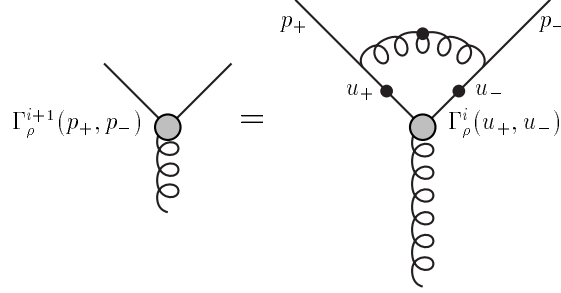


Fig. 2.2. Recursion relation for the iterates in the fully-resummed dressed-gluon-ladder vertex: filled circles denote a fully-dressed propagator or vertex. Using Eq. (2.15),  $p_+ = p_-$ . (Adapted from Ref. [23].)

related to its precursor via the simple recursion relation depicted in Fig. 2.2 and, substituting Eq. (2.19), this recursion yields ( $s = p^2$ )

$$\boldsymbol{\alpha}^{i+1}(s) := \begin{pmatrix} \alpha_1^{i+1}(s) \\ \alpha_2^{i+1}(s) \\ \alpha_3^{i+1}(s) \end{pmatrix} = \mathcal{O}(s; A, B) \boldsymbol{\alpha}^i(s), \quad (2.21)$$

$$\mathcal{O}(s; A, B) = \frac{1}{4} \frac{1}{\Delta^2} \begin{pmatrix} -\Delta & 0 & 0 \\ 2A^2 & sA^2 - B^2 & 2AB \\ 4AB & 4sAB & 2(B^2 - sA^2) \end{pmatrix}, \quad (2.22)$$

$\Delta = sA^2(s) + B^2(s)$ . It follows that

$$\boldsymbol{\alpha} = \left( \sum_{i=1}^{\infty} \mathcal{O}^i \right) \boldsymbol{\alpha}^0 = \frac{1}{1 - \mathcal{O}} \boldsymbol{\alpha}^0 \quad (2.23)$$

and hence, using Eq. (2.20),

$$\begin{aligned} \alpha_1 &= \frac{4\Delta}{1 + 4\Delta}, \\ \alpha_2 &= \frac{-8A^2}{1 + 2(B^2 - sA^2) - 8\Delta^2} \frac{1 + 2\Delta}{1 + 4\Delta}, \\ \alpha_3 &= \frac{-8AB}{1 + 2(B^2 - sA^2) - 8\Delta^2}. \end{aligned} \quad (2.24)$$

The recursion relation thus leads to a closed form for the gluon-ladder-dressed quark-gluon vertex in Fig. 2.1; viz., Eqs. (2.18), (2.24). Its momentum-dependence is determined by that of the dressed-quark propagator, which is obtained by solving the gap equation, itself constructed with this vertex. Using Eq. (2.15), that gap equation is

$$S^{-1}(p) = i\boldsymbol{\gamma} \cdot p + m + \boldsymbol{\gamma}_\mu S(p) \boldsymbol{\Gamma}_\mu(p) \quad (2.25)$$

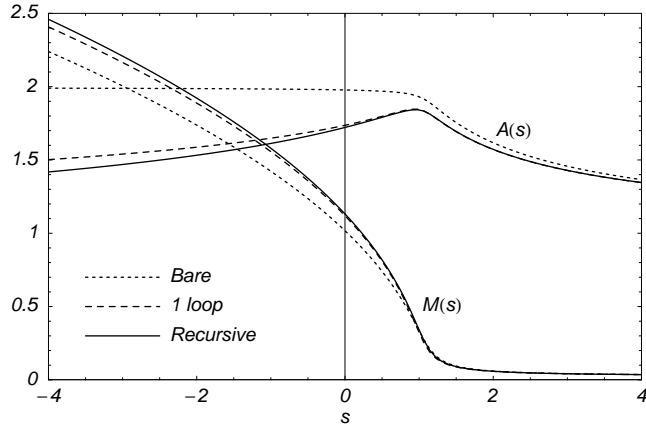


Fig. 2.3.  $A(s)$ ,  $M(s)$  obtained from Eqs. (2.24), (2.26), (2.27) with  $m = 0.023$ : solid line. All dimensioned quantities are expressed in units of  $\mathcal{G}$  in Eq. (2.15). For comparison, the results obtained with the zeroth-order vertex: dotted line; and the one-loop vertex: dashed line, are also plotted. (Adapted from Ref. [23].)

and substituting Eq. (2.18) gives

$$A(s) = 1 + \frac{1}{sA^2 + B^2} [A(2\alpha_1 - s\alpha_2) - B\alpha_3], \quad (2.26)$$

$$B(s) = m + \frac{1}{sA^2 + B^2} [B(4\alpha_1 + s\alpha_2) - sA\alpha_3]. \quad (2.27)$$

Equations (2.26), (2.27), completed using Eqs. (2.24), form a closed algebraic system. It can easily be solved numerically, and that yields simultaneously the complete gluon-ladder-dressed vertex and the propagator for a quark fully dressed via gluons coupling through this nonperturbative vertex. Furthermore, it is apparent that in the chiral limit,  $m = 0$ , a realisation of chiral symmetry in the Wigner-Weyl mode, which is expressed via the  $B \equiv 0$  solution of the gap equation, is always admissible. This is the solution anticipated in Eq. (2.7).

The chiral limit gap equation also admits a Nambu-Goldstone mode solution whose  $p^2 \simeq 0$  properties are unambiguously related to those of the  $m \neq 0$  solution, a feature also evident in QCD.<sup>25</sup> A complete solution of Eq. (2.25) is available numerically, and results for the dressed-quark propagator and gluon-ladder-dressed vertex are depicted in Figs. 2.3, 2.4. It is readily seen that the complete resummation of dressed-gluon ladders gives a dressed-quark propagator that is little different from that obtained with the one-loop-corrected vertex; and there is no material difference from the result obtained using the zeroth-order vertex. Similar observations apply to the vertex itself. Of course, there is a qualitative difference between the zeroth-order vertex and the one-loop-corrected result:  $\alpha_{2,3} \neq 0$  in the latter case. However, once that effect is seeded, the higher-loop corrections do little. The scale of these modest effects can be quantified by a comparison between the values of  $M(s=0) =$

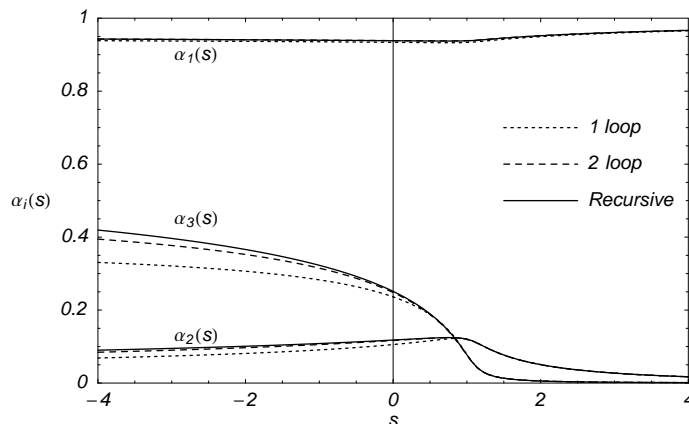


Fig. 2.4.  $\alpha_i$ ,  $i = 1, 2, 3$ , calculated from Eqs. (2.24), (2.26), (2.27) with  $m = 0.023$ . These functions calculated at one-loop (dotted line) and two-loop (dashed line) are also plotted for comparison. (Adapted from Ref. [23].)

$B(0)/A(0)$  calculated using vertices dressed at different orders:

$$\frac{\sum_{i=0,N} \Gamma_{\mu}^i}{M(0)} \left| \begin{array}{cccc} N=0 & N=1 & N=2 & N=\infty \\ 1 & 1.105 & 1.115 & 1.117 \end{array} \right. \quad (2.28)$$

The rainbow truncation of the gap equation is accurate to within 12% and adding just one gluon ladder gives 1% accuracy. It is now important to couple this with an understanding of how the vertex resummation affects the Bethe-Salpeter kernel.

### 2.2.2. Vertex-consistent Bethe-Salpeter kernel

The renormalised homogeneous BSE for the quark-antiquark channel denoted by  $M$  can be expressed

$$[\Gamma_M(k; P)]_{tu} = \int_q^{\Lambda} [\chi_M(q; P)]_{sr} [K(k, q; P)]_{tu}^{rs} \quad (2.29)$$

where:  $\Gamma_M(k; P)$  is the meson's Bethe-Salpeter amplitude,  $k$  is the relative momentum of the quark-antiquark pair,  $P$  is their total momentum; and

$$\chi_M(k; P) = S(k_+) \Gamma_M(k; P) S(k_-). \quad (2.30)$$

Equation (2.29), depicted in Fig. 2.5, describes the residue at a pole in the solution of an inhomogeneous BSE; e.g., the lowest mass pole solution of Eq. (2.9) is identified with the pion. (NB. The normalisation of a Bethe-Salpeter amplitude is fixed by requiring that the bound state contribute with unit residue to the fully-amputated quark-antiquark scattering amplitude:  $M = K + K(SS)K + \dots$ , see, e.g., Ref. [28].)

On p. 5 we observed that the automatic preservation of Ward-Takahashi identities in those channels related to strong interaction observables requires a conspiracy

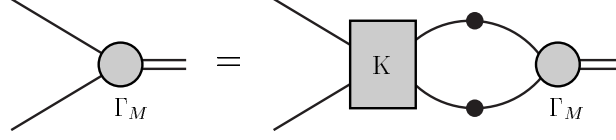


Fig. 2.5. Homogeneous BSE, Eq. (2.29). Filled circles: dressed propagators or vertices;  $K$  is the dressed-quark-antiquark scattering kernel. A systematic truncation of  $S^2K$  is the key to preserving Ward-Takahashi identities.<sup>22,29</sup> (Adapted from Ref. [23].)

between the dressed-quark-gluon vertex and the Bethe-Salpeter kernel.<sup>22,29</sup> A systematic procedure for building that kernel follows<sup>23</sup> from the observation<sup>29</sup> that the gap equation can be expressed via

$$\frac{\delta\Gamma[S]}{\delta S} = 0, \quad (2.31)$$

where  $\Gamma[S]$  is a Cornwall-Jackiw-Tomboulis-like effective action. The Bethe-Salpeter kernel is then obtained via an additional functional derivative:

$$K_{tu}^{rs} = -\frac{\delta\Sigma_{tu}}{\delta S_{rs}}. \quad (2.32)$$

With the recursive vertex depicted in Fig. 2.1, the  $n$ -th order contribution to the kernel is obtained from the  $n$ -loop contribution to the self energy:

$$\Sigma^n(p) = -\int_q^\Lambda \mathcal{D}_{\mu\nu}(p-q) l^\alpha \gamma_\mu S(q) l^\alpha \Gamma_\nu^n(q, p). \quad (2.33)$$

Since  $\Gamma_\mu(p, q)$  itself depends on  $S$  then Eq. (2.32) yields the Bethe-Salpeter kernel as a sum of two terms and hence Eq. (2.29) assumes the form

$$\Gamma_M(k; P) = \int_q^\Lambda \mathcal{D}_{\mu\nu}(k-q) l^\alpha \gamma_\mu \left[ \chi_M(q; P) l^\alpha \Gamma_\nu(q_-, k_-) + S(q_+) \Lambda_{M\nu}^a(q, k; P) \right], \quad (2.34)$$

where we have used the mnemonic

$$\Lambda_{M\nu}^a(q, k; P) = \sum_{n=0}^{\infty} \Lambda_{M\nu}^{a;n}(q, k; P). \quad (2.35)$$

While  $\mathcal{D}_{\mu\nu}$  also depends on  $S$  because of quark vacuum polarisation diagrams, the additional term arising from the derivative of  $\mathcal{D}_{\mu\nu}$  does not contribute to the Bethe-Salpeter kernel for flavour nonsinglet systems, which are our current focus, and hence is neglected for simplicity.

Equation (2.34) is depicted in Fig. 2.6. The first term is instantly available once one has an explicit form for  $\Gamma_\nu^n$  and the second term, identified by the shaded box

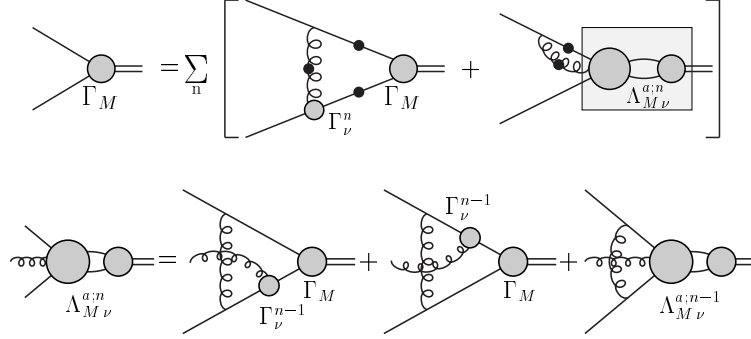


Fig. 2.6. Upper panel: BSE, Eq. (2.34), which is valid whenever  $\Gamma_\mu$  can be obtained via a recursion relation. Lower panel: Recursion relation for  $\Lambda_{M\nu}^{a;n}$ , Eq. (2.36). (Adapted from Ref. [23].)

in Fig. 2.6, can be obtained via an inhomogeneous recursion relation<sup>23</sup>

$$\begin{aligned}
& \Lambda_{M\nu}^{a;n}(\ell, k; P) \\
&= \int_q^\Lambda \mathcal{D}_{\rho\sigma}(\ell - q) l^b \gamma_\rho \chi_M(q; P) l^a \Gamma_\nu^{n-1}(q_-, q_- + k - \ell) S(q_- + k - \ell) l^b \gamma_\sigma \\
&+ \int_q^\Lambda \mathcal{D}_{\rho\sigma}(k - q) l^b \gamma_\rho S(q_+ + \ell - k) l^a \Gamma_\nu^{n-1}(q_+ + \ell - k, q_+) \chi_M(q; P) l^b \gamma_\sigma \\
&+ \int_{q'}^\Lambda \mathcal{D}_{\rho\sigma}(\ell - q') l^b \gamma_\rho S(q'_+) \Lambda_{M\nu}^{a;n-1}(q', q' + k - \ell; P) S(q'_- + k - \ell) l^b \gamma_\sigma.
\end{aligned} \tag{2.36}$$

This equation is also depicted in Fig. 2.6. Combining the two figures, it is apparent that to form the Bethe-Salpeter kernel the free gluon line is attached to the upper dressed-quark line. It follows that the first term in Eq. (2.36) invariably generates crossed gluon lines; i.e., nonplanar contributions to the kernel. The character of the vertex-consistent Bethe-Salpeter kernel is now clear: it consists of countably many contributions, a subclass of which are crossed-ladder diagrams and hence nonplanar. Only the rainbow gap equation, obtained with  $i = 0$  in Eq. (2.19), yields a planar vertex-consistent Bethe-Salpeter kernel, namely the ladder kernel of Eq. (2.12). In this case alone is the number of diagrams in the dressed-vertex and kernel identical. Otherwise there are always more terms in the kernel.

### 2.2.3. Solutions for the $\pi$ - and $\rho$ -mesons

Section 2.2.2 recapitulates on a general procedure that provides the vertex-consistent channel-projected Bethe-Salpeter kernel once  $\Gamma_\nu^n$  and the propagator functions:  $A$ ,  $B$ , are known. That kernel must be constructed independently for each channel because, e.g.,  $\Lambda_{M\nu}^a$  depends on  $\chi_M(q; P)$ . As with the study of the vertex in Sec. 2.2.1, an elucidation of the resulting BSEs' features is simplified by using the model of Eq.

Table 2.1. Calculated  $\pi$  and  $\rho$  meson masses, in GeV, quoted with  $\mathcal{G} = 0.48$  GeV, in which case  $m = 0.023\mathcal{G} = 11$  MeV.  $n$  is the number of dressed-gluon rungs retained in the planar vertex, see Fig. 2.1, and hence the order of the vertex-consistent Bethe-Salpeter kernel: the rapid convergence of the kernel is apparent from the tabulated results. (Adapted from Ref. [23].)

	$M_H^{n=0}$	$M_H^{n=1}$	$M_H^{n=2}$	$M_H^{n=\infty}$
$\pi, m = 0$	0	0	0	0
$\pi, m = 0.011$	0.152	0.152	0.152	0.152
$\rho, m = 0$	0.678	0.745	0.754	0.754
$\rho, m = 0.011$	0.695	0.762	0.770	0.770

(2.15), for then the Bethe-Salpeter kernels are finite matrices [cf.  $(1 - \mathcal{O})^{-1}$  in Eq. (2.23)] and the homogeneous BSEs are merely linear, coupled algebraic equations.

Reference [23] describes the solution of the coupled gap and Bethe-Salpeter equations for the  $\pi$ - and  $\rho$ -mesons in detail. Herein we focus on the results, which are summarised in Table 2.1. It is evident that, irrespective of the order of the truncation; viz., the number of dressed gluon rungs in the quark-gluon vertex, the pion is massless in the chiral limit. This is in spite of the fact that the pion is composed of heavy dressed-quarks, as is evident in the calculated scale of the dynamically generated dressed-quark mass function: see Fig. 2.3,  $M(0) \approx \mathcal{G} \approx 0.5$  GeV. These observations emphasise that the masslessness of the  $\pi$  is a model-independent consequence of consistency between the Bethe-Salpeter kernel and the kernel in the gap equation. Furthermore, the bulk of the  $\rho$ - $\pi$  mass splitting is present for  $m = 0$  and with the simplest ( $n = 0$ ; i.e., rainbow-ladder) kernel, which demonstrates that this mass difference is driven by the DCSB mechanism: it is not the result of a carefully tuned chromo-hyperfine interaction. Finally, the quantitative effect of improving on the rainbow-ladder truncation; i.e., including more dressed-gluon rungs in the gap equation's kernel and consistently improving the kernel in the Bethe-Salpeter equation, is a 10% correction to the vector meson mass. Simply including the first correction (viz., retaining the first two diagrams in Fig. 2.1) yields a vector meson mass that differs from the fully resummed result by  $\lesssim 1\%$ . The rainbow-ladder truncation is clearly accurate in these channels.

#### 2.2.4. Summary

It is now evident that a Ward-Takahashi identity preserving Bethe-Salpeter kernel can always be calculated explicitly from a dressed-quark-gluon vertex whose diagrammatic content is enumerable.<sup>e</sup> Furthermore, in all but the simplest case, namely, the rainbow-ladder truncation, that kernel is nonplanar.

While we described results obtained with a rudimentary interaction model in order to make the construction transparent, the procedure is completely general. However, the algebraic simplicity of the analysis is naturally peculiar to the model. With a more realistic interaction, the gap and vertex equations yield a system of

<sup>e</sup>That is not true if one employs an *Ansatz* for the dressed-quark-gluon vertex whose diagrammatic content cannot be made explicit; e.g., that of Ref. [30].

twelve coupled integral equations. The Bethe-Salpeter kernel for any given channel then follows as the solution of a determined integral equation.

We have reviewed those points in the construction of Refs. [22,23] that bear upon the fidelity of the rainbow-ladder truncation in the gap equation, and in the vector and flavour non-singlet pseudoscalar channels. The error is small. In modelling it is therefore justified to fit one's parameters to physical observables at this level in these channels and then make predictions for other phenomena involving vector and pseudoscalar bound states in the expectation they will be reliable. That approach has been successful, as we shall illustrate.

By identifying the rainbow-ladder truncation as the lowest order in a systematic scheme, the procedure also provides a means of anticipating the channels in which that truncation must fail. The scalar mesons are an example. Parametrisations of the rainbow-ladder truncation, fitted as described above, give masses for scalar mesons that are too high.<sup>31,32,33,34</sup> That was thought to be a problem. However, we now know this had to happen because cancellations that occur between higher order terms in the pseudoscalar and vector channels, thereby reducing the magnitude of corrections, do not occur in the scalar channel,<sup>35</sup> wherein the full kernel contains additional attraction.<sup>36</sup> Indeed, it follows that an interaction model employed in rainbow-ladder truncation that simultaneously provides a good description of scalar and pseudoscalar mesons must contain spurious degrees of freedom. Quantitative studies of the effect of the higher-order terms have begun.<sup>37,38,39,40</sup>

The placement of the rainbow-ladder truncation as the first term in a procedure that can systematically be improved explains clearly why this truncation has been successful, the boundaries of its success, why it has failed outside these boundaries, and why straightening out the failures will not undermine the successes.

### 2.3. Selected model-independent results

In the hadron spectrum the pion is identified as both a Goldstone mode, associated with DCSB, and a bound state composed of constituent  $u$ - and  $d$ -quarks, whose effective mass is  $\sim 350$  MeV. Naturally, in quantum mechanics, one can fabricate a potential that yields a bound state whose mass is much less than the sum of the constituents' masses. However, that requires *fine tuning* and, without additional fine tuning, such models predict properties for spin- and/or isospin-flip relatives of the pion which conflict with experiment. A correct resolution of this apparent dichotomy is one of the fundamental challenges to establishing QCD as the theory underlying strong interaction physics, and the DSEs provide an ideal framework within which to achieve that end, as we now explain following the proof of Ref. [19].

#### 2.3.1. A proof of Goldstone's theorem

Consider the BSE of Eq. (2.29) expressed for the isovector pseudoscalar channel:

$$[\Gamma_{\pi}^j(k; P)]_{tu} = \int_q^{\Lambda} [\chi_{\pi}^j(q; P)]_{sr} K_{tu}^{rs}(q, k; P), \quad (2.37)$$

with  $\chi_\pi^j(q; P) = S(q_+) \Gamma_\pi^j(q; P) S(q_-)$  obvious from Eq. (2.30) and  $j$  labelling isospin, of which the solution has the general form

$$\begin{aligned} \Gamma_\pi^j(k; P) = & \tau^j \gamma_5 \left[ i E_\pi(k; P) + \gamma \cdot P F_\pi(k; P) \right. \\ & \left. + \gamma \cdot k k \cdot P G_\pi(k; P) + \sigma_{\mu\nu} k_\mu P_\nu H_\pi(k; P) \right]. \end{aligned} \quad (2.38)$$

It is again apparent that the dressed-quark propagator, the solution of Eq. (2.1), is an important part of the BSE's kernel.

In studying the pion it is crucial to understand chiral symmetry, and its explicit and dynamical breaking. These features are expressed in the axial-vector Ward-Takahashi identity, Eq. (2.8), which involves the axial-vector vertex:

$$\left[ \Gamma_{5\mu}^j(k; P) \right]_{tu} = Z_2 \left[ \gamma_5 \gamma_\mu \frac{\tau^j}{2} \right]_{tu} + \int_q^\Lambda [\chi_{5\mu}^j(q; P)]_{sr} K_{tu}^{rs}(q, k; P), \quad (2.39)$$

that has the general form

$$\begin{aligned} \Gamma_{5\mu}^j(k; P) = & \frac{\tau^j}{2} \gamma_5 [\gamma_\mu F_R(k; P) + \gamma \cdot k k_\mu G_R(k; P) - \sigma_{\mu\nu} k_\nu H_R(k; P)] \\ & + \tilde{\Gamma}_{5\mu}^j(k; P) + \frac{P_\mu}{P^2 + m_\phi^2} \phi^j(k; P), \end{aligned} \quad (2.40)$$

where  $F_R, G_R, H_R$  and  $\tilde{\Gamma}_{5\mu}^i$  are regular as  $P^2 \rightarrow -m_\phi^2$ ,  $P_\mu \tilde{\Gamma}_{5\mu}^i(k; P) \sim O(P^2)$  and  $\phi^j(k; P)$  has the structure depicted in (2.38). This form admits the possibility of at least one pole term in the axial-vector vertex but does not require it.

Substituting (2.40) into (2.39) and equating putative pole terms, it is clear that, if present,  $\phi^j(k; P)$  satisfies Eq. (2.37). Since this is an eigenvalue problem that only admits a  $\Gamma_\pi^j \neq 0$  solution for  $P^2 = -m_\pi^2$ , it follows that  $\phi^j(k; P)$  is nonzero only for  $P^2 = -m_\pi^2$  and the pole mass is  $m_\phi^2 = m_\pi^2$ . Hence, if  $K$  supports such a bound state, the axial-vector vertex contains a pion-pole contribution whose residue,  $r_A$ , is not fixed by these arguments; i.e., Eq. (2.40) becomes

$$\begin{aligned} \Gamma_{5\mu}^j(k; P) = & \frac{\tau^j}{2} \gamma_5 [\gamma_\mu F_R(k; P) + \gamma \cdot k k_\mu G_R(k; P) - \sigma_{\mu\nu} k_\nu H_R(k; P)] \\ & + \tilde{\Gamma}_{5\mu}^j(k; P) + \frac{r_A P_\mu}{P^2 + m_\pi^2} \Gamma_\pi^j(k; P). \end{aligned} \quad (2.41)$$

Consider now the chiral limit axial-vector Ward-Takahashi identity, Eq. (2.8). If one assumes  $m_\pi^2 = 0$  in Eq. (2.41), substitutes it into the l.h.s. of Eq. (2.8) along with Eq. (2.4) on the right, and equates terms of order  $(P_\nu)^0$  and  $P_\nu$ , one obtains the chiral-limit relations<sup>19</sup>

$$r_A E_\pi(k; 0) = B(k^2), \quad (2.42)$$

$$F_R(k; 0) + 2 r_A F_\pi(k; 0) = A(k^2), \quad (2.43)$$

$$G_R(k; 0) + 2 r_A G_\pi(k; 0) = 2A'(k^2), \quad (2.44)$$

$$H_R(k; 0) + 2 r_A H_\pi(k; 0) = 0. \quad (2.45)$$

We know  $B(k^2) \equiv 0$  in the chiral limit [Eq. (2.7)] and that a  $B(k^2) \neq 0$  solution of Eq. (2.1) in the chiral limit signals DCSB. Indeed, in this case

$$M(p^2) \stackrel{\text{large-}p^2}{=} \frac{2\pi^2\gamma_m}{3} \frac{(-\langle\bar{q}q\rangle^0)}{p^2 \left(\frac{1}{2} \ln \left[p^2/\Lambda_{\text{QCD}}^2\right]\right)^{1-\gamma_m}}, \quad (2.46)$$

where  $\langle\bar{q}q\rangle^0$  is the renormalisation-point-independent vacuum quark condensate.<sup>41</sup> Furthermore, there is at least one nonperturbative DSE truncation scheme that preserves the axial-vector Ward-Takahashi identity, order by order. Hence Eqs. (2.42)-(2.45) are exact quark-level Goldberger-Treiman relations, which state that when chiral symmetry is dynamically broken:<sup>19</sup>

1. the homogeneous isovector pseudoscalar BSE has a massless,  $P^2 = 0$ , solution;
2. the Bethe-Salpeter amplitude for the massless bound state has a term proportional to  $\gamma_5$  alone, with  $E_\pi(k; 0)$  completely determined by the scalar part of the quark self energy, in addition to other pseudoscalar Dirac structures,  $F_\pi$ ,  $G_\pi$  and  $H_\pi$ , that are nonzero;
3. and the axial-vector vertex is dominated by the pion pole for  $P^2 \simeq 0$ .

The converse is also true. Hence DCSB is a sufficient and necessary condition for the appearance of a massless pseudoscalar bound state (of what can be very-massive constituents) that dominates the axial-vector vertex for  $P^2 \sim 0$ .

### 2.3.2. A mass formula

When chiral symmetry is explicitly broken the axial-vector Ward-Takahashi identity becomes:

$$P_\mu \Gamma_{5\mu}^j(k; P) = S^{-1}(k_+) i\gamma_5 \frac{\tau^j}{2} + i\gamma_5 \frac{\tau^j}{2} S^{-1}(k_-) - 2i m(\zeta) \Gamma_5^j(k; P), \quad (2.47)$$

where the pseudoscalar vertex is given by

$$\left[\Gamma_5^j(k; P)\right]_{tu} = Z_4 \left[\gamma_5 \frac{\tau^j}{2}\right]_{tu} + \int_q^\Lambda \left[\chi_5^j(q; P)\right]_{sr} K_{tu}^{rs}(q, k; P). \quad (2.48)$$

As argued in connection with Eq. (2.39), the solution of Eq. (2.48) has the form

$$\begin{aligned} i\Gamma_5^j(k; P) &= \frac{\tau^j}{2} \gamma_5 \left[ iE_R^P(k; P) + \gamma \cdot P F_R^P + \gamma \cdot k k \cdot P G_R^P(k; P) \right. \\ &\quad \left. + \sigma_{\mu\nu} k_\mu P_\nu H_R^P(k; P) \right] + \frac{r_P}{P^2 + m_\pi^2} \Gamma_\pi^j(k; P), \end{aligned} \quad (2.49)$$

where  $E_R^P$ ,  $F_R^P$ ,  $G_R^P$  and  $H_R^P$  are regular as  $P^2 \rightarrow -m_\pi^2$ ; i.e., the isovector pseudoscalar vertex also receives a contribution from the pion pole. In this case equating pole terms in the Ward-Takahashi identity, Eq. (2.47), entails<sup>19</sup>

$$r_A m_\pi^2 = 2 m(\zeta) r_P(\zeta). \quad (2.50)$$

This is another exact relation in QCD. Now it is important to determine the residues  $r_A$  and  $r_P$ .

A consideration of the renormalised axial-vector vacuum polarisation shows:<sup>19</sup>

$$r_A \delta^{ij} P_\mu = f_\pi \delta^{ij} P_\mu = Z_2 \text{tr} \int_q^\Lambda \frac{1}{2} \tau^i \gamma_5 \gamma_\mu S(q_+) \Gamma_\pi^j(q; P) S(q_-); \quad (2.51)$$

i.e., the residue of the pion pole in the axial-vector vertex is the pion decay constant. The factor of  $Z_2$  on the r.h.s. in Eq. (2.51) is crucial: it ensures the result is gauge invariant, and cutoff and renormalisation-point independent. Equation (2.51) is the exact expression in quantum field theory for the pseudovector projection of the pion's wave function on the origin in configuration space.

A close inspection of Eq. (2.48), following its re-expression in terms of the renormalised, fully-amputated quark-antiquark scattering amplitude:  $M = K + K(SS)K + \dots$ , yields<sup>19</sup>

$$i\delta^{ij} r_P = Z_4 \text{tr} \int_q^\Lambda \frac{1}{2} \tau^i \gamma_5 S(q_+) \Gamma_\pi^j(q; P) S(q_-), \quad (2.52)$$

wherein the dependence of  $Z_4$  on the gauge parameter, the regularisation mass-scale and the renormalisation point is exactly that required to ensure: 1)  $r_P$  is finite in the limit  $\Lambda \rightarrow \infty$ ; 2)  $r_P$  is gauge-parameter independent; and 3) the renormalisation point dependence of  $r_P$  is just such as to guarantee the r.h.s. of Eq. (2.50) is renormalisation point *independent*. Equation (2.52) expresses the pseudoscalar projection of the pion's wave function on the origin in configuration space.

Let us focus for a moment on the chiral limit behaviour of Eq. (2.52) whereat, using Eqs. (2.38), (2.42)-(2.45), one readily finds

$$-\langle \bar{q}q \rangle_\zeta^0 = f_\pi r_P^0(\zeta) = Z_4(\zeta, \Lambda) N_c \text{tr}_D \int_q^\Lambda S_{\hat{m}=0}(q). \quad (2.53)$$

Equation (2.53) is unique as the expression for the chiral limit *vacuum quark condensate*. It is  $\zeta$ -dependent but independent of the gauge parameter and the regularisation mass-scale, and Eq. (2.53) thus proves that the chiral-limit residue of the pion pole in the pseudoscalar vertex is  $(-\langle \bar{q}q \rangle_\zeta^0)/f_\pi$ . Now Eqs. (2.50), (2.53) yield

$$(f_\pi^0)^2 m_\pi^2 = -2 m(\zeta) \langle \bar{q}q \rangle_\zeta^0 + \text{O}(\hat{m}^2), \quad (2.54)$$

where  $f_\pi^0$  is the chiral limit value from Eq. (2.51). Hence what is commonly known as the Gell-Mann–Oakes–Renner relation is a *corollary* of Eq. (2.50).

One can now understand the results in Table 2.1: a massless bound state of massive constituents is a necessary consequence of DCSB and will emerge in any few-body approach to QCD that employs a systematic truncation scheme which preserves the Ward-Takahashi identities.

We stress that Eqs. (2.50)-(2.52) are valid for any values of the current-quark masses and the generalisation to  $N_f$  quark flavours is<sup>20,24,25</sup>

$$f_H^2 m_H^2 = -\langle \bar{q}q \rangle_\zeta \mathcal{M}_H^\zeta, \quad (2.55)$$

$\mathcal{M}_\zeta^H = m_{q_1}^\zeta + m_{q_2}^\zeta$  is the sum of the current-quark masses of the meson's constituents;

$$f_H P_\mu = Z_2 \text{tr} \int_q^\Lambda \frac{1}{2} (T^H)^T \gamma_5 \gamma_\mu \mathcal{S}(q_+) \Gamma^H(q; P) \mathcal{S}(q_-), \quad (2.56)$$

with  $\mathcal{S} = \text{diag}(S_u, S_d, S_s, \dots)$ ,  $T^H$  a flavour matrix specifying the meson's quark content, e.g.,  $T^{\pi^+} = \frac{1}{2}(\lambda^1 + i\lambda^2)$ ,  $\{\lambda^i\}$  are  $N_f$ -flavour generalisations of the Gell-Mann matrices, and

$$\langle \bar{q}q \rangle_\zeta^H = i f_H Z_4 \text{tr} \int_q^\Lambda \frac{1}{2} (T^H)^T \gamma_5 \mathcal{S}(q_+) \Gamma^H(q; P) \mathcal{S}(q_-). \quad (2.57)$$

Owing to its chiral limit behaviour,  $\langle \bar{q}q \rangle_\zeta^H$  has been called an in-hadron condensate.

In the heavy-quark limit, Eq. (2.56) yields the model-independent result<sup>24,25</sup>

$$f_H \propto \frac{1}{\sqrt{M_H}}; \quad (2.58)$$

i.e., it reproduces a well-known consequence of heavy-quark symmetry.<sup>42</sup> A similar analysis of Eq. (2.57) gives a new result

$$-\langle \bar{q}q \rangle_\zeta^H = \text{constant} + O\left(\frac{1}{m_H}\right) \text{ for } \frac{1}{m_H} \sim 0. \quad (2.59)$$

Combining Eqs. (2.58), (2.59), one finds<sup>24,25</sup>

$$m_H \propto \hat{m}_f \text{ for } \frac{1}{\hat{m}_f} \sim 0, \quad (2.60)$$

where  $\hat{m}_f$  is the renormalisation-group-invariant current-quark mass of the flavour-nonsinglet pseudoscalar meson's heaviest constituent. This is the result one would have anticipated from constituent-quark models but here we have reviewed a direct proof in QCD. Equation (2.50) is a single formula that unifies aspects of light- and heavy-quark physics and, as we shall illustrate, can be used to gain an insightful understanding of modern lattice simulations.

### 3. Foundation for a Description of Mesons

The renormalisation-group-improved rainbow-ladder truncation has long been employed to study light mesons and [Sec. 2] it can be a quantitatively reliable tool for vector and flavour nonsinglet pseudoscalar mesons. In connection with Eqs. (2.12), (2.13) we argued that the truncation preserves the ultraviolet behaviour of the quark-antiquark scattering kernel in QCD but requires an assumption about that kernel in the infrared; viz., on the domain  $Q^2 \lesssim 1 \text{ GeV}^2$ , which corresponds to length-scales  $\gtrsim 0.2 \text{ fm}$ . The calculation of this behaviour is a primary challenge in contemporary hadron physics and there is progress.<sup>43,44,45,46,47,48,49,50</sup> However, at present the efficacious approach is to model the kernel in the infrared, which

enables quantitative comparisons with experiments that can be used to inform theoretical analyses.

The most extensively applied model is specified by using<sup>20,51</sup>

$$\frac{\alpha(Q^2)}{Q^2} = \frac{4\pi^2}{\omega^6} D Q^2 e^{-Q^2/\omega^2} + \frac{8\pi^2 \gamma_m}{\ln \left[ \tau + \left( 1 + Q^2/\Lambda_{\text{QCD}}^2 \right)^2 \right]} \mathcal{F}(Q^2), \quad (3.1)$$

in Eqs. (2.12), (2.13). Here,  $\mathcal{F}(Q^2) = [1 - \exp(-Q^2/[4m_t^2])]/Q^2$ ,  $m_t = 0.5 \text{ GeV}$ ;  $\tau = e^2 - 1$ ;  $\gamma_m = 12/25$ ; and<sup>52</sup>  $\Lambda_{\text{QCD}} = \Lambda_{\overline{\text{MS}}}^{(4)} = 0.234 \text{ GeV}$ .<sup>f</sup> The true parameters in Eq. (3.1) are  $D$  and  $\omega$ , which together determine the integrated infrared strength of the rainbow-ladder kernel; i.e., the so-called interaction tension,<sup>44</sup>  $\sigma^\Delta$ . However, we emphasise that they are not independent:<sup>51</sup> in fitting to a selection of observables, a change in one is compensated by altering the other; e.g., on the domain  $\omega \in [0.3, 0.5] \text{ GeV}$ , the fitted observables are approximately constant along the trajectory<sup>49</sup>

$$\omega D = (0.72 \text{ GeV})^3. \quad (3.2)$$

This correlation: a reduction in  $D$  compensating an increase in  $\omega$ , acts to keep a fixed value of the interaction tension. Equation (3.1) is thus a one-parameter model.

### 3.1. Rainbow gap equation

Inserting Eq. (3.1) into Eq. (2.13) provides a model for QCD's gap equation and in applications to hadron physics one is naturally interested in the nonperturbative DCSB solution. A familiar property of gap equations is that they only support such a solution if the interaction tension exceeds some critical value. In the present case that value is<sup>44</sup>  $\sigma_c^\Delta \sim 2.5 \text{ GeV/fm}$ . This amount of infrared strength is sufficient to generate a nonzero vacuum quark condensate *but only just*. An acceptable description of hadrons requires<sup>20</sup>  $\sigma^\Delta \sim 25 \text{ GeV/fm}$  and that is obtained with<sup>51</sup>

$$D = (0.96 \text{ GeV})^2. \quad (3.3)$$

This value of the model's infrared mass-scale parameter and the two current-quark masses

$$m_u(1 \text{ GeV}) = 5.5 \text{ MeV}, \quad m_s(1 \text{ GeV}) = 125 \text{ MeV}, \quad (3.4)$$

defined using the one-loop expression

$$\frac{m(\zeta)}{m(\zeta')} = Z_m(\zeta', \zeta) \approx \left( \frac{\ln[\zeta'/\Lambda_{\text{QCD}}]}{\ln[\zeta/\Lambda_{\text{QCD}}]} \right)^\gamma \quad (3.5)$$

to evolve  $m_u(19 \text{ GeV}) = 3.7 \text{ MeV}$ ,  $m_s(19 \text{ GeV}) = 85 \text{ MeV}$ , were obtained in Ref. [51] by requiring a least-squares fit to the  $\pi$ - and  $K$ -meson observables listed in

<sup>f</sup>NB. Eq. (3.1) gives  $\alpha(m_Z^2) = 0.126$ . Comparison with a modern value:<sup>53</sup>  $0.117 \pm 0.002$ , means that a smaller  $\Lambda_{\text{QCD}}$  is acceptable in the model, if one wants to avoid overestimating the coupling in the ultraviolet, but not a larger value.

Table 3.1. Comparison of experimental values with results for  $\pi$  and  $K$  observables calculated using the renormalisation-group-improved rainbow-ladder interaction specified by Eq. (3.1), quoted in MeV. The model's sole parameter and the current-quark masses were varied to obtain these results. The best fit parameter values are given in Eqs. (3.3), (3.4). (Adapted from Ref. [51].)

	$m_\pi$	$m_K$	$f_\pi$	$f_K$
Calc. <sup>51</sup>	138	497	93	109
Expt. <sup>53</sup>	138	496	92	113

Table 3.1. The procedure was straightforward: the rainbow gap equation [Eqs. (2.5), (2.13), (3.1)] was solved with a given parameter set and the output used to complete the kernels in the homogeneous ladder BSEs for the  $\pi$ - and  $K$ -mesons [Eqs. (2.12), (2.13), (2.37), (2.38) with  $\tau^j$  for the  $\pi$  channel and  $\tau^j \rightarrow T^{K^+} = \frac{1}{2}(\lambda^4 + i\lambda^5)$  for the  $K$ ]. These BSEs were solved to obtain the  $\pi$ - and  $K$ -meson masses, and the Bethe-Salpeter amplitudes. Combining this information gives the leptonic decay constants via Eq. (2.56). This was repeated as necessary to arrive at the results in Table 3.1, which were judged satisfactory. The model gives a vacuum quark condensate

$$-\langle \bar{q}q \rangle_{1\text{GeV}}^0 = (0.242\text{ GeV})^3, \quad (3.6)$$

calculated from Eq. (2.53) and evolved using the one-loop expression in Eq. (3.5).

With the model's single parameter fixed, and the dressed-quark propagator obtained, it is straightforward to compose and solve the homogeneous BSE for vector mesons and calculate properties analogous to those in Table 3.1. The predictions<sup>51</sup> of the model are reproduced in Table 3.2. The expression in QCD for a vector meson's electroweak decay constant is<sup>25</sup>

$$f_H^V M_H^V = \frac{1}{3} Z_2 \text{tr} \int_q^\Lambda (T^H)^T \gamma_\mu \mathcal{S}(q_+) \Gamma_\mu^H(q; P) \mathcal{S}(q_-), \quad (3.7)$$

where  $M_H^V$  is the meson's mass. This quantity characterises decays such as  $\rho \rightarrow e^+e^-$ ,  $\tau \rightarrow K^*\nu_\tau$ , and in the heavy-quark limit<sup>25</sup>

$$f_H^V \propto \frac{1}{\sqrt{M_H^V}}, \quad f_H^V \approx f_H, \quad (3.8)$$

reproducing additional familiar consequences of heavy-quark symmetry.

Given the discussion in Sec. 2.2, the phenomenological success of the rainbow-ladder kernel, evident in the results in Tables 3.1 and 3.2, is unsurprising and, indeed, was to be expected.

### 3.2. Comparison with lattice simulations

Since the solution of the gap equation has long been of interest in grappling with DCSB in QCD, in Figs. 3.1, 3.2 we depict the scalar functions characterising the renormalised dressed-quark propagator: the wave function renormalisation,  $Z(p^2)$ , and mass function,  $M(p^2)$ , obtained by solving Eq. (2.13) using Eq. (3.1). The infrared suppression of  $Z(p^2)$  and enhancement of  $M(p^2)$  are longstanding predictions

Table 3.2. Experiment cf. predictions of a rainbow-ladder kernel for simple vector meson observables. No parameters were varied to obtain the results. The root-mean-square error over predicted quantities is  $< 8\%$ . NB. A charged particle normalisation is used for  $f_H^V$  in Eq. (3.7), which differs from that in Eq. (2.56) by a multiplicative factor of  $\sqrt{2}$ . (Adapted from Ref. [51].)

	$m_\rho$	$m_{K^*}$	$m_\phi$	$f_\rho$	$f_{K^*}$	$f_\phi$
Calc. <sup>51</sup>	742	936	1072	207	241	259
Expt. <sup>53</sup>	771	892	1019	217	227	228
Rel.-Error	0.04	-0.05	-0.05	0.05	-0.06	-0.14

of DSE studies,<sup>21</sup> which could have been anticipated from Ref. [55]. This prediction has recently been confirmed in numerical simulations of quenched lattice-QCD, as is evident in the figures.

It is not yet possible to reliably determine the behaviour of lattice Schwinger functions for current-quark masses that are a realistic approximation to those of the  $u$ - and  $d$ -quarks. Therefore a lattice estimate of  $m_\pi$ ,  $f_\pi$ ,  $\langle \bar{q}q \rangle^0$  is absent. To obtain such an estimate, Ref. [49] used the rainbow kernel described herein and varied  $(D, \omega)$  in order to reproduce the lattice data. A best fit was obtained with

$$D = (0.74 \text{ GeV})^2, \quad \omega = 0.3 \text{ GeV}, \quad (3.9)$$

at a current-quark mass of  $0.6 m_s^{1 \text{ GeV}} \approx 14 m_u$  [Eq. (3.4)] chosen to coincide with that employed in the lattice simulation. Constructing and solving the homogeneous BSE for a pion-like bound state composed of quarks with this current-mass yields

$$m_\pi^{m_q \sim 14 m_u} = 0.48 \text{ GeV}, \quad f_\pi^{m_q \sim 14 m_u} = 0.094 \text{ GeV}. \quad (3.10)$$

The parameters in Eq. (3.9) give chiral limit results:<sup>49</sup>

$$f_\pi^0 = 0.068 \text{ GeV}, \quad -\langle \bar{q}q \rangle_{1 \text{ GeV}}^0 = (0.19 \text{ GeV})^3, \quad (3.11)$$

whereas Eqs. (3.2), (3.3) give  $f_\pi^0 = 0.088 \text{ GeV}$ , which agrees with the estimate of chiral perturbation theory, and the vacuum quark condensate in Eq. (3.6). Following this preliminary study it is important to reanalyse the lattice data using different models for the infrared behaviour of the scattering kernel,  $K$ , so that the quenching error can be estimated.

The unification of light and heavy pseudoscalar meson masses via the mass formula in Eq. (2.50) has also been quantitatively explored using the rainbow-ladder kernel. That is illustrated in Fig. 3.3 wherein the calculated mass of a  $u\bar{q}$  pseudoscalar meson is plotted as a function of  $m_q(\zeta)$ , with  $m_u(\zeta)$  fixed via Eq. (3.4). The calculations are depicted in the figure by the solid curve, which is, in MeV,<sup>57</sup>

$$m_H = 83 + 500\sqrt{\mathcal{X}} + 310 \mathcal{X}, \quad \mathcal{X} = m_q^\zeta / \Lambda_{\text{QCD}}. \quad (3.12)$$

The curvature appears slight in the figure but that is misleading: the nonlinear term in Eq. (3.12) accounts for almost all of  $m_\pi$  (the Gell-Mann–Oakes–Renner relation is nearly exact for the pion) and 80% of  $m_K$ . NB. The dashed line in Fig. 3.3

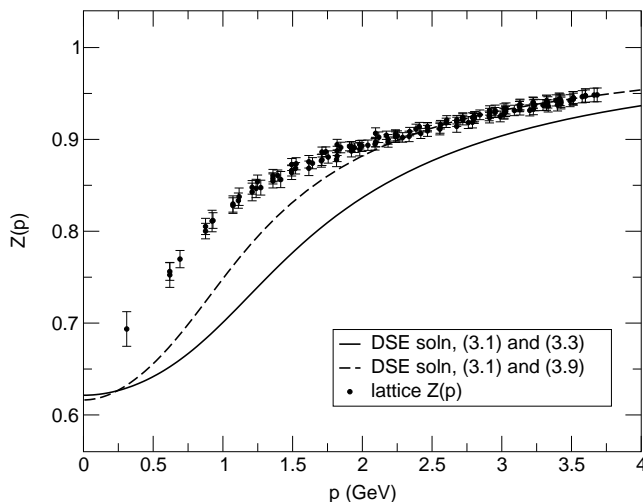


Fig. 3.1. Wave function renormalisation. Solid line: solution of the gap equation using Eqs. (3.1), (3.3); data: lattice simulations,<sup>54</sup> obtained with  $m = 0.036/a \sim 60$  MeV; dashed-line: gap equation solution using Eqs. (3.1), (3.9). The DSE study used a renormalisation point  $\zeta = 19$  GeV and a current-quark mass  $0.6 m_s^{1\text{GeV}}$  [Eq. (3.4)] so as to enable a direct comparison with the lattice data. (Adapted from Ref. [49].)

fits the  $K$ ,  $D$ ,  $B$  subset of the data exactly. It is drawn to illustrate how easily one can be misled. Without careful calculation one might infer from this apparent agreement that the large- $m_q$  limit of Eq. (2.50) is already manifest at the  $s$ -quark mass whereas, in reality, the linear term only becomes dominant for  $m_q \gtrsim 1$  GeV, providing 50% of  $m_D$  and 67% of  $m_B$ . The model predicts  $m_c^{1\text{GeV}} = 1.1$  GeV,  $m_b^{1\text{GeV}} = 4.2$  GeV, values typical of Poincaré covariant treatments.<sup>25</sup>

Equation (3.12) can be used as a basis for extrapolating the results of lattice simulations to realistic values of the light current-quark masses. It is a true expression of essential consequences of DCSB and the importance of incorporating such constraints in the analysis of lattice data is beginning to be appreciated.<sup>59</sup> The rainbow-ladder kernel has also been employed in an analysis of a trajectory of fictitious pseudoscalar mesons, all composed of equally massive constituents.<sup>57</sup> (The only physical state on this trajectory is the pion.) The DSE study predicts<sup>60</sup>

$$\frac{m_{H_{m=2m_s}}}{m_{H_{m=m_s}}} = 2.2, \quad (3.13)$$

in agreement with a result of recent quenched lattice simulations.<sup>61</sup> It provides an understanding of this result, showing that the persistent dominance by the term nonlinear in the current-quark mass owes itself to a large value of the in-meson condensates for light-quark mesons; e.g.,<sup>20</sup>  $\langle \bar{q}q \rangle_{1\text{GeV}}^{s\bar{s}} = (-0.32 \text{ GeV})^3$ , and thereby confirms the large-magnitude condensate version of chiral perturbation theory. (NB. This last observation is also supported by Eq. (3.11) and the associated discussion.) References [57,58] provide vector meson trajectories too.

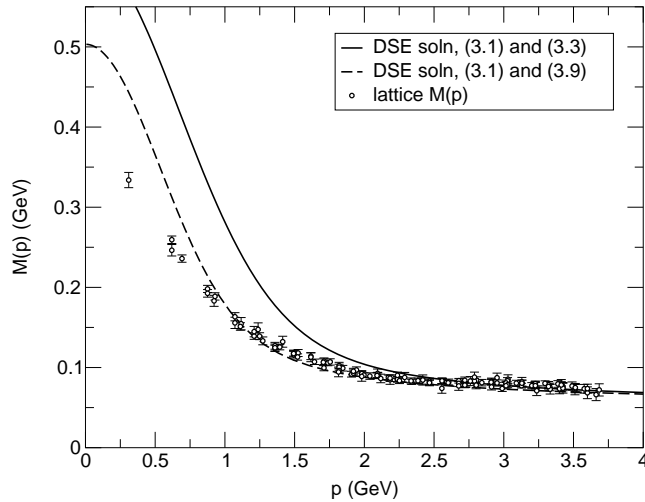


Fig. 3.2. Mass function. Solid line: solution of the gap equation using Eqs. (3.1), (3.3); data: lattice simulations,<sup>54</sup> obtained with  $m = 0.036/a \sim 60$  MeV; dashed-line: gap equation solution using Eqs. (3.1), (3.9). The DSE study used a renormalisation point  $\zeta = 19$  GeV and a current-quark mass  $0.6 m_s^{1 \text{ GeV}}$  [Eq. (3.4)]. (Adapted from Ref. [49].)

### 3.3. Pion's valence-quark distribution function

The momentum-dependent dressing of quark and gluon propagators is a fact. It is certainly the keystone of DCSB, materially influences hadron observables and quite likely plays a central role in confinement. This was anticipated in the Global Colour Model.<sup>62,63,64</sup> As we shall subsequently illustrate, the rainbow-ladder kernel is unique today in providing a direct description and unification of a wide range of meson phenomena in terms of a single parameter that characterises the long-range behaviour of the quark-antiquark interaction. Establishing this is a reward for substantial effort. However, it is a recent development. Historically, algebraic parametrisations of the dressed-quark propagator and Bethe-Salpeter amplitudes, based on the known behaviour of numerical solutions, were used to expedite a comparison between theory and experiment. Successes with that approach<sup>25,32,33,65,66,67,68,69,70,71,72,73,74,75</sup> provided the impetus for refining the DSE method and its direct numerical applications.

The utility of an algebraic form for the dressed-quark propagator and Bethe-Salpeter amplitudes is self-evident: calculating the simplest elastic form factor requires the repeated evaluation of a multidimensional integral whose integrand is a complex-valued function, and a functional of the propagator and amplitudes. The expedient remains of use, notably in connection with baryons, and can be illustrated by reviewing a recent calculation of the pion's valence-quark distribution function.<sup>76</sup>

The cross section for deep inelastic lepton-hadron scattering can be interpreted in terms of the momentum-fraction probability distributions of quarks and gluons

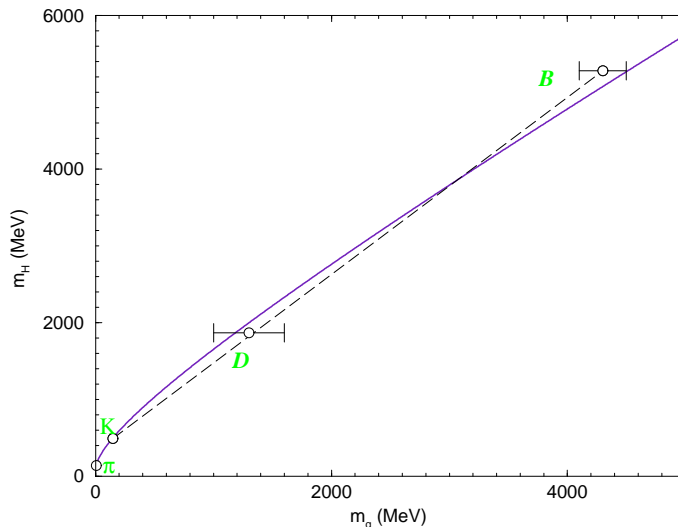


Fig. 3.3. Solid line: pseudoscalar  $u\bar{q}$  meson’s mass as a function of  $m_q^\zeta$ ,  $\zeta = 19$  GeV, with a fixed value of  $m_\zeta$  corresponding to  $m_u^{1\text{GeV}} = 5.5$  MeV, Eq. (3.4). The experimental data points are from Ref. [53] as are the errors assigned to the associated heavy-quark masses. The dashed curve is a straight line drawn through the  $K$ ,  $D$ ,  $B$  masses. (Adapted from Ref. [56]. See also Ref. [58].)

in the hadronic target, and since the pion is a two-body bound state with only  $u$ - and  $d$ -valence-quarks it is the least complicated system for which these distribution functions can be calculated. However, in the absence of pion targets, their measurement is not straightforward and they have primarily been inferred from Drell-Yan measurements in pion-nucleus collisions.<sup>77</sup>

The distribution functions provide a measure of the pion’s quark-gluon substructure but they cannot be calculated perturbatively. Fortunately, DSEs furnish a sound theoretical description of pion properties, providing a model-independent explanation of its essentially dichotomous nature as both a Goldstone boson and a low-mass bound state of massive constituents, and also supply an efficacious phenomenological tool. Hence they are ideal for exploring the nature of the pion’s parton distribution functions. The valence-quark distribution function,  $u_v^\pi(x)$ , is of particular interest because its pointwise behaviour is affected by aspects of confinement dynamics; e.g., by the mechanisms responsible for the finite extent and essentially nonpointlike nature of the pion. (NB.  $u^{\pi^+} = \bar{d}^{\pi^+}$  in the  $\mathcal{G}$ -parity symmetric limit of QCD.)

### 3.3.1. Handbag contributions

Reference [76] focuses on a calculation of the “handbag diagrams” illustrated in Fig. 3.4, which are the only impulse approximation contributions to virtual photon-pion

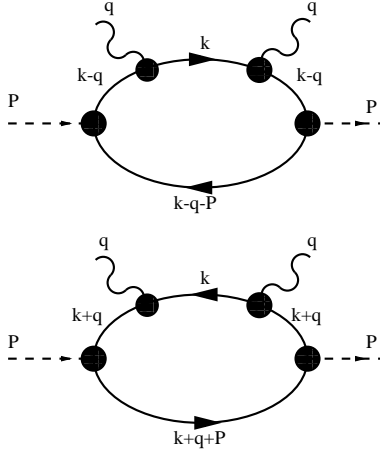


Fig. 3.4. “Handbag” contributions to the virtual photon-pion forward Compton scattering amplitude.  $\pi$ , dashed-line;  $\gamma$ , wavy-line;  $S$ , internal solid-line, dressed-quark propagator, Eq. (3.24). The filled circles represent the pion’s Bethe-Salpeter amplitude,  $\Gamma_\pi$  in Eqs. (2.38), (3.30)-(3.33), and the dressed-quark-photon vertex,  $\Gamma_\mu$  in Eq. (3.35), depending on which external line they begin/end. (Adapted from Ref. [76].)

forward Compton scattering that survive in the deep inelastic Bjorken limit:

$$q^2 \rightarrow \infty, \quad P \cdot q \rightarrow -\infty \quad \text{but} \quad x := -\frac{q^2}{2P \cdot q} \quad \text{fixed.} \quad (3.14)$$

The upper diagram represents the renormalised matrix element

$$T_{\mu\nu}^+(q, P) = \text{tr} \int_k^\Lambda \tau_- \Gamma_\pi(k_\Gamma; -P) \\ \times S(k_t) ieQ\Gamma_\nu(k_t, k) S(k) ieQ\Gamma_\mu(k, k_t) S(k_t) \tau_+ \Gamma_\pi(k_\Gamma; P) S(k_s), \quad (3.15)$$

where:  $\tau_\pm = \frac{1}{2}(\tau_1 \pm i\tau_2)$ ;  $S(\ell) = \text{diag}[S_u(\ell), S_d(\ell)]$ , with  $S_u = S_d = S$ , assuming isospin symmetry; and  $k_\Gamma = k - q - P/2$ ,  $k_t = k - q$ ,  $k_s = k - q - P$ . A new element in Eq. (3.15) is  $\Gamma_\mu(\ell_1, \ell_2)$ , the dressed-quark-photon vertex, with  $Q = \text{diag}(2/3, -1/3)$  the quark-charge matrix. It can be obtained by solving the inhomogeneous vector BSE;<sup>27</sup> i.e., Eq. (2.9) with  $\gamma_5\gamma_\mu \rightarrow \gamma_\mu$ , or modelled, based on symmetry considerations, as we describe below. The matrix element represented by the lower diagram is the crossing partner of Eq. (3.15) and is obvious by analogy.

The hadronic tensor relevant to inclusive deep inelastic lepton-pion scattering can be obtained from the forward Compton process via the optical theorem:

$$W_{\mu\nu}(q; P) = W_{\mu\nu}^+(q; P) + W_{\mu\nu}^-(q; P) = \frac{1}{2\pi} \text{Im} [T_{\mu\nu}^+(q; P) + T_{\mu\nu}^-(q; P)]. \quad (3.16)$$

In the Bjorken limit one finds<sup>76</sup>

$$W_{\mu\nu}^+(q; P) = F_1^+(x) t_{\mu\nu} + F_2^+(x) \frac{q_\mu^t q_\nu^t}{2x}, \quad (3.17)$$

$t_{\mu\nu} = \delta_{\mu\nu} - q_\mu q_\nu / q^2$ ,  $q_\mu^t = q_\mu + 2xP_\mu$ , and

$$F_2^+(x) = 2xF_1^+(x), \quad F_{1,2}^+(x) \rightarrow 0 \text{ as } x \rightarrow 1. \quad (3.18)$$

Combining these results with their analogues for  $W_{\mu\nu}^-$ , one recovers Bjorken scaling of the deep inelastic cross section, namely, the cross section depends only on  $x$ , and not on  $P \cdot q$  and  $q^2$  separately. Furthermore, the derivation shows that, in the Bjorken limit,  $x$  is truly the fraction of the pion's momentum carried by the struck quark, and one may therefore write

$$F_2^{e\pi}(x) = F_2^+(x) + F_2^-(x) = \frac{4}{9}[xu(x) + x\bar{u}(x)] + \frac{1}{9}[xd(x) + x\bar{d}(x)] + \dots, \quad (3.19)$$

where  $u(x)$ ,  $\bar{u}(x)$ , etc., are the quark and antiquark distribution functions, and the ellipsis denotes contributions from the  $s$ - and  $c$ -quarks. (Heavier quarks are assumed not to contribute at all.)

As we now explain, the calculation in Ref. [76] produces the valence-quark distributions:

$$q_v^\pi(x) := q^\pi(x) - \bar{q}^\pi(x). \quad (3.20)$$

It is plain from Eqs. (3.15), (3.16) that the hadronic tensor depends on the dressed-quark propagator, pion Bethe-Salpeter amplitude and dressed-quark-photon vertex, and although sea-quarks are implicitly contained in these elements, the ‘‘handbag’’ impulse approximation diagrams in Fig. 3.4 only admit a coupling of the photon to the propagator of the dressed-quark constituent. The quark's internal structure is not resolved. The calculation therefore yields the valence-quark distribution at a scale  $q_0$  that is characteristic of the resolution and  $\ell_0 = 1/q_0$  is a length-scale that typifies the size of the valence quark. As with all calculations of this type hitherto,  $q_0$  is an *a priori* undetermined parameter, although one anticipates  $0.3 \lesssim q_0 \lesssim 1.0$  GeV ( $0.7 \gtrsim \ell_0 \gtrsim 0.2$  fm), with the lower bound set by the constituent-quark mass and the upper by the onset of the perturbative domain. A sea-quark distribution is generated via the evolution equations when the valence distribution is evolved to that  $q^2$ -scale appropriate to a given experiment. An explicit sea-quark distribution at the scale  $q_0$  can arise from non-impulse diagrams; e.g., contributions that one might identify with photon couplings to intermediate-state quark-meson-loops that can appear as a dressing of the quark propagator:

$$\pi^+ = u\bar{d} \rightarrow (u\bar{s}s)\bar{d} = (K^+s)\bar{d} \rightarrow u\bar{d} = \pi^+, \quad (3.21)$$

with deep inelastic scattering in this instance taking place on the kaon:  $\gamma K^+s \rightarrow K^+s\gamma$ , etc. Such intermediate states arise as vertex corrections in the quark-DSE and were neglected merely to simplify the first calculation of  $u_v^\pi(x)$ , the improvement of which is a modern challenge. With these observations in mind,

$$F_2^+(x; q_0) = \frac{4}{9} x u_v^\pi(x; q_0), \quad F_2^-(x; q_0) = \frac{1}{9} x \bar{d}_v^\pi(x; q_0). \quad (3.22)$$

The calculations are required to yield

$$\int_0^1 dx u_v^\pi(x; q_0) = 1 = \int_0^1 dx \bar{d}_v^\pi(x; q_0); \quad (3.23)$$

viz., to ensure that the  $\pi^+$  contains one, and only one,  $u$ -valence-quark and one  $\bar{d}$ -valence-quark.

### 3.3.2. Algebraic parametrisations

To complete the calculation one must specify the elements in the integrand of Eq. (3.15). This is where the algebraic parametrisations appear. The dressed-light-quark propagator is

$$S(p) = -i\gamma \cdot p \sigma_V(p^2) + \sigma_S(p^2) = [i\gamma \cdot p A(p^2) + B(p^2)]^{-1}, \quad (3.24)$$

$$\bar{\sigma}_S(x) = 2\bar{m} \mathcal{F}(2(x + \bar{m}^2)) + \mathcal{F}(b_1 x) \mathcal{F}(b_3 x) [b_0 + b_2 \mathcal{F}(\varepsilon x)], \quad (3.25)$$

$$\bar{\sigma}_V(x) = \frac{1}{x + \bar{m}^2} [1 - \mathcal{F}(2(x + \bar{m}^2))], \quad (3.26)$$

with  $\mathcal{F}(y) = (1 - e^{-y})/y$ ,  $x = p^2/\lambda^2$ ,  $\bar{m} = m/\lambda$ ,  $\bar{\sigma}_S(x) = \lambda \sigma_S(p^2)$  and  $\bar{\sigma}_V(x) = \lambda^2 \sigma_V(p^2)$ . The mass-scale,  $\lambda = 0.566$  GeV, and dimensionless parameter values:<sup>g</sup>

$$\frac{\bar{m} \quad b_0 \quad b_1 \quad b_2 \quad b_3}{0.00897 \quad 0.131 \quad 2.90 \quad 0.603 \quad 0.185}, \quad (3.27)$$

were fixed in a least-squares fit to light-meson observables,<sup>68</sup> and the dimensionless  $u$ -current-quark mass corresponds to

$$m_u(1 \text{ GeV}) = 5.1 \text{ MeV}. \quad (3.28)$$

The pointwise form of the dressed-quark wave function renormalisation and mass function obtained with this simple parametrisation is qualitatively identical to that of the numerical DSE solutions depicted in Figs. 3.1, 3.2, and hence is consistent with lattice-QCD simulations. However, it was proposed long before both, and provided the first clear evidence that nonperturbative momentum-dependent dressing of parton propagators is fundamentally important in QCD and provides a key to understanding hadron properties. The parametrisation represents the propagator as an entire function<sup>78,79</sup> and thereby exhibits confinement through the violation of reflection positivity,<sup>h</sup> which means, loosely speaking, that the quark fragments before it can reach a detector;<sup>83</sup> and manifests DCSB with

$$-\langle \bar{q}q \rangle_{1 \text{ GeV}^2} = \lambda^3 \frac{3}{4\pi^2} \frac{b_0}{b_1 b_3} \ln \frac{1}{\Lambda_{\text{QCD}}^2} = (0.221 \text{ GeV})^3, \quad (3.29)$$

which is calculated directly from Eqs. (2.53), (3.5) after noting that Eqs. (3.25), (3.26) yield Eq. (2.46) with  $\gamma_m = 1$ .

<sup>g</sup> $\varepsilon = 10^{-4}$  in Eq. (3.25) acts only to decouple the large- and intermediate- $p^2$  domains. The study used Landau gauge because it is a fixed point of the QCD renormalisation group and  $Z_2 \approx 1$ , even nonperturbatively.<sup>20</sup>

<sup>h</sup>This sufficient condition for confinement is discussed at length in Sec. 6.2 of Ref. [21], Ref. [80], Sec. 2.2 of Ref. [81] and Sec. 2.4 of Ref. [82].

The general form of the pion's Bethe-Salpeter amplitude is given in Eq. (2.38). The behaviour of the invariant functions therein is largely constrained by the axial-vector Ward-Takahashi identity, as we explained in connection with Eqs. (2.42)-(2.45). These relations and numerical studies<sup>20</sup> support the parametrisation<sup>84</sup>

$$E_\pi(k; P) = \frac{1}{N_\pi} B_\pi(k^2), \quad (3.30)$$

where  $B_\pi$  is obtained from Eqs. (3.24)-(3.26), evaluated using  $\bar{m} = 0$  and

$$b_0 \rightarrow b_0^\pi = 0.19 \quad (3.31)$$

with the other parameters unchanged, and:

$$F_\pi(k; P) = E_\pi(k; P)/(110f_\pi); \quad (3.32)$$

$$G_\pi(k; P) = 2F_\pi(k; P)/[k^2 + M_{UV}^2], \quad (3.33)$$

$M_{UV} = 10 \Lambda_{\text{QCD}}$ ; and  $H_\pi(k; Q) \equiv 0$ . The amplitude is canonically normalised consistent with the impulse approximation:

$$P_\mu = \int \frac{d^4k}{(2\pi)^4} \left\{ \text{tr}_{\text{CD}} \left[ \Gamma_\pi(k; -P) \frac{\partial S(k_+)}{\partial P_\mu} \Gamma_\pi(k; P) S(k_-) \right] + \text{tr}_{\text{CD}} \left[ \Gamma_\pi(k; -P) S(k_+) \Gamma_\pi(k; P) \frac{\partial S(k_-)}{\partial P_\mu} \right] \right\}. \quad (3.34)$$

This fixes  $N_\pi$ . The decay constant is subsequently obtained from Eq. (2.51).

The manner whereby an Abelian gauge boson couples to a dressed-fermion has been studied extensively and a range of qualitative constraints have been elucidated.<sup>85</sup> This research supports an *Ansatz*.<sup>86</sup>

$$i\Gamma_\mu(\ell_1, \ell_2) = i\Sigma_A(\ell_1^2, \ell_2^2) \gamma_\mu + (\ell_1 + \ell_2)_\mu \left[ \frac{1}{2} i\gamma \cdot (\ell_1 + \ell_2) \Delta_A(\ell_1^2, \ell_2^2) + \Delta_B(\ell_1^2, \ell_2^2) \right], \quad (3.35)$$

wherein

$$\Sigma_F(\ell_1^2, \ell_2^2) = \frac{1}{2} [F(\ell_1^2) + F(\ell_2^2)], \quad \Delta_F(\ell_1^2, \ell_2^2) = \frac{F(\ell_1^2) - F(\ell_2^2)}{\ell_1^2 - \ell_2^2}, \quad (3.36)$$

with  $F = A, B$  the scalar functions in Eq. (3.24), which preserves many of the constraints, in particular, the vector Ward-Takahashi identity. Furthermore, the *Ansatz* is expressed solely in terms of the dressed-quark propagator.

Using the elements just described, one obtains the following calculated values for an illustrative range of pion observables (adapted from Ref. [84]):

	$m_\pi$ (GeV)	$f_\pi$ (GeV)	$r_\pi$ (fm)	
Calc.	0.139	0.090	0.56	(3.37)
Expt. <sup>53,87</sup>	0.138	0.092	0.66	

with the pion's charge radius,  $r_\pi$ , calculated in impulse approximation.<sup>66</sup>

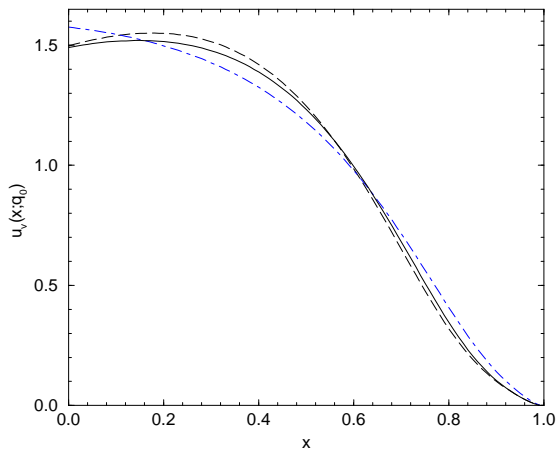


Fig. 3.5. Solid line:  $u_v(x; q_0)$  calculated using the DSE model described in Sec. 3.3. The resolving scale  $q_0 = 0.54 \text{ GeV} = 1/(0.37 \text{ fm})$  is fixed as described in connection with Eq. (3.40). Dashed line:  $u_v(x; q_0)$  calculated in the absence of the pseudovector components of the pion's Bethe-Salpeter amplitude; i.e.,  $F = 0 = G$  in Eq. (2.38) instead of Eqs. (3.32) and (3.33). Dot-dashed line: distribution calculated with  $m_\pi \rightarrow 0.1 m_\pi$ ,  $\tilde{M} = 0.36 \text{ GeV}$ . (Adapted from Ref. [76].)

### 3.3.3. Calculated distribution function

In the Bjorken limit, Eq. (3.15) reduces to a one-dimensional integral that depends parametrically on the valence-quark mass,  $\tilde{M}$ , and using the parametrisations described above that equation yields the valence-quark distribution function via Eqs. (3.16), (3.17), (3.22). The value

$$\tilde{M} = 0.30 \text{ GeV} \quad (3.38)$$

is fixed by normalisation, Eq. (3.23), and gives the distribution function depicted in Fig. 3.5. It vanishes at  $x = 1$ , in accordance with the kinematic constraint expressed in Eq. (3.18), and corresponds to a finite value of  $F_1(x = 0)$ , which signals the absence of sea-quark contributions. Unsurprisingly, since the pion is a light bound state of heavy constituents, the shape of the distribution is characteristic of a strongly bound system: cf. for a weakly bound system<sup>88</sup>  $u_v(x) \approx \delta(x - \frac{1}{2})$ .

The momentum-fraction carried by the valence-quarks at this resolving scale is

$$\langle x_q \rangle^\pi = \int_0^1 dx x [u_v(x; q_0) + \bar{d}_v(x; q_0)] = 0.71, \quad (3.39)$$

with the remainder,  $\langle x_g \rangle^\pi = 0.29$ , carried by the gluons that bind the pion bound state, which are invisible to the electromagnetic probe.<sup>i</sup> As with all calculations of parton distributions hitherto, in Ref. [76] the resolving scale

$$q_0 = 0.54 \text{ GeV} = 1/(0.37 \text{ fm}) \quad (3.40)$$

<sup>i</sup>NB. The parametrised pionic parton distributions in Ref. [89] yield a gluon momentum-fraction of  $\langle x_g \rangle^\pi = 0.29$  at  $q_0 = 0.51 \text{ GeV}$ .

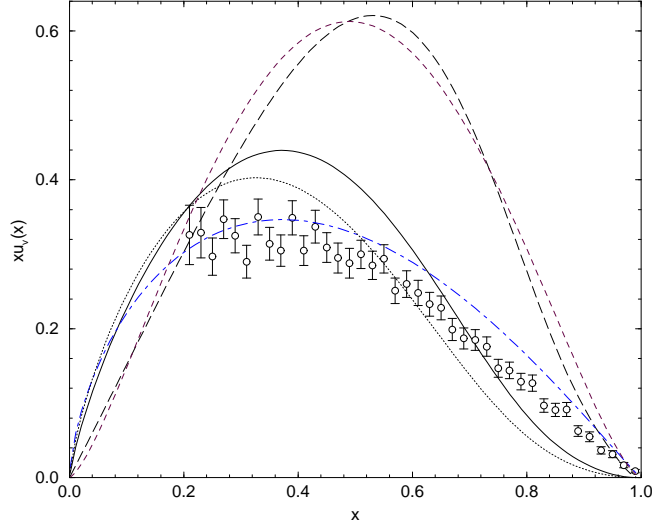


Fig. 3.6. Dashed line:<sup>76</sup>  $xu_v(x; q_0)$ ; short-dashed line: fit of Eqs. (3.42) and (3.46). Solid line: the evolved distribution,  $xu_v(x; q = 2 \text{ GeV})$ ; dotted line:  $xu_v(x; q = 4.05 \text{ GeV})$ , evolved with a 4-flavour value of  $\Lambda_{\text{QCD}} = 0.204 \text{ GeV}$ ; and dot-dashed line: the phenomenological fit of Ref. [90]. The Drell-Yan data are from Ref. [77]. (Adapted from Ref. [76].)

was chosen so that when using the nonsinglet evolution equations (see, e.g., Ref. [53]) to evolve the distribution in Fig. 3.5 up to  $q = 2 \text{ GeV}$ , agreement was obtained between the first and second moments of the calculated distribution and those determined from a phenomenological fit to data, in this case the fit of Ref. [90], viz.

	$\langle x_q \rangle_{2 \text{ GeV}}^{\pi}$	$\langle x_q^2 \rangle_{2 \text{ GeV}}^{\pi}$	$\langle x_q^3 \rangle_{2 \text{ GeV}}^{\pi}$
Calc. <sup>76</sup>	0.24	0.098	0.049
Fit <sup>90</sup>	$0.24 \pm 0.01$	$0.10 \pm 0.01$	$0.058 \pm 0.004$
Latt. <sup>91</sup>	$0.27 \pm 0.01$	$0.11 \pm 0.03$	$0.048 \pm 0.020$

The original and evolved distributions are depicted in Fig. 3.6.

A fit to  $xu_v(x; q)$ , acceptable for the estimation of moments, is obtained with

$$xu_v^{\text{mom}}(x; q) = \mathcal{A}_{\alpha, \beta} x^{\alpha} (1-x)^{\beta}, \quad \mathcal{A}_{\alpha, \beta} = \Gamma(1 + \alpha + \beta) / [\Gamma(\alpha) \Gamma(1 + \beta)], \quad (3.42)$$

whereupon the moments of  $u_v^{\text{mom}}(x; q)$  are given by

$$\langle x^n \rangle = \prod_{i=1}^n \frac{i + \alpha - 1}{i + \alpha + \beta}. \quad (3.43)$$

The Drell-Yan data<sup>77</sup> are described by Eq. (3.42) with  $q = 2 \text{ GeV}$  values

$$\alpha^{\text{DY}} = 0.57 \pm 0.03, \quad \beta^{\text{DY}} = 1.27 \pm 0.04, \quad (3.44)$$

while a global fit to Drell-Yan and prompt photon data yields the consistent result<sup>90</sup>

$$\alpha^{\text{fit}} = 0.64 \pm 0.03, \quad \beta^{\text{fit}} = 1.15 \pm 0.02. \quad (3.45)$$

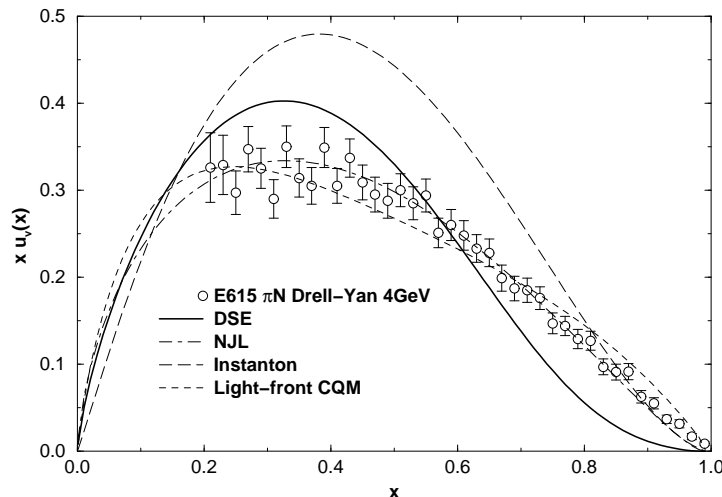


Fig. 3.7. Fuller comparison of theory with experiment. Solid line: DSE result;<sup>76</sup> dot-dashed line: NJL model;<sup>93</sup> long-dashed line: instanton model;<sup>94</sup> short-dashed line: light-front constituent quark model.<sup>95</sup> All calculations have been evolved to  $q = 4.0$  GeV using a 4-flavour value of  $\Lambda_{\text{QCD}} = 0.204$  GeV. The Drell-Yan data are from Ref. [77]. (Adapted from Ref. [96].)

The calculation of Ref. [76] is described by the values

$q$ (GeV)	0.57	2.0	4.05
$\alpha$	1.34	0.92	0.84
$\beta$	1.31	1.80	1.98

(3.46)

A material feature of this DSE result is the value of  $\beta \simeq 2$  because although perturbative QCD cannot be used to obtain the pointwise dependence of the distribution function it does predict<sup>92</sup> the power-law dependence at  $x \simeq 1$ :

$$\text{pQCD: } u_v^\pi(x) \stackrel{x \sim 1}{\propto} (1-x)^2, \quad (3.47)$$

in agreement with the DSE result (corrections are logarithmic). However, as is apparent in Fig. 3.6 and emphasised by Eqs. (3.44), (3.45), this prediction *disagrees* with extant experimental data.<sup>j</sup> That is very disturbing because a verification of the experimental result would present a profound threat to QCD, even challenging the assumed vector-exchange nature of the force underlying the strong interaction.

In Fig. 3.7 we illustrate that the only extant calculation which agrees with the distribution inferred from  $\pi N$  Drell-Yan data is that performed with a particular regularisation of the Nambu–Jona-Lasinio model.<sup>93</sup> That calculation yields a distribution

$$u_v^{\text{pt}}(x; q_0^{\text{NJL}} = 0.35 \text{ GeV}) = \theta(x)\theta(1-x) \quad (3.48)$$

<sup>j</sup>This is in spite of the fact that the first four moments agree: Eq. (3.41). Plainly, the low moments contain little information about the distribution on the valence-quark domain. Lattice-simulations are currently limited to the low moments.

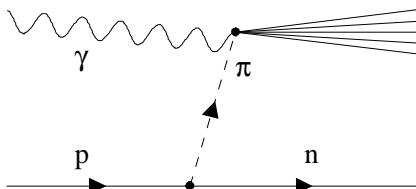


Fig. 3.8. Deep inelastic scattering from the proton's  $\pi$ -cloud (Sullivan process) could provide a means of measuring  $u_v^\pi(x)$  at JLab. (Adapted from Ref. [96].)

which corresponds to the valence-quark carrying each and every fraction of the pion's momentum with equal probability. The result is an artefact tied to this model's representation of the pion bound state by a momentum-*independent* Bethe-Salpeter amplitude;<sup>76,97</sup> i.e., representing the pion as a point-particle, which is a necessary consequence of the model's momentum-independent interaction. It is clearly the hardest distribution that is physically possible.

This observation underscores the serious nature of the discrepancy described above in connection with Eq. (3.47), and in highlighting that disagreement the DSE study<sup>76</sup> has catalysed interest in  $u_v^\pi(x)$  and proposals for its remeasurement. One proposal that could use existing facilities would employ the process depicted in Fig. 3.8 at JLab.<sup>96</sup> This process could also be used efficaciously at a future electron-proton collider to accurately probe  $u_v^\pi(x)$  on the valence-quark domain.<sup>98</sup>

### 3.3.4. Summary

This application illustrates the power of using algebraic parametrisations of key DSE elements: one can proceed rapidly to an insightful analysis of hadronic phenomena and arrive at robust conclusions. Now, however, this type of analysis is supported, improved and in some cases superseded by a direct application of the one-parameter rainbow-ladder model specified by Eq. (3.1).

## 4. *Ab Initio* Calculation of Meson Properties

In this section we review the systematic application of the renormalisation-group-improved rainbow-ladder kernel defined by Eq. (3.1) to a wide range of meson observables. We emphasise at the outset that each result is a prediction, in the sense that the model's mass-scale is fixed, Eq. (3.3), and every element in each calculation is completely determined by, and calculated from, that kernel.

### 4.1. Elastic electromagnetic form factors

We first consider processes that involve only three external particles, at least one of which is a hadron. The simplest of these are the pion and kaon electromagnetic form factors. The matrix element describing the coupling of a photon with momentum  $q$  to a pseudoscalar meson composed of quark  $a$  with electric charge  $e_a$  and antiquark

$\bar{b}$ , electric charge  $e_{\bar{b}}$ , can be written as the sum of two terms

$$\Lambda_{\nu}^{a\bar{b}}(P, q) = e_a \Lambda_{\nu}^{a\bar{b}a}(P, q) + e_{\bar{b}} \Lambda_{\nu}^{a\bar{b}\bar{b}}(P, q), \quad (4.1)$$

which, respectively, describe the coupling of the photon to the quark and the anti-quark. In the Breit frame, where the incoming meson has total momentum  $P - q/2$ ,

$$\Lambda_{\nu}^{a\bar{b}}(P, q) = 2 P_{\nu} F(q^2), \quad (4.2)$$

where  $F(q^2)$  is the meson's elastic electromagnetic form factor. ( $r^2 = -6F'(0)$  is the square of the meson's charge radius.) Each term on the r.h.s. of Eq. (4.1) has this property and hence one can also write

$$\Lambda_{\nu}^{a\bar{b}}(P, q) = 2 P_{\nu} \left[ e_a F^a(q^2) + e_{\bar{b}} F^{\bar{b}}(q^2) \right], \quad (4.3)$$

and thereby explicate the contribution of each quark to the total elastic form factor.

The matrix element describing the scattering process is most easily calculated using the renormalised impulse approximation,<sup>66</sup> in which, e.g.,

$$\Lambda_{\nu}^{a\bar{b}}(P, q) = N_c \text{tr}_D \int_k^{\Lambda} S^a(\ell) \Gamma^{a\bar{b}}(r_+; P_-) S^b(\ell_+) i \Gamma_{\nu}^b(\ell_+, \ell_-) S^b(\ell_-) \Gamma^{b\bar{a}}(r_-; -P_+), \quad (4.4)$$

where:  $\ell = k + P/2$ ,  $\ell_{\pm} = k - P/2 \pm q/2$ ,  $r_{\pm} = k \pm q/4$ ,  $P_{\pm} = P \pm q/2$ ; and, similar to what we saw with Eq. (3.15),  $S^{a,b}$  is a dressed-quark propagator,  $\Gamma^{a\bar{b}}$  is the meson's Bethe-Salpeter amplitude, and  $\Gamma_{\mu}^{a,b}$  is a dressed-quark-photon vertex.

In this section the dressed-quark propagators are obtained by solving the mass-dependent rainbow gap equations, Eq. (2.13), and the Bethe-Salpeter amplitudes come from Eqs. (2.12), (2.37). Furthermore, the dressed-quark-photon vertex is calculated by solving a renormalised inhomogeneous BSE, viz.

$$\Gamma_{\mu}^a(k_+, k_-) = Z_2 \gamma_{\mu} + \int_{\ell}^{\Lambda} K(k, \ell; q) S^a(\ell_+) \Gamma_{\mu}^a(\ell_+, \ell_-) S^a(\ell_-), \quad (4.5)$$

wherein  $k_{\pm} = k \pm q/2$ ,  $\ell_{\pm} = \ell \pm q/2$ , with the kernel again given by Eq. (2.12). At this point it is important to remember that because the rainbow-ladder truncation is the first term in a systematic DSE truncation scheme [Sec. 2.2] the vertex thus obtained satisfies the Ward-Takahashi identity

$$i q_{\mu} \Gamma_{\mu}^a(k_+, k_-) = S_a^{-1}(k_+) - S_a^{-1}(k_-). \quad (4.6)$$

(NB. This is only true if a Poincaré covariant regularisation scheme is employed.)

#### 4.1.1. *Current conservation*

It is electromagnetic current conservation that reduces to one the number of form factors on the r.h.s. of Eq. (4.2) and it also requires  $F^a(0) = 1 = F^{\bar{b}}(0)$ . As with the realisation of Goldstone's theorem, these consequences of symmetry are exhibited

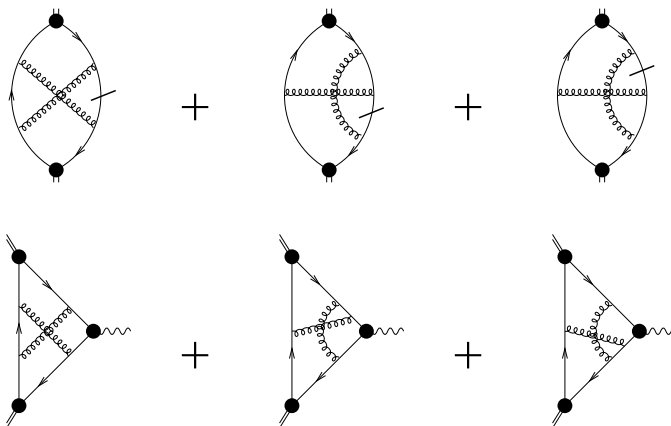


Fig. 4.1. Top row: The three additional contributions to the normalisation of the Bethe-Salpeter amplitude, Eq. (3.34), generated when the second term in Eq. (2.14) is included in the gap equation's kernel. (Without loss of generality, for this illustration the integration variable is chosen such that the total momentum,  $P$ , flows only through the antiquark line, upon which the slash represents  $\partial S/\partial P_\mu$ .) Bottom row: The corrections to the impulse approximation, Eq. (4.4), necessary to maintain current conservation. (Adapted from Ref. [37].)

by the electromagnetic matrix elements if, and only if, there is an intimate relation between each of the elements in the calculation. The impulse approximation, calculated with propagators and vertices obtained using the rainbow-ladder truncation, preserves these constraints without fine-tuning;<sup>66</sup> i.e., independent of the detailed form of the interaction, Eq. (3.1).

Suppose now that one adds the second term of Eq. (2.14) to the kernel of the gap equation. Following the systematic procedure reviewed in Sec. 2.2, that term generates three additional contributions to the kernel of the BSE and also introduces a dependence on the bound state's total momentum. That in turn gives rise to a modification of the canonical normalisation condition for the Bethe-Salpeter amplitude; viz.,<sup>28</sup> the integrals represented by the three diagrams in the top row of Fig. 4.1 must be added to the r.h.s. of Eq. (3.34). The dressed-quark-photon vertex calculated from Eq. (4.5) with the modified kernel automatically satisfies the Ward-Takahashi identity, Eq. (4.6), and current conservation is guaranteed without fine-tuning provided one augments the impulse approximation by the three diagrams depicted in the bottom row of Fig. 4.1.<sup>37</sup> That these diagrams are necessary and sufficient is obvious once one realises that, according to the differential Ward identity:  $i\Gamma_\mu(k, k) = \partial S(k)/\partial k_\mu$ , the derivative of a quark line is equivalent to the insertion of a zero momentum photon. The generalisation of this procedure is straightforward and it is therefore apparent that for any given gap equation kernel it is systematically possible to construct the current-conserving matrix element that describes the coupling of the photon to a composite meson.

4.1.2. *Pion and kaon electromagnetic form factors*

To be concrete we review a calculation of the  $\pi$  and  $K$  form factors:<sup>37</sup>

$$F_\pi(q^2) = \frac{2}{3}F_\pi^u(q^2) + \frac{1}{3}F_\pi^{\bar{d}}(q^2), \quad (4.7)$$

$$F_{K^+}(q^2) = \frac{2}{3}F_{K^+}^u(q^2) + \frac{1}{3}F_{K^+}^{\bar{s}}(q^2), \quad (4.8)$$

$$F_{K^0}(Q^2) = -\frac{1}{3}F_{K^0}^d(Q^2) + \frac{1}{3}F_{K^0}^{\bar{s}}(Q^2). \quad (4.9)$$

So far as the strong interaction is concerned  $u$  and  $d$  quarks are identical in the isospin symmetric limit and hence there are only three independent form factors,  $F_\pi^u(q^2) = F_\pi^{\bar{d}}(q^2)$ ,  $F_{K^+}^u(q^2) = F_{K^0}^d(q^2)$ , and  $F_{K^+}^{\bar{s}}(q^2) = F_{K^0}^{\bar{s}}(q^2)$ , which in impulse approximation are given by Eqs. (4.3), (4.4).

These form factors were calculated in Ref. [37] as an *ab initio* and parameter-free application of the model defined by Eqs. (3.1), (3.3). Therein the dressed-quark propagators were calculated and used in constructing the kernel of the BSE; the BSE was solved to determine the mesons' bound state amplitudes *completely*, i.e., all the amplitudes in Eq. (2.38) were calculated and shown to play an important role; and then the elements were combined to yield a manifestly Poincaré covariant prediction of meson electromagnetic form factors.

The result for the pion form factor is depicted in Fig. 4.2,<sup>k</sup> wherein it is compared with the most recent experimental data.<sup>100</sup> The pion's calculated charge radius is compared with experiment in Table 4.1. The excellent agreement is misleading because  $\pi$ - $\pi$  final-state interactions add  $\lesssim 15\%$  to the impulse approximation result for  $r_\pi$ .<sup>101</sup> (NB. This rescattering contribution to the form factor vanishes with increasing  $q^2$ .) However, that only makes the result more plausible by leading to a disagreement with experiment commensurate with that one would anticipate based on the discussion in Sec. 2.2.

It is evident in Table 4.1 that the calculated charged kaon form factor, Eq. (4.8), agrees with available data,<sup>103</sup> which unfortunately is not a stringent test of theory because it covers only a small low- $q^2$  domain and has large errors. The  $q^2$ -dependence of the form factor again deviates from a simple monopole on  $q^2 \gtrsim 2 \text{ GeV}^2$ .

The neutral kaon form factor, Eq. (4.9), as the difference between two terms, reacts most to a model's details. Of course,  $F_{K^0}(q^2 = 0) = 0$  as a direct result of current conservation and Ref. [37] is guaranteed to reproduce that. However, the evolution away from  $q^2 = 0$  is sensitive to differences between the dressed  $d$ - and  $s$ -quark mass functions. (This is obvious because if they were the same then  $F_{K^0} \equiv 0$ , just as  $F_{\pi^0} \equiv 0$ .) The calculation yields  $r_{K^0}^2 < 0$ , Table 4.1, which is readily understood: the heavier and positively charged  $\bar{s}$ -quark in the  $K^0$  is more

<sup>k</sup>The nature and meaning of vector dominance is discussed in Sec. 2.3.1 of Ref. [66], Sec. 2.3 of Ref. [81] and Sec. 4.3 below: the low- $q^2$  behaviour of the pion form factor is necessarily dominated by the lowest mass resonance in the  $J^{PC} = 1^{--}$  channel. Any realistic calculation will predict that and also a deviation from dominance by the  $\rho$ -meson pole alone as spacelike- $q^2$  increases.

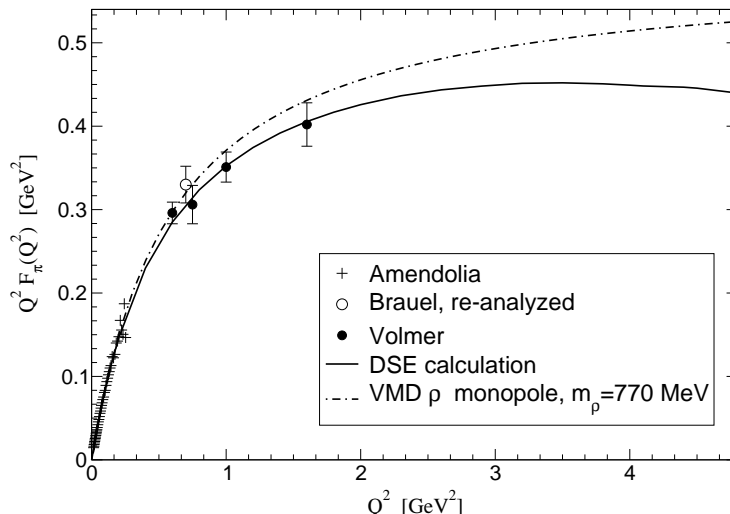


Fig. 4.2. Impulse approximation DSE prediction for  $q^2 F_\pi(q^2)$  obtained in an *ab initio*, parameter-free application of the renormalisation-group-improved rainbow-ladder truncation, Eqs. (3.1), (3.3). The data are from Refs. [87,99,100] (Adapted from Ref. [102].)

often to be found at the meson's core so that the lighter  $d$ -quark provides an excess of negative charge at the surface. The result is therefore qualitatively reliable. However, as the squared-charge radius is small,<sup>104</sup>  $K^0$ - $\bar{K}^0$  final state interactions, neglected in Ref. [37], can have more of an impact on this observable. These effects disappear with increasing  $q^2$  but data are difficult to obtain for  $q^2 \neq 0$ .

It is a model independent prediction<sup>84</sup> of the DSE framework reviewed herein that the elastic electromagnetic meson form factors display

$$q^2 F(q^2) = \text{constant}, \quad q^2 \gg \Lambda_{\text{QCD}}^2, \quad (4.10)$$

with calculable  $\ln^d q^2 / \Lambda_{\text{QCD}}^2$  corrections, where  $d$  is an anomalous dimension.<sup>l</sup> This agrees with earlier perturbative QCD analyses.<sup>107,108</sup> However, to obtain this result in covariant gauges it is crucial to retain the pseudovector components of the Bethe-Salpeter amplitude in Eq. (2.38):  $F_\pi$ ,  $G_\pi$ . (NB. The quark-level Goldberger-Treiman relations, Eqs. (2.43), (2.45), prove them to be nonzero.) Without these amplitudes,<sup>66</sup>  $q^2 F(q^2) \propto 1/q^2$ . Similar statements are true of the role played by nonleading components in the Bethe-Salpeter amplitudes of vector mesons. The calculation of Ref. [84], which uses the propagator and vertex parametrisations described in Sec. 3.3, suggests that the perturbative behaviour of Eq. (4.10) is unambiguously evident for  $q^2 \gtrsim 15 \text{ GeV}^2$ . Owing to challenges in the numerical analysis, the *ab initio* calculations of Ref. [37] cannot yet make a prediction for the onset of the perturbative domain but progress in remedying that is being made.<sup>109</sup>

<sup>l</sup> Corrections to the rainbow-ladder-impulse approximation, such as those depicted in Fig. 4.2, contribute to the anomalous dimension but do not modify the power law dependence.

Table 4.1. Comparison of calculated<sup>27,37</sup> squared-charge-radii (in fm<sup>2</sup>) with data.<sup>87,103,104</sup> The  $\gamma^*\pi^0\gamma$  interaction radius is also included.<sup>105,106</sup> (Adapted from Ref. [37].)

	$r_\pi^2$	$r_{K^+}^2$	$r_{K^0}^2$	$r_{\pi\gamma\gamma}^2$
Calc.	0.45	0.38	-0.086	0.41
Expt.	$0.44 \pm 0.01$	$0.34 \pm 0.05$	$-0.054 \pm 0.026$	$0.42 \pm 0.04$
Rel.-Error	0.023	0.118	0.59	0.024

#### 4.2. $K_{l3}$ decays

Related to the elastic form factors are the semileptonic transition form factors describing  $K^+ \rightarrow \pi^0 \ell \nu_\ell$  [ $K_{\ell 3}^+$ ],  $K^0 \rightarrow \pi^- \ell \nu_\ell$  [ $K_{\ell 3}^0$ ] and  $\pi^+ \rightarrow \pi^0 e \nu_e$  [ $\pi_{e3}$ ]. They proceed via the flavour-changing vector piece of the  $V - A$  electroweak interaction, in particular  $j_\mu^{su}$  and  $j_\mu^{du}$ . The axial-vector component does not contribute because the two mesons involved have the same parity. Neither  $j_\mu^{su}$  nor  $j_\mu^{du}$  is conserved and the symmetry breaking term measures the dressed-quark mass difference [see Eq. (4.13)]. These processes can therefore be employed to probe flavour symmetry violation,<sup>70,115</sup> and this more effectively than the neutral kaon form factor.

The matrix element for the  $K_{\ell 3}^0$  transition is characterised by two form factors:

$$\Lambda_\mu^{dsu}(p_K, q, -p_\pi) = \langle \pi^-(p_\pi) | \bar{s} \gamma_\mu u | K^0(p_K) \rangle = 2 P_\mu f_+^{K^0}(q^2) + q_\mu f_-^{K^0}(q^2), \quad (4.11)$$

where  $p_\pi = P - q/2$ ,  $p_K = (P + q/2)$  and  $q$  is the  $W$ -boson's momentum, with  $t = -q^2$ . In the isospin symmetric case considered in Refs. [70,110],  $m_u = m_d$  and  $j_\mu^{du}$  is conserved so that  $f_+^\pi(t) = -F_\pi(t)$ ,  $f_-^\pi \equiv 0$ . In addition,  $f_\pm^{K^0} \equiv f_\pm^{K^+}$  and hence all new information is contained in the two form factors of Eq. (4.11). Their calculation in impulse approximation involves only one element not already used in Sec. 4.1.2, namely, the dressed- $suW$ -vertex, which replaces the dressed-quark-photon vertex. That piece which contributes to  $K_{\ell 3}$  decays is obtained from

$$\Gamma_\mu^{su}(k_+, k_-) = Z_2 \gamma_\mu + \int_\ell^\Lambda K(k, \ell; q) S_s(\ell_+) \Gamma_\mu^{su}(\ell_+, \ell_-) S_u(\ell_-), \quad (4.12)$$

where again, for a consistent truncation, the renormalisation-group-improved ladder kernel must be used. The vertex thus calculated satisfies

$$iq_\mu \Gamma_\mu^{su}(k_+, k_-) = S_s^{-1}(k_+) - S_u^{-1}(k_-) - (m_s - m_u) \Gamma_1^{su}(k_+, k_-), \quad (4.13)$$

where  $\Gamma_1^{su}$  is a flavour-dependent scalar vertex analogous to the pseudoscalar vertex in Eq. (2.48). The parameter-free prediction<sup>110</sup> for  $f_+^K$  is depicted in Fig. 4.3.

On the physical domain for  $K_{\ell 3}$  decays:  $m_\ell^2 < t < (m_K - m_\pi)^2 = 0.13 \text{ GeV}^2$ , the calculated form factors<sup>110</sup> are well approximated by a straight line:

$$f(t) = f(0) \left[ 1 + \frac{\lambda}{m_\pi^2} t \right], \quad \lambda := -m_\pi^2 f'(m_\ell^2) / f(0), \quad (4.14)$$

supporting an assumption common in the analysis of experimental data.<sup>53</sup>

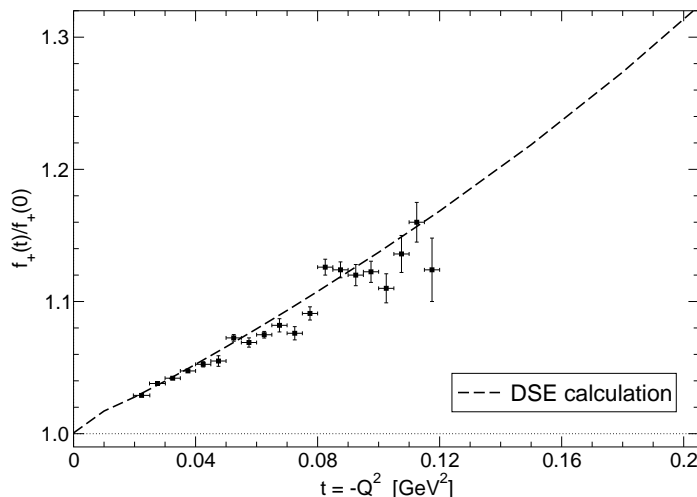


Fig. 4.3. DSE results for the  $K_{l3}$  form factor  $f_+(t = -q^2)$ . Experimental data from CPLEAR.<sup>111</sup> (Adapted from Ref. [110].)

The last term in Eq. (4.13) indicates the manner in which  $K_{\ell 3}$  decays are sensitive to the current-quark-mass difference and its enhancement through nonperturbative effects.<sup>70</sup> Experimentally this is best explored via the scalar form factor

$$f_0(q^2) = f_+(q^2) - \frac{q^2}{m_K^2 - m_\pi^2} f_-(q^2), \quad (4.15)$$

which measures the divergence  $q_\mu \Lambda_\mu^{dsu}(p_K, q, -p_\pi)$ . Current algebra predicts the value of  $f_0^K$  at the Callan-Treiman point,<sup>112</sup>  $t = m_K^2 - m_\pi^2 =: \Delta$ ,  $f_0^K(\Delta) = -f_K/f_\pi = -1.23$ , while a systematic analysis of corrections yields:<sup>113</sup>  $f_0^K(\Delta) = -1.18$ . The Callan-Treiman point is not experimentally accessible but the robust nature of its derivation makes the value of  $f_0(\Delta)$  a tight constraint on any theoretical framework.

In Table 4.2 we display a representative sample of the results calculated in Ref. [110]. We note that  $|f_+(0)| \approx 1$  and that is consistent with the Ademollo-Gatto theorem,<sup>114</sup> which states that flavour symmetry breaking effects are suppressed at  $t = 0$ . Furthermore, it was observed in Ref. [115] and confirmed in Ref. [70], that  $f_-(0)$  is a measure of the  $s:u$  constituent-quark mass ratio. Applying this notion to Ref. [110], in which the calculated value of that ratio is  $\sim 1.25$ , one estimates  $f_-(0) \approx -0.15$ , from Fig. 1 of Ref. [115]. The calculated value is actually  $f_-(0) = -0.10$ . These observations again emphasise the power of a systematic symmetry preserving DSE truncation.

### 4.3. Form factors in the timelike region

The electromagnetic pion form factor,  $F_\pi(Q^2)$ , exhibits a peak at  $q^2 = -t = -m_\rho^2$

Table 4.2. Calculated<sup>110</sup>  $K_{l3}$  observables, compared with experimental data<sup>53</sup> and chiral perturbation theory.<sup>113</sup> The partial widths are calculated in the usual way. (Adapted from Ref. [110].)

	DSE	Expt.	ChPT
$-f_+(0)$	0.96		0.98
$-f_0(0)$	0.10		0.16
$-f_0(\Delta)$	1.18		1.18
$\lambda_+^{K^0}$	0.027	$0.0300 \pm 0.0020$	0.031
$\lambda_+^{K^+}$	0.027	$0.0282 \pm 0.0027$	0.031
$\lambda_0^{K^0}$	0.018	$0.030 \pm 0.005$	0.017
$\lambda_0^{K^+}$	0.018	$0.013 \pm 0.005$	0.017
$\Gamma(K_{e3}^0) \times 10^{-8} \text{ eV}$	0.49	$0.494 \pm 0.005$	
$\Gamma(K_{\mu 3}^0) \times 10^{-8} \text{ eV}$	0.32	$0.346 \pm 0.004$	
$\Gamma(K_{e3}^+) \times 10^{-8} \text{ eV}$	0.24	$0.259 \pm 0.003$	
$\Gamma(K_{\mu 3}^+) \times 10^{-8} \text{ eV}$	0.16	$0.174 \pm 0.003$	

that is associated with  $e^+e^- \rightarrow \rho \rightarrow \pi^+\pi^-$ . This is a general feature of the electroweak form factors of pseudoscalar mesons, all of which can be expressed as

$$F_P(t) = g_{VPP} \frac{1}{m_V^2 - im_V \Gamma_V - t} \frac{m_V^2}{g_V} \quad (4.16)$$

in the neighbourhood of the relevant flavour channel's lowest-mass vector meson resonance, assuming it is narrow. In Eq. (4.16),  $g_{VPP}$  is the coupling constant modulating the  $V \rightarrow P\bar{P}$  decay,  $\Gamma_V$  is the total width of the vector meson and  $m_V^2/g_V$  characterises the strength of the vector-meson-photon coupling.

This behaviour arises naturally in applications of the rainbow-ladder kernel. In the case of the pion and kaon form factors the poles appear as a straightforward consequence of solving the inhomogeneous BSE, Eq. (4.5); a result we have already illustrated in connection with the axial-vector vertex, Eq. (2.40). In the neighbourhood of the pole the solutions of Eq. (4.5) assume the form<sup>27</sup>

$$\Gamma_\mu^a(p_+, p_-) \approx f_V m_V \frac{1}{m_V^2 - t} \Gamma_\mu^{a\bar{a}}(p; q), \quad (4.17)$$

where  $\Gamma_\mu^{a\bar{a}}$  is the vector meson's Bethe-Salpeter amplitude and  $f_V$  was introduced in Eq. (3.7).<sup>m</sup> The absence of a width in Eq. (4.17) is a defect of the rainbow-ladder truncation, which can be remedied without overcounting by including diagrams in the kernel that represent the vector meson's coupling to the  $P\bar{P}$  intermediate state. Alternatively, if the width:mass ratio is small, that can be done via bound state perturbation theory.<sup>74,116,117,118</sup>

The timelike behaviour of the form factors describing electroweak  $\pi$  and  $K$  transitions is depicted in Fig. 4.4. It is apparent that  $F_\pi$  is singular at  $t = (0.74 \text{ GeV})^2$  and  $F_{K^+}^\pm$  at  $t = (1.05 \text{ GeV})^2$ ; namely, at the masses of the  $\rho$ - and  $\phi$ -mesons (see <sup>m</sup> $f_V$  and  $g_V$  are algebraically related; e.g., for the  $\rho^0$ ,  $f_\rho m_\rho = \sqrt{2} m_\rho^2 / g_\rho$ ; and  $f_\phi m_\phi = 3 m_\phi^2 / g_\phi$ ).

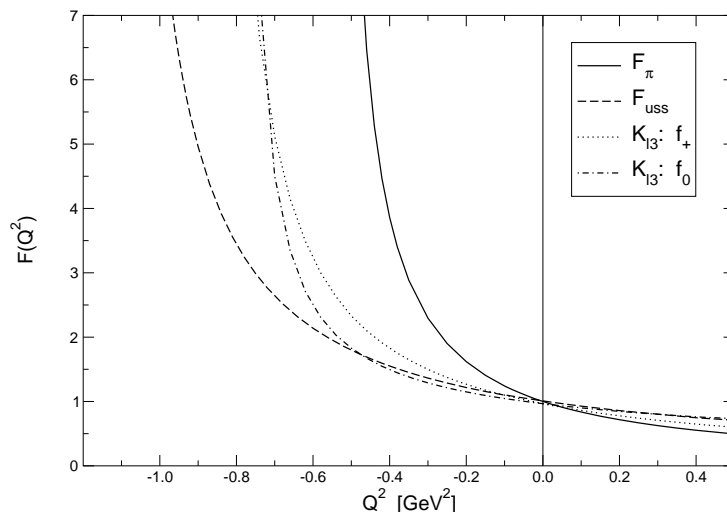


Fig. 4.4. Timelike ( $t = -Q^2$ ) behaviour of the individual form factors describing electroweak  $\pi$  and  $K$  transitions. The vector meson poles are apparent. (Adapted from Ref. [119].)

Table 3.2). Since every other element has already been calculated, the coupling constants  $g_{\rho\pi\pi}$ ,  $g_{\phi KK}$  can be determined by fitting Eq. (4.16) in the neighbourhood of the pole.<sup>119</sup> Alternatively, one can directly calculate the coupling constants using impulse approximation three-hadron triangle diagrams. The results coincide<sup>120</sup> and are listed in Table 4.3. The agreement with experiment at the 9% level is good, given the rainbow-ladder truncation's established accuracy.

Figure 4.4 also reveals poles in the  $K_{\ell 3}$  electroweak transition form factors. The transverse form factor,  $f_+(t)$ , exhibits a pole at  $t = (0.94 \text{ GeV})^2$ ; i.e., at the mass of the  $K^*$  meson (see Table 3.2), as expected, and it is this singularity that facilitates the successful description illustrated in Table 4.2.<sup>70</sup> The scalar form factor,  $f_0(t)$ , possesses a pole at  $t = (0.89 \text{ GeV})^2$ . As the discussion makes clear, this is the model's prediction for the mass of the lightest  $0_{u\bar{s}}^+$  meson. The model also yields a  $0_{u\bar{u}+d\bar{d}}^+$  meson with mass  $0.67 \text{ GeV}$ .<sup>34</sup> However, as observed in Sec. 2.2, the rainbow-ladder truncation is known to be unreliable in the scalar channel and, until a quantitative analysis of the corrections is complete, it is impossible to associate these dressed-quark-antiquark bound states with any mesons in the hadron spectrum or with the scalar states in model studies.<sup>121,122,123</sup>

Table 4.3. Calculated coupling constants for the two-pseudoscalar decays of vector mesons. The rms rel.-error is 9%. (Adapted from Ref. [120].)

Calc.	5.2	4.3	4.3	4.1
Expt.	$5.99 \pm 0.02$	$4.48 \pm 0.04$	$4.58 \pm 0.05$	$4.59 \pm 0.05$
Rel.-Error	0.13	0.04	0.07	0.11

Table 4.4. Calculated<sup>102,105</sup> coupling constants for radiative vector meson decays and associated widths compared with data.<sup>53</sup> The calculations yield the ratios  $g_{VP\gamma}/m_V$ , which are tabulated: the rms rel.-error is 12%. Errors in the calculated values of meson masses propagate into the values of the widths [see Eq. (4.19)] (Adapted from Ref. [102].)

$\frac{g_{VP\gamma}}{m_V}$ (GeV <sup>-1</sup> )	$\rho^\pm \rightarrow \pi^\pm \gamma$	$\omega \rightarrow \pi \gamma$	$K^{*\pm} \rightarrow K^\pm \gamma$	$K^{*0} \rightarrow K^0 \gamma$
Calc.	0.69	2.07	0.99	1.19
Expt.	$0.73 \pm 0.05$	$2.35 \pm 0.07$	$0.84 \pm 0.05$	$1.27 \pm 0.07$
Rel.-Error	0.055	0.119	0.18	0.063

---

$\Gamma_{V \rightarrow P\gamma}$ (keV)	$\rho^\pm \rightarrow \pi^\pm \gamma$	$\omega \rightarrow \pi \gamma$	$K^{*\pm} \rightarrow K^\pm \gamma$	$K^{*0} \rightarrow K^0 \gamma$
Calc.	53	479	90	130
Expt.	$67 \pm 7.5$	$734 \pm 35$	$50.3 \pm 4.6$	$117 \pm 10$

#### 4.4. Vector meson transition form factors

Vector meson transition form factors, such as  $\gamma^* \pi \rightarrow \rho$  and  $\gamma^* \pi \rightarrow \omega$ , are important in the description of hadron photo- and electro-production reactions, and their analysis can help in developing a deeper understanding of the relation between QCD and efficacious meson-exchange models of the  $N$ - $N$  interaction.<sup>124</sup> A large variety of these form factors have been calculated in impulse approximation,<sup>102,105</sup> which for the  $\rho \rightarrow \pi \gamma$  transition is

$$\begin{aligned}
 \Lambda_{\mu\nu}^{\rho\pi\gamma}(P; q) &= \frac{e N_c}{3} \text{tr}_D \int_k^\Lambda S(q_2) \Gamma^\pi(r_{+-}; -P - q) S(q_1) \Gamma_\mu^\rho(r_{+0}; P) S(k) i\Gamma_\nu^\gamma(k, q_2) \\
 &= e \frac{g_{\rho\pi\gamma}}{m_\rho} \epsilon_{\mu\nu\alpha\beta} P_\alpha q_\beta F_{\rho\pi\gamma}(q^2), \tag{4.18}
 \end{aligned}$$

where  $P$  is the  $\rho$ -meson's momentum,  $q$  is that of the photon and  $q_1 = k + P$ ,  $q_2 = k - q$ ,  $r_{\alpha\beta} = k + \alpha P/2 + \beta q/2$ . The coupling  $g_{\rho\pi\gamma}$  is defined such that  $F_{\rho\pi\gamma}(q^2 = 0) = 1$  and then

$$\Gamma_{\rho \rightarrow \pi \gamma} = \frac{\alpha_{\text{em}}}{24} g_{\rho\pi\gamma}^2 m_\rho \left(1 - \frac{m_\pi^2}{m_\rho^2}\right)^3, \tag{4.19}$$

where  $\alpha_{\text{em}}$  is QED's fine structure constant. For  $m_u = m_d$ ,  $\Gamma_{\rho^\pm \rightarrow \pi^\pm \gamma} = \Gamma_{\rho^0 \rightarrow \pi^0 \gamma}$  and  $\Gamma_{\omega \rightarrow \pi \gamma} = 9 \Gamma_{\rho \rightarrow \pi \gamma}$ . The analysis of  $K^* \rightarrow K \gamma$  is also straightforward and in the limit of  $SU(3)$ -flavour symmetry:<sup>102</sup>  $\Gamma_{K^{*\pm} \rightarrow K^\pm \gamma} = \Gamma_{\rho^\pm \rightarrow \pi^\pm \gamma}$  and  $\Gamma_{K^{*0} \rightarrow K^0 \gamma} = 4 \Gamma_{K^{*\pm} \rightarrow K^\pm \gamma}$ , so one anticipates  $\Gamma_{K^{*0} \rightarrow K^0 \gamma} > \Gamma_{K^{*\pm} \rightarrow K^\pm \gamma}$  in reality.

The calculated results<sup>102,105</sup> are summarised in Table 4.4. The agreement is consistent with the established accuracy of the rainbow-ladder truncation. The transition form factors are depicted in Fig. 4.5 and, on the physical domain,  $F_{\rho\pi\gamma}(q^2)$  agrees with extant data<sup>125</sup> to a degree consistent with the absence of a width for the  $\rho$ -meson in rainbow-ladder truncation. An algebraic analysis of the behaviour of the form factors at large spacelike- $q^2$  has not been completed but they do appear to fall faster than  $1/q^2$  (see the  $\omega$ -dominance curve in the figure). This is consistent with analyses in perturbative QCD, which indicate that such processes are suppressed

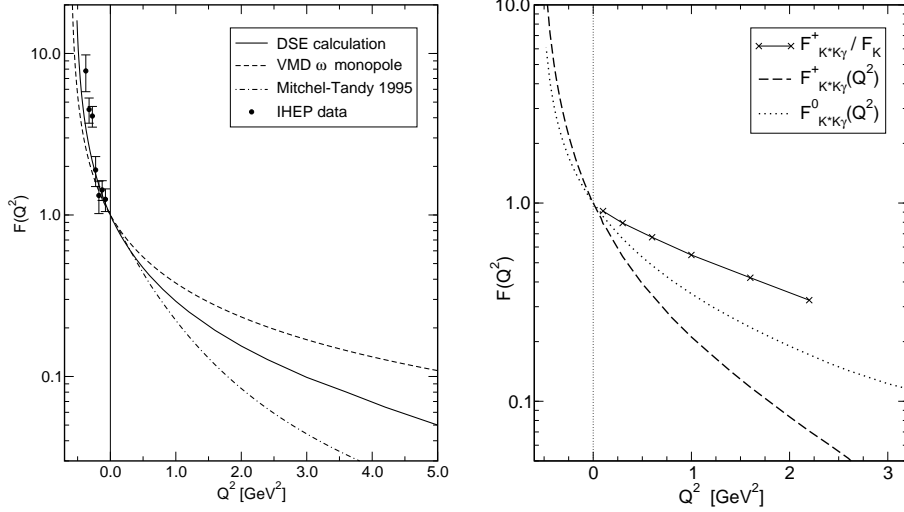


Fig. 4.5. Left panel: DSE result for  $F_{\omega\pi\gamma}(q^2) = F_{\rho\pi\gamma}(q^2)$  compared with experimental data.<sup>125</sup> The dot-dashed line is an earlier, rudimentary DSE calculation<sup>126</sup> proceeding from parametrisations of the propagators and vertices after the fashion described in Sec. 3.3. Right panel: DSE result for  $F_{K^*K\gamma}(q^2)$ , charged (dashed line) and neutral (dotted line). The solid line is the ratio  $F_{K^*+K+\gamma}(q^2)/F_K(q^2)$ . (Adapted from Refs. [105,128].)

because they do not conserve hadron helicity.<sup>127</sup> The charged  $K^*K\gamma$  form factor falls very rapidly because of cancellations between the contributing  $\gamma$ - $u$ - and  $\gamma$ - $s$ -quark diagrams. The analogous contributions for  $K^{*0}$  interfere constructively.

#### 4.5. $\pi^0 \rightarrow \gamma\gamma$

The decay  $\pi^0 \rightarrow \gamma\gamma$  and associated  $\gamma\gamma^* \rightarrow \pi^0$  transition form factor are closely related to the processes discussed in the last subsection and furthermore they have long been recognised to possess a number of unique features that are especially important for testing QCD.<sup>108</sup>

In impulse approximation the transition form factor is obtained from the vertex

$$\begin{aligned}
 \Lambda_{\mu\nu}^{\pi\gamma\gamma}(k_1; k_2) &= \alpha_{\text{em}} \frac{4\pi\sqrt{2}}{3} N_c \text{tr}_D \int_{\ell}^{\Lambda} S(\ell_1) \Gamma^{\pi}(\hat{\ell}; -P) S(\ell_2) i\Gamma_{\mu}(\ell_2, \ell_{12}) S(\ell_{12}) i\Gamma_{\nu}(\ell_{12}, \ell_1) \\
 &= 2i \frac{\alpha_{\text{em}} g_{\pi\gamma\gamma}}{\pi f_{\pi}} \epsilon_{\mu\nu\rho\sigma} k_{1\rho} k_{2\sigma} F_{\pi\gamma\gamma}(k_1; k_2), \tag{4.20}
 \end{aligned}$$

where  $\ell_1 = \ell - k_1$ ,  $\ell_2 = \ell + k_2$ ,  $\hat{\ell} = (\ell_1 + \ell_2)/2$ ,  $\ell_{12} = \ell - k_1 + k_2$ , and the coupling constant  $g_{\pi\gamma\gamma}$  is defined such that  $F_{\pi\gamma\gamma}(k_1 = 0 = k_2) = 1$ . For  $k_1^2 = 0 = k_2^2$ , the vertex describes  $\pi^0$  decay and yields the width

$$\Gamma_{\pi^0\gamma\gamma} = \frac{m_{\pi}^3}{16\pi} \left( \frac{\alpha_{\text{em}}}{\pi f_{\pi}} \right)^2 g_{\pi\gamma\gamma}^2. \tag{4.21}$$

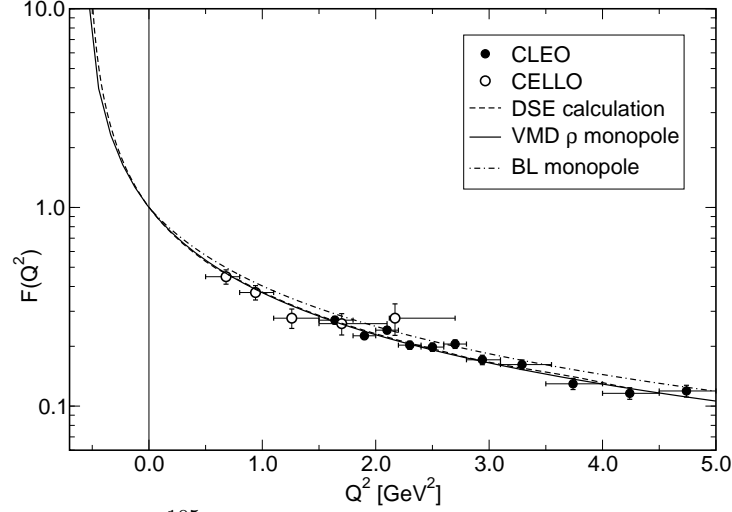


Fig. 4.6. DSE prediction,<sup>105</sup> dashed line, for the  $\gamma^*\pi \rightarrow \gamma$  transition form factor; solid line, a monopole with mass scale  $m_\rho^2 = 0.59 \text{ GeV}^2$ ; and dot-dashed line, monopole based on the asymptotic form:<sup>131</sup>  $1/(1 + Q^2/[8\pi^2 f_\pi^2])$ . The data are from the CELLO<sup>106</sup> and CLEO<sup>130</sup> collaborations (Adapted from Ref.[105].)

It is a textbook example that  $g_{\pi\gamma\gamma} \equiv 0$  and  $\pi^0 \rightarrow \gamma\gamma$  is forbidden in the absence of the Abelian anomaly; i.e., if the axial-vector quark current  $J_{5\mu}^3 = \bar{q}\frac{1}{2}\lambda^3\gamma_5\gamma_\mu q$  is conserved in the chiral limit. However, this current is anomalous, as may be demonstrated in many ways, and one arrives instead at the model-independent chiral limit result:  $g_{\pi\gamma\gamma} = \frac{1}{2}$ , wherewith Eq. (4.21) predicts  $\Gamma_{\pi^0\gamma\gamma} = 7.73 \text{ eV}$  cf. the experimental value:<sup>53</sup>  $7.84 \pm 0.56$ , which corresponds to  $g_{\pi\gamma\gamma}^{\text{expt.}} = 0.504 \pm 0.018$ .

It is a key feature of the DSEs that, with a systematic and nonperturbative truncation scheme, all consequences of the Wess-Zumino term and Abelian anomaly are obtained exactly, without fine tuning. A true representation of DCSB and the preservation of Ward-Takahashi identities is crucial in achieving this.<sup>66,67,84,129</sup> Hence, one obtains algebraically  $g_{\pi\gamma\gamma}(m_\pi = 0) = \frac{1}{2}$  and<sup>105</sup>

$$g_{\pi\gamma\gamma}(m_\pi) = 0.502. \quad (4.22)$$

The  $\gamma^*\pi \rightarrow \gamma$  transition form factor, which was measured by the CELLO<sup>106</sup> and CLEO<sup>130</sup> collaborations, is defined as

$$F_{\gamma^*\pi\gamma}(q^2) = F_{\pi\gamma\gamma}(k_1^2 = q^2, k_2^2 = 0); \quad (4.23)$$

i.e., as the form factor in Eq. (4.20) evaluated with one photon on-shell, and the impulse approximation result is plotted in Fig. 4.6. The calculated interaction radius  $r_{\pi\gamma\gamma}^2 := -6F'_{\gamma^*\pi\gamma}(0) = 0.41 \text{ fm}^2$  agrees with the experimental estimate:<sup>106</sup>  $0.42 \pm 0.04$ . It is evident that the constraints of DCSB are very tight.

The behaviour of the form factor at large spacelike- $q^2$  has been analysed in

perturbative QCD,<sup>n</sup> with the leading order result:<sup>108,131,132</sup>

$$F_{\gamma^*\pi\gamma}^{\text{pQCD}}(q^2) = J(1) \frac{4\pi^2 f_\pi^2}{q^2} + \mathcal{O}\left(\frac{\alpha(q^2)}{q^2}, \frac{1}{q^4}\right), \quad (4.24)$$

$$J(w) = \frac{4}{3} \int_0^1 dx \frac{\phi_\pi(x; \ln q)}{1 - w^2(2x - 1)^2}, \quad (4.25)$$

where  $w = (k_1^2 - k_2^2)/(k_1^2 + k_2^2) = 1$  for  $\gamma^*\pi \rightarrow \gamma$ , and  $\phi_\pi(x; \ln q)$  is the pion's light-cone quark distribution amplitude,  $\int_0^1 dx \phi_\pi(x; \ln q) = 1$ . In this context accurate measurements of the transition form factor can be interpreted as constraining the  $x$ -dependence of  $\phi_\pi(x; \ln q)$  at the experimental scale,  $\ln q$ . At very large  $q^2$ ; viz.,  $\ln[q^2/\Lambda_{\text{QCD}}^2] \gg 1$ ,  $\phi_\pi(x; \infty) = 6x(1-x)$  and consequently  $J(1) = 2$ . Existing data at  $\ln[q/\Lambda_{\text{QCD}}] \sim 2$  favour<sup>130</sup>  $J(1) \approx 1.5$ , a value which requires either  $\phi_\pi(x; \sim 2)$  to be far from asymptotic (e.g.  $\phi_\pi(x; \sim 2) = 630x^4(1-x)^4$  gives  $J(w) = 1.5$ ) or material corrections to the leading order result.<sup>133</sup>

The expression in Eq. (4.20) has also been used to analyse the large spacelike- $q^2$  behaviour of the  $\gamma^*\pi \rightarrow \gamma$  transition form factor, with the result<sup>73,134,135</sup>

$$F_{\gamma^*\pi\gamma}(q^2) = \frac{4}{3} \frac{4\pi^2 f_\pi^2}{q^2}. \quad (4.26)$$

This was obtained by assuming that for  $k_2^2 = 0$  and  $k_1^2 = q^2 \rightarrow \infty$ ,  $2k_1 \cdot k_2 = -q^2$  because  $P = k_1 + k_2$  and the pion is on-shell, and

$$S(\ell_{12}) = \frac{1}{Z_2} \frac{1}{q^2} i\gamma \cdot (k_1 - k_2), \quad \Gamma_\mu(\ell_2, \ell_{12}) = Z_1 \gamma_\mu = \Gamma_\mu(\ell_{12}, \ell_1). \quad (4.27)$$

The effect of Eq. (4.27) is to treat the photons symmetrically in the integrand of Eq. (4.20). In reality that might effect the situation  $k_1^2 = q^2 = k_2^2$ , which corresponds to  $w = 0$ . Since  $J(w = 0) = 4/3$ , this interpretation would reconcile Eqs. (4.24) and (4.26). In essence, this expresses the relevant observation in Ref. [136] and suggests that Eq. (4.20) should be reanalysed with a more conscious focus on the asymmetric  $\gamma^*\pi \rightarrow \gamma$  transition.

The calculations reported in Ref. [105] are not affected by these considerations. They simply provide the prediction of the rainbow-ladder DSE model for  $F_{\gamma^*\pi\gamma}(q^2)$  on the domain covered by extant experiments, which do not extend into the truly asymptotic domain,  $\ln[q^2/\Lambda_{\text{QCD}}^2] \gg 1$ . The result is plotted in Fig. 4.6, and on the scale of the figure is well approximated by a simple  $\rho$ -meson monopole. It agrees with existing data, within errors, and interpreted in terms of Eq. (4.24), corresponds to  $J(w = 1; \ln q/\Lambda_{\text{QCD}} \sim 2) \approx 1.7$ .

#### 4.6. Scattering processes

Consider now the more complex situation of four external lines. We have repeatedly emphasised that the DSEs provide for a resolution of the dichotomy of the pion as

<sup>n</sup>NB. The anomalous dimension is zero; i.e., at leading order, in contrast to the elastic electromagnetic pion form factor,  $F_{\gamma^*\pi\gamma}$  does not depend on the strong running coupling,  $\alpha_s(q^2)$ .

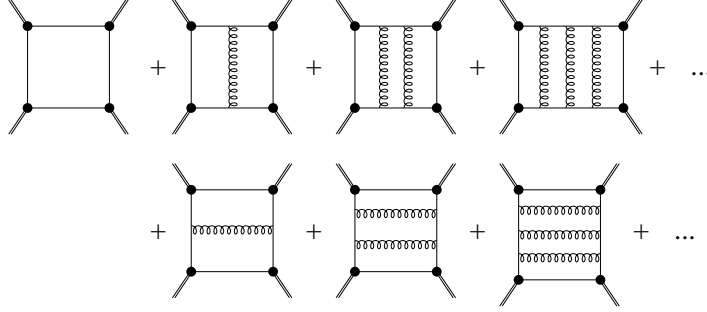


Fig. 4.7. Sum of terms required to describe  $\pi$ - $\pi$  scattering when the rainbow-ladder truncation is used to calculate the dressed-quark propagator and pion Bethe-Salpeter amplitude. In every case, the interaction line is specified by Eq. (3.1). The first diagram on the top line,  $D_\diamond(s, t, u)$ , is expressed in Eq. (4.28); the remaining sum on the top line is denoted by  $D\mathcal{T}_s(s, t, u)$ ; and the sum on the bottom line by  $D\mathcal{T}_t(s, t, u)$ . (Adapted from Ref.[36].)

both a Goldstone mode and a bound state of massive dressed-quarks, and the role played in this by the systematic, nonperturbative truncation scheme reviewed in Sec. 2. As our exemplar we therefore choose  $\pi$ - $\pi$  scattering. It will immediately be appreciated that this process has long been of interest and, indeed, that its particular features and the effective Lagrangian that describe them<sup>137</sup> are a keystone of chiral perturbation theory.

Based on the analyses reviewed in the preceding subsections one would naively suppose that the dominant contribution to  $\pi$ - $\pi$  scattering arises from the first diagram in Fig. 4.7, which represents the renormalised expression

$$D_\diamond(s, t, u) = \text{tr} \int_\ell^\Lambda S(\ell_{--}) \Gamma_\pi(\ell; -p_4) S(\ell_{++}) \\ \times \Gamma_\pi(\ell_{++0}; -p_3) S(\ell_{+++}) \Gamma_\pi(\ell_{+0+}; p_2) S(\ell_{+-}) \Gamma_\pi(\ell_{0-+}; p_1), \quad (4.28)$$

with  $s = -(p_1 + p_2)^2$ ,  $t = -(p_1 - p_3)^2$ ,  $u = -(p_1 - p_4)^2$ ,  $p_1 + p_2 = p_3 + p_4$  and  $\ell_{\alpha\beta\gamma} = \ell + \frac{\alpha}{2}p_1 + \frac{\beta}{2}p_2 + \frac{\gamma}{2}p_3$ . However, it follows immediately from Eqs. (2.38), (2.42), (2.51) that in the chiral limit

$$D_\diamond(0, 0, 0) = \text{tr}_{\text{isospin}}[\tau^i \tau^j \tau^m \tau^n] \frac{4N_c}{f_\pi^4} \int_\ell \frac{B^4(\ell^2)}{[\ell^2 A^2(\ell^2) + B^2(\ell^2)]^2} \quad (4.29)$$

and hence  $D_\diamond(0, 0, 0) \neq 0$  when chiral symmetry is dynamically broken. It is clear now that this contribution alone violates the current algebra results for low-energy  $\pi$ - $\pi$  scattering; viz., at threshold the scattering amplitude must vanish as  $m_\pi^2/f_\pi^2$ .

The observation is not new. In fact, it has long been known that in the chiral limit  $D_\diamond(0, 0, 0)$  is cancelled by contributions that may be described as scalar-isoscalar two-pion correlations. That mechanism is readily realised; e.g., by analysing the auxiliary field effective action in four-fermion interaction theories.<sup>65,129,138</sup> It can also be achieved directly using a systematic truncation of the DSEs, by which manner it is firmly placed in context with the material reviewed herein.

For the latter, if one employs a dressed-quark propagator and Bethe-Salpeter amplitude obtained in the rainbow-ladder truncation, then the combination of diagrams depicted in Fig. 4.7 is guaranteed to reproduce the current-algebra results for near-threshold  $\pi$ - $\pi$  scattering.<sup>36,139</sup> To illustrate, we note that the sum in the figure can be expressed

$$D(s, t, u) = D_\diamond(s, t, u) + D_{\mathcal{T}_s}(s, t, u) + D_{\mathcal{T}_t}(s, t, u) \quad (4.30)$$

and, in the chiral limit, it is readily established<sup>o</sup> that if any one of the external pion momenta vanish then

$$D_{\mathcal{T}_s}(0, 0, 0) = -\frac{1}{2}D_\diamond(0, 0, 0) = D_{\mathcal{T}_t}(0, 0, 0) \quad (4.31)$$

and thus  $D(0, 0, 0) = 0$ . Extending this, one finds at leading order in powers of mass and momenta<sup>139</sup>

$$D(s, t, u) = \frac{1}{8f_\pi^2}(s + t - u), \quad (4.32)$$

from which follows the isospin-zero, -one and -two scattering amplitudes:

$$\begin{aligned} A_0(s, t, u) &= 3D(s, t, u) + 3D(s, u, t) - D(u, t, s) = \frac{2s - m_\pi^2}{2f_\pi^2}, \\ A_1(s, t, u) &= 2D(s, t, u) - 2D(s, u, t) = \frac{t - u}{2f_\pi^2}, \\ A_2(s, t, u) &= 2D(u, t, s) = \frac{2m_\pi^2 - s}{2f_\pi^2}; \end{aligned} \quad (4.33)$$

viz., precisely the current algebra results for low-energy  $\pi$ - $\pi$  scattering, *independent* of the detailed form of the interaction.

In Fig. 4.8 we plot the mass-dependence of the isospin-zero and -two scattering amplitudes at threshold. At the physical value of the light current-quark-mass, 95% of  $D_\diamond(4m_\pi^2, 0, 0)$  is cancelled by the remaining terms in Fig. 4.7. Furthermore, the direct calculation yields  $A_0 = 8.6$ ,  $A_2 = -2.3$  cf. the current-algebra results:  $A_W^0 = 7m_\pi^2/(2f_\pi^2) = 7.8$ ,  $A_W^2 = -m_\pi^2/f_\pi^2 = -2.2$ ; i.e., the complete result exhibits a 10% increase over the leading order value in the isospin-zero channel, which is an harbinger of the resonant behaviour of  $\pi$ - $\pi$  scattering in this channel.

For a detailed comparison with experiment, as with meson charge radii,<sup>101</sup> the DSE calculation should be augmented by the inclusion of pion initial and final state interactions. Omitting them, the results described herein are kindred to those obtained at tree-level in chiral perturbation theory. Bearing this in mind, in Table 4.5 we compare the DSE predictions for  $\pi$ - $\pi$  scattering lengths with fits to data using tree-level<sup>140</sup> and two-loop<sup>141</sup> chiral perturbation theory. The comparison shows that final state interactions only materially affect the scalar-isoscalar scattering length. It is this channel that putatively exhibits a low-mass scalar meson.

<sup>o</sup>To complete the proof one uses the axial-vector Ward-Takahashi identity, Eq. (2.8), the quark-level Goldberger-Treiman relation, Eq. (2.42), and the Bethe-Salpeter equation for the fully-amputated quark-antiquark scattering matrix, Eq. (20) of Ref. [19].

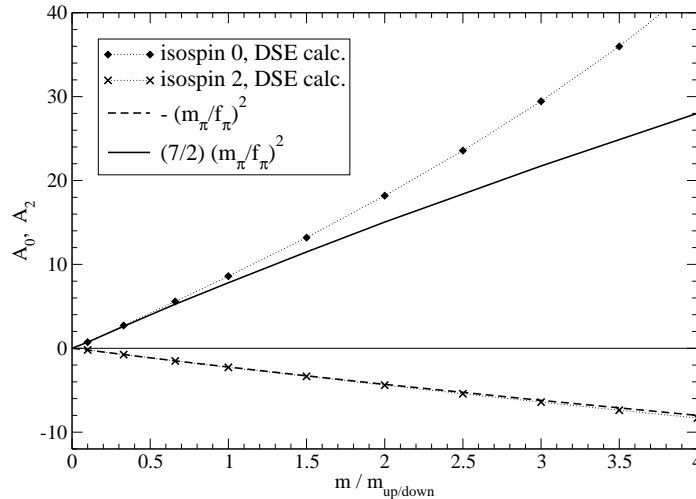


Fig. 4.8. Current-quark-mass-dependence of the isospin-zero and -two scattering amplitudes at threshold:  $A_0(4m_\pi^2, 0, 0)$ ,  $A_2(4m_\pi^2, 0, 0)$ , respectively, calculated by summing the contributions in Fig. 4.7 (Adapted from Ref. [139].)

It is an opportune point to reemphasise a key aspect of the framework, namely, because it works explicitly from a single enunciated kernel, final state interactions of the type we have just described can be incorporated cleanly and without overcounting. For instance, in Sec. 4.3 we saw that the dressed-quark-photon vertex exhibits a real-axis pole when  $s = -q^2$  coincides with a bound state mass and that a width was acquired only after including meson rescattering effects. In precisely the same manner, the sum of terms in Fig. 4.7 produces the resonance poles one expects in  $\pi$ - $\pi$  scattering; e.g., a  $\rho$ -meson pole appears in the isospin-one scattering amplitude.<sup>36</sup> The systematic nature of the truncation means that one can subsequently add loops that represent initial and/or final state interactions between the DSE-described rainbow-ladder pions and be certain that these contributions are truly new and previously unaccounted for, and just those terms needed to provide the strong width of the  $\rho$ -meson.

It is important to note that in a Ward-Takahashi identity preserving implementation of the rainbow-ladder truncation, contributions analogous to the additional diagrams in Fig. 4.7, which we have denoted  $D\mathcal{T}_s(s, t, u)$ ,  $D\mathcal{T}_t(s, t, u)$ , can only appear in the calculation of amplitudes describing processes with *four or more* external

Table 4.5. Rainbow-ladder DSE prediction for  $\pi$ - $\pi$  scattering lengths,<sup>36</sup> compared with those fitted in analyses of data using chiral perturbation theory at tree-level<sup>140</sup> and at second-order.<sup>141</sup>

	$a_0^0$	$a_1^1$	$a_0^2$
DSE calc.	0.17	0.036	-0.045
Tree-level ChPT	0.15	0.036	-0.045
2nd order	0.22	0.038	-0.044

particles. In those involving only two or three external lines, the addition of a single gluon rung connecting any two quarks can be absorbed into the ladder sum that generated the vertex or bound state amplitude which joins the two quark lines; i.e., it adds to what was already present, and is therefore overcounting. Hitherto,  $\pi$ - $\pi$  scattering is the only amplitude with four external lines that has been fully explored and many other processes are worthy of study or reexamination. Of particular interest, perhaps, are the anomalous  $\gamma\pi\pi\pi$  amplitude, wherein the interplay between the vector and axial-vector Ward-Takahashi identities is known to be important,<sup>67</sup> and, indeed, the Wess-Zumino five-pseudoscalar interaction term itself.<sup>129</sup>

#### 4.7. Summary

We reiterate that every DSE result reviewed in this section is a prediction. All follow from the strict implementation of the renormalisation-group-improved rainbow-ladder truncation defined in Eqs. (2.12), (2.13), with the model of the effective coupling specified in Eq. (3.1) whose single parameter takes the value in Eq. (3.3), which was chosen to fit  $f_\pi$ ,  $m_\pi$ ,  $f_K$ ,  $m_K$ . The analyses demonstrate that the DSEs provide a mature approach that links hadron physics experiments with elementary properties of QCD and allows for their direct interpretation as critical data on the nature of quark confinement and the quark/gluon wave functions of hadrons. The success is firm evidence that the quark-quark interaction possesses significant integrated strength on the infrared domain  $k^2 \lesssim 2 \text{ GeV}^2$ , and lattice-QCD simulations and DSE studies of QCD's gauge sector are now searching for its origin.

### 5. On Baryons

Contemporary experimental facilities employ large momentum transfer reactions to probe the structure of hadrons and thereby attempt to elucidate the role played by quarks and gluons in building them. Since the proton is a readily accessible target its properties have been studied most extensively and hence an understanding of a large fraction of the available data requires a Poincaré covariant theoretical description of the nucleon.

The material we have reviewed thus far demonstrates that the properties of light mesons are well described by a Poincaré covariant rainbow-ladder truncation of QCD's DSEs. An extension to baryons begins with a Poincaré covariant Faddeev equation. That, too, requires an assumption about the interaction between quarks. An analysis<sup>142</sup> of the Global Colour Model<sup>62,63,64</sup> suggests that the nucleon can be viewed as a quark-diquark composite. Pursuing that picture yields<sup>143</sup> a Faddeev equation, in which two quarks are always correlated as a colour-antitriplet diquark quasiparticle (because ladder-like gluon exchange is attractive in the  $\bar{3}_c$  quark-quark scattering channel) and binding in the nucleon is effected by the iterated exchange of roles between the dormant and diquark-participant quarks.

A first numerical study of the Faddeev equation for the nucleon was reported in Ref. [144], and there have subsequently been numerous more extensive analyses;

e.g., Refs. [145,146]. In particular, the formulation of Ref. [146] employs confined quarks, and confined pointlike-scalar and -axial-vector diquark correlations, to obtain a spectrum of octet and decuplet baryons in which the rms-deviation between the calculated mass and experiment is only 2%. The model also reproduces nucleon form factors over a large range of momentum transfer,<sup>147</sup> and its descriptive success in that application is typical of such Poincaré covariant treatments.<sup>60,148,149,150</sup>

However, these early successes were achieved without considering the role played by light pseudoscalar mesons. In the context of spectroscopy, studies using the Cloudy Bag Model (CBM)<sup>13</sup> indicate that the dressed-nucleon's mass receives a negative contribution of as much as 300-400 MeV from pion self-energy corrections; i.e.,<sup>151,152</sup>  $\delta M_+ = -300$  to  $-400$  MeV. Furthermore, a perturbative study, using the Faddeev equation, of the mass shift induced by pointlike  $\pi$ -exchange between quark and diquark constituents of the nucleon obtains<sup>153</sup>  $\delta M_+ = -150$  to  $-300$  MeV. Such corrections much diminish the value of the 2% spectroscopic accuracy obtained using only quark and diquark degrees of freedom. The size and qualitative impact of contributions from light-pseudoscalars to baryon masses may therefore provide material constraints on the development of a realistic quark-diquark picture. This has recently been explored in detail<sup>154</sup> and we now review the findings.

### 5.1. Diquarks and a Faddeev equation

The rainbow-ladder DSE truncation yields asymptotic diquark states in the strong interaction spectrum.<sup>32,34</sup> Such states are not observed. Their appearance is an artefact of this lowest-order truncation. Higher order terms in the quark-quark scattering kernel<sup>p</sup> (crossed-box and vertex corrections) act to ensure that QCD's quark-quark scattering matrix does not exhibit singularities that correspond to asymptotic diquark bound states.<sup>22,23</sup> Nevertheless, studies with kernels that don't produce diquark bound states, do support a physical interpretation of the masses obtained using the rainbow-ladder truncation:  $m_{qq}$  plays the role of a confined-quasiparticle mass in the sense that  $l_{qq} = 1/m_{qq}$  may be interpreted as a range over which the diquark can propagate inside a baryon. These observations motivate the following *Ansatz* for the quark-quark scattering matrix:

$$[M_{qq}(k, q; K)]_{rs}^{tu} = \sum_{J^P=0^+,1^+, \dots} \Gamma^{J^P}(q; K) \Delta^{J^P}(K) \bar{\Gamma}^{J^P}(k; -K), \quad (5.1)$$

wherein  $\Delta^{J^P}(K)$  act as diquark propagators and  $\Gamma^{J^P}(q; K)$  are Bethe-Salpeter-like amplitudes describing the relative momentum correlation of the quarks constituting the diquark.

The validity of Eq. (5.1) is key to the derivation of a quark-diquark Faddeev equation for baryons. The simplification is amplified when the summation can be

<sup>p</sup>NB. We saw in Sec. 2.2 that such contributions to the quark-*antiquark* scattering kernel do not materially affect the properties of vector and flavour nonsinglet pseudoscalar mesons, a result which underlies the successes reviewed in Sec. 4.

Table 5.1. Diquark pseudoparticle masses (in GeV) calculated in Ref. [32]. The magnitudes and ordering are characteristic and model independent: see, e.g., Refs. [34,155] and recent lattice-QCD estimates.<sup>156</sup> (Adapted from Ref. [154].)

$\frac{(qq)_J^P}{m_{qq}}$	$(ud)_0^+$	$(us)_0^+$	$(uu)_1^+$	$(us)_1^+$	$(ss)_1^+$	$(uu)_1^-$	$(us)_1^-$	$(ss)_1^-$
	0.74	0.88	0.95	1.05	1.13	1.47	1.53	1.64

truncated after only a few terms. That is indeed possible, as can be argued from Table 5.1, which lists calculated diquark pseudoparticle masses.<sup>32</sup> It is apparent that for octet and decuplet baryons it should be a good approximation to retain only the scalar and axial-vector diquark correlations because they alone have masses less than the bound states they will constitute. (Naturally, spin-3/2 baryons cannot be described unless pseudovector correlations are retained.) Capitalising on this, one arrives at a remarkably simple matrix-integral equation.

For example, one represents the bound state nucleon by a Faddeev amplitude:

$$\Psi = \Psi_1 + \Psi_2 + \Psi_3, \quad (5.2)$$

in which the subscript identifies the dormant quark and, e.g.,  $\Psi_{1,2}$  are obtained from  $\Psi_3$  by a correlated cyclic permutation of all the quark labels. According to the above assumption, the individual sub-amplitudes are written as just a sum of scalar and pseudovector diquark correlations:

$$\Psi_3(p_i, \alpha_i, \tau_i) = \Psi_3^{0+} + \Psi_3^{1+}, \quad (5.3)$$

with  $(p_i, \alpha_i, \tau_i)$  the momentum, spin and isospin labels of the quarks constituting the nucleon, and  $P = p_1 + p_2 + p_3$  the nucleon's total momentum. The scalar diquark component in Eq. (5.3) is

$$\Psi_3^{0+}(p_i, \alpha_i, \tau_i) = [\Gamma^{0+}(\frac{1}{2}p_{[12]}; K)]_{\alpha_1\alpha_2}^{\tau_1\tau_2} \Delta^{0+}(K) [\mathcal{S}(\ell; P)u(P)]_{\alpha_3}^{\tau_3}, \quad (5.4)$$

where: the spinor satisfies  $(i\gamma \cdot P + M)u(P) = 0 = \bar{u}(P)(i\gamma \cdot P + M)$ , with  $M$  the mass obtained in solving the Faddeev equation, and is also a spinor in isospin space, with  $\varphi_+ = \text{col}(1, 0)$  for the proton and  $\varphi_- = \text{col}(0, 1)$  for the neutron; and  $K = p_1 + p_2 =: p_{\{12\}}$ ,  $p_{[12]} = p_1 - p_2$ ,  $\ell := (-p_{\{12\}} + 2p_3)/3$ . The pseudovector component is

$$\Psi_3^{1+}(p_i, \alpha_i, \tau_i) = [\mathbf{t}^i \Gamma_\mu^{1+}(\frac{1}{2}p_{[12]}; K)]_{\alpha_1\alpha_2}^{\tau_1\tau_2} \Delta_{\mu\nu}^{1+}(K) [\mathcal{A}_\nu^i(\ell; P)u(P)]_{\alpha_3}^{\tau_3}, \quad (5.5)$$

where the symmetric isospin-triplet matrices are:  $\mathbf{t}^+ = \frac{1}{\sqrt{2}}(\tau^0 + \tau^3)$ ,  $\mathbf{t}^0 = \tau^1$ ,  $\mathbf{t}^- = \frac{1}{\sqrt{2}}(\tau^0 - \tau^3)$ , with  $(\tau^0)_{ij} = \delta_{ij}$  and  $\tau^{1,3}$  the usual Pauli matrices. The colour antisymmetry of  $\Psi_3$  is implicit in  $\Gamma^{JP}$ .

The Faddeev equation satisfied by  $\Psi_3$  now reduces to a set of coupled equations for the matrix valued functions  $\mathcal{S}$ ,  $\mathcal{A}_\nu^i$  in Eqs. (5.4), (5.5):

$$\begin{bmatrix} \mathcal{S}(k; P) u(P) \\ \mathcal{A}_\mu^i(k; P) u(P) \end{bmatrix} = -4 \int \frac{d^4\ell}{(2\pi)^4} \mathcal{M}(k, \ell; P) \begin{bmatrix} \mathcal{S}(\ell; P) u(P) \\ \mathcal{A}_\nu^j(\ell; P) u(P) \end{bmatrix}, \quad (5.6)$$

wherein the kernel is

$$\mathcal{M}(k, \ell; P) = \begin{bmatrix} \mathcal{M}_{00} & (\mathcal{M}_{01})_{\nu}^j \\ (\mathcal{M}_{10})_{\mu}^i & (\mathcal{M}_{11})_{\mu\nu}^{ij} \end{bmatrix} \quad (5.7)$$

with, e.g.,

$$\mathcal{M}_{00} = \Gamma^{0+}(k_q - \ell_{qq}/2; \ell_{qq}) S^T(\ell_{qq} - k_q) \Gamma^{0+}(\ell_q - k_{qq}/2; -k_{qq}) S(\ell_q) \Delta^{0+}(\ell_{qq}), \quad (5.8)$$

$\ell_q = \ell + P/3$ ,  $k_q = k + P/3$ ,  $\ell_{qq} = -\ell + 2P/3$ ,  $k_{qq} = -k + 2P/3$ , and  $S$  is the propagator of the dormant quark constituent of the nucleon. The other entries are also expressed merely in terms of the Bethe-Salpeter-like amplitudes and propagators.

It is implicit in Eqs. (5.6)-(5.8) that  $u(P)$  is a normalised average of  $\varphi_{\pm}$  so that, e.g., the equation for the proton is obtained by projection on the left with  $\varphi_{+}^{\dagger}$  and  $\mathcal{M}_{01}$  generates an isospin coupling between  $u(P)_{\varphi_{+}}$  on the l.h.s. of Eq. (5.6) and, on the r.h.s.,

$$\sqrt{2} \mathcal{A}_{\nu}^{+} u(P)_{\varphi_{-}} - \mathcal{A}_{\nu}^{0} u(P)_{\varphi_{+}}. \quad (5.9)$$

This is merely the Clebsch-Gordon coupling of isospin- $1 \oplus$  isospin- $\frac{1}{2}$  to total isospin- $\frac{1}{2}$  and means that the scalar diquark amplitude in the proton,  $(ud)_{0+} u$ , is coupled to itself *and* the linear combination:  $\sqrt{2} (uu)_{1+} d - (ud)_{1+} u$ .

The matrix-valued functions  $\mathcal{S}$  and  $\mathcal{A}_{\mu}^i$  are Bethe-Salpeter-like amplitudes that describe the momentum-space correlation between the quark and diquark in the nucleon and can, in general, assume quite complex forms.<sup>146</sup> However, reduced forms can be used to good effect:<sup>154</sup>

$$\mathcal{S}(\ell; P) = f_1(\ell^2, P^2) I_D + \frac{1}{M} \left( i\gamma \cdot \ell - \ell \cdot \hat{P} I_D \right) f_2(\ell^2, P^2), \quad (5.10)$$

$$\mathcal{A}_{\mu}^i(\ell; P) = a_1^i(\ell^2, P^2) \gamma_5 \gamma_{\mu} + a_2^i(\ell^2, P^2) \gamma_5 \gamma \cdot \hat{\ell} \hat{\ell}_{\mu}, \quad (5.11)$$

where  $(I_D)_{rs} = \delta_{rs}$ ,  $\hat{P}^2 = -1$ ,  $\hat{\ell}^2 = 1$ , and, assuming isospin symmetry,  $a_j^1 = a_j^2 = a_j^3$ ,  $j = 1, 2$ . In the nucleon's rest frame,  $f_{1,2}$  in Eq. (5.10) describe the upper, lower component of the bound-state nucleon's spinor. It will readily be appreciated that a sizable value of  $f_2/f_1$  corresponds to a significant amount of the nucleon's spin being stored as quark orbital angular momentum. In this connection the amplitude  $a_2^i$  corresponds to a  $D$ -wave in the nucleon's wave function: in the rest frame, the quark and diquark spins are coupled to total-spin  $\frac{3}{2}$ , which must be combined with angular momentum  $L = 2$  to obtain a  $J = \frac{1}{2}$  nucleon. The physical content is frame invariant because the Faddeev amplitudes are Poincaré covariant.

Equation (5.6) can be solved once the kernel is specified and for that Ref. [154] adopted the expedient, described in Sec. 3.3, of using algebraic parametrisations of the propagators and Bethe-Salpeter amplitudes. The rationale is the same: DSE studies of baryons are not yet mature and hence there is merit in employing sound simplifications. The dressed-quark propagator of Eqs. (3.24)-(3.27) was used, without change. The Bethe-Salpeter-like amplitudes describing the relative-momentum

Table 5.2. Calculated nucleon and  $\Delta$  masses.<sup>154</sup> The results in the first and third rows were obtained using scalar and pseudovector diquark correlations:  $m_{1^+} = 0.90$  GeV in row 1,  $m_{1^+} = 0.94$  GeV in row 3. ( $m_{0^+} = 0.74$  GeV, always.) Pseudovector diquarks were omitted in the second and fourth rows.  $\omega_{f_{1,2}}$  are discussed after Eq. (5.16), and  $R$  in and after Eq. (5.19). All dimensioned quantities are in GeV. (Adapted from Ref. [154].)

	$\omega_{0^+}$	$\omega_{1^+}$	$M_N$	$M_\Delta$	$\omega_{f_1}$	$\omega_{f_2}$	$R$
$0^+ \ \& \ 1^+$	0.64	1.19	0.94	1.23	0.49	0.44	0.25
$0^+$	0.64	-	1.59	-	0.39	0.41	1.28
$0^+ \ \& \ 1^+$	0.45	1.36	1.14	1.33	0.44	0.36	0.54
$0^+$	0.45	-	1.44	-	0.36	0.35	2.32

correlations of quarks within the diquark were represented by

$$\Gamma^{0^+}(k; K) = \frac{1}{\mathcal{N}^{0^+}} H^a C i\gamma_5 i\tau_2 \mathcal{F}(k^2/\omega_{0^+}^2), \quad (5.12)$$

$$\mathfrak{t}^i \Gamma_\mu^{1^+}(k; K) = \frac{1}{\mathcal{N}^{1^+}} H^a i\gamma_\mu C \mathfrak{t}^i \mathcal{F}(k^2/\omega_{1^+}^2), \quad (5.13)$$

with  $\mathcal{F}(y)$  given after Eq. (3.26), the colour matrix  $[H^{c_3}]_{c_1 c_2} = \epsilon_{c_1 c_2 c_3}$  and  $\mathcal{N}^{J^P}$ , the canonical normalisation, fixed by an expression very much like Eq. (3.34); and the propagators for the confined diquarks by:

$$\Delta^{0^+}(K) = \frac{1}{m_{0^+}^2} \mathcal{F}(K^2/\omega_{0^+}^2), \quad (5.14)$$

$$\Delta_{\mu\nu}^{1^+}(K) = \left( \delta_{\mu\nu} + \frac{K_\mu K_\nu}{m_{1^+}^2} \right) \frac{1}{m_{1^+}^2} \mathcal{F}(K^2/\omega_{1^+}^2). \quad (5.15)$$

These expressions define a four-parameter model:  $m_{J^P}$  are diquark masses and  $\omega_{J^P}$  are widths characterising the size of the diquark correlation inside baryons.

The nucleon's Faddeev equation is complete with these definitions. An analogous equation for the  $\Delta$  is readily obtained and does not require additional input. The equations can be solved for the nucleon and  $\Delta$  masses, and also yield their Faddeev amplitudes with which one can define an impulse approximation to  $N$  and  $\Delta$  elastic and transition form factors.<sup>148,157</sup> Regarding the four parameters, the scalar diquark mass can be taken from Table 5.1, as may the constraint  $m_{1^+}/m_{0^+} \approx 1.3$ . That leaves the diquark width parameters,  $\omega_{J^P}$ .

One goal of Ref. [154] was to illustrate and emulate the success of Ref. [146] by showing there are intuitively reasonable values of the parameters for which one obtains the nucleon and  $\Delta$  masses:  $M_N = 0.94$  GeV,  $M_\Delta = 1.23$  GeV. The results of that exercise are listed in Table 5.2. It is clear that the observed masses are easily obtained using solely the dressed-quark and -diquark degrees of freedom described above. The first two rows of the table show that the additional quark exchange associated with the presence of pseudovector correlations provides considerable attraction. Here it reduces the nucleon's mass by 41% and, of course, the  $\Delta$  would not be bound in this approach without the  $1^+$  correlation. Furthermore, in agreement with intuition, the nucleon and  $\Delta$  masses increase with increasing  $m_{J^P}$ . The

diquark width parameters are also reasonable. For example, with calculated results

$$l_{0+} := 1/\omega_{0+} = 0.31 \text{ fm} > l_{1+} := 1/\omega_{1+} = 0.17 \text{ fm}, \quad (5.16)$$

these correlations lie within the nucleon (experimentally, the proton's charge radius  $r_p = 0.87 \text{ fm}$ ), a point also emphasised by the scalar diquark's charge radius, calculated as described in Ref. [148]:  $r_{0+}^2 = (0.55 \text{ fm})^2$ . Moreover, defining  $\omega_{f_{1,2}}$  by requiring a least-squares fit of  $\mathcal{F}(\ell^2/\omega_{f_{1,2}})$  to  $f_{1,2}(\ell^2)$ , matched in magnitude at  $\ell^2 \simeq 0$ , one obtains a scale characterising the quark-diquark separation:

$$l_{q(qq)_{f_1}} := 1/\omega_{f_1} = 0.40 \text{ fm} > 0.15 \text{ fm} = \frac{1}{2} l_{0+}. \quad (5.17)$$

These scales reveal a significant spatial separation between the dormant quark and the diquark-participant quarks while permitting both the quark and diquark to remain within the baryon's volume, and thereby provide an intuitively appealing picture of confined constituents. For the pseudovector analogue

$$l_{q(qq)_{a_1}} = 0.36 \text{ fm} > \frac{1}{2} l_{1+}. \quad (5.18)$$

Finally, the ratio

$$R = f_2(\ell^2 = 0)/f_1(\ell^2 = 0) \quad (5.19)$$

is a measure of the importance of the lower component of the positive energy nucleon's spinor. It is not small, a fact that emphasises the need to treat baryons using a Poincaré covariant framework. As a point of comparison, an analogue in the MIT bag model is  $R_{\text{MIT}} := \max_{x \in [0,1]} j_1(2.04x)/j_0(0) = 0.43$ .

## 5.2. Nucleon mass and pion loops

We have illustrated that an internally consistent and accurate description of the nucleon and  $\Delta$  masses is readily obtained using a Poincaré covariant Faddeev equation based on confined diquarks and quarks. However, the  $\pi NN$  and  $\pi N\Delta$  couplings are large so it is important to estimate the shift in the masses owing to  $\pi$ -dressing. That was the primary goal of Ref. [154] but in seeking the estimate a number of additional important results were confirmed or established.

### 5.2.1. One-loop mass shift

As a first step, the shift in the mass of a positive-energy nucleon,  $\delta M_+$ , was evaluated perturbatively; i.e., the effect of just one pion loop on the nucleon's mass was calculated. Assuming a pseudoscalar coupling:  $g\bar{N}i\gamma_5\vec{\tau}\cdot\vec{\pi}N$ ,  $g = M/f_\pi$  with  $M$  the mass of the nucleon in the loop, this can be separated into a sum of three terms:

$$\delta M_+ = \delta_F M_+^+ + \delta_F M_+^- + \delta_H M_+, \quad (5.20)$$

where  $\delta_F M_+^+$  represents the Fock diagram with a positive-energy nucleon in the loop,  $\delta_F M_+^-$  is the  $Z$ -diagram; i.e., the Fock diagram with a negative-energy nucleon

in the loop, and  $\delta_H M_+$  is the tadpole (or Hartree) contribution arising from the contact term:  $[M/(2f_\pi^2)] \bar{N} \vec{\pi} \cdot \vec{\pi} N$ .

The loop integrals in Eq. (5.20) must be defined and that was achieved in Ref. [154] by implementing a Poincaré invariant Pauli-Villars regularisation. It was immediately apparent that this is equivalent to employing a monopole form factor at each  $\pi NN$  vertex:  $g/(1+k^2/\lambda^2)$ , and since the procedure modifies the pion propagator it may be interpreted as expressing compositeness of the pion and regularising its off-shell contribution. A related effect was identified in Refs. [118,158].

Each term in Eq. (5.20) is finite after regularisation and straightforward to evaluate numerically. However, some insight can be gained algebraically by supposing that the mass of the nucleon in the loop is much greater than any other scale present. In that case,<sup>154</sup>

$$\delta_F M_+^+ = -\frac{3}{32\pi} \frac{1}{f_\pi^2} m_\pi^3 - m_\pi^2 f_{(1)}^+(\lambda) - f_{(0)}^+(\lambda), \quad (5.21)$$

$$\delta_F M_+^- = \frac{3}{32\pi^2} \frac{M}{f_\pi^2} m_\pi^2 (\ln[m_\pi^2/\lambda^2] - 1) + m_\pi^2 f_{(1)}^-(\lambda) + f_{(0)}^-(\lambda), \quad (5.22)$$

$$\delta_H M_+ = -\frac{3}{32\pi^2} \frac{M}{f_\pi^2} (m_\pi^2 (\ln[m_\pi^2/\lambda^2] - 1) + \lambda^2), \quad (5.23)$$

where all the regularisation-scheme-dependence resides in  $f_{(0,1)}^\pm(\lambda) > 0$ , which are only functions of the regularisation mass-scale. One sees immediately that, for sufficiently small  $m_\pi > \lambda$ ,  $\delta_F M_+^+ + \delta_F M_+^- > 0$ , and it is only when the Hartree term is included that  $\delta M_+ < 0$ . Furthermore, the leading behaviour of the nucleon's mass shift that is nonanalytic in the current-quark mass,  $m \propto \sqrt{m_\pi}$ , is only given by Eq. (5.21) because DCSB constrains the couplings and ensures a precise cancellation between the  $\ln m_\pi$ -terms in Eqs. (5.22), (5.23). In general, with the pseudoscalar coupling,  $\delta M_+(\lambda) < 0$  and decreases monotonically from zero with increasing  $\lambda$  only because of destructive interference between the tadpole- and  $Z$ -diagrams.<sup>154</sup> At realistic values of  $m_\pi$  the actual value of  $\delta M_+(\lambda)$  is determined by the regularisation-scale-dependent terms, as visible in Fig. 5.1.

There is no tadpole contribution to the nucleon's mass shift if one elects to use an axial-vector  $\pi N$  coupling:<sup>159</sup>  $[1/(2f_\pi)] \bar{N} \gamma_5 \gamma^\mu \vec{\tau} \cdot \partial_\mu \vec{\pi} N$ . In this case  $\delta^A M_+ = \delta^A M_+^+ + \delta^A M_+^-$ ; i.e., there are two contributions, one with a positive-energy nucleon in the loop and the other with a negative-energy nucleon. Some insight is again obtained by considering the large- $M$  limit, wherein<sup>154</sup>

$$\delta^A M_+^+ = -\frac{3}{32\pi} \frac{1}{f_\pi^2} m_\pi^3 + m_\pi^2 f_{(1^A)}^+(\lambda) + f_{(0^A)}^+(\lambda); \quad (5.24)$$

i.e., the same contribution, nonanalytic in the current-quark mass, as in Eq. (5.21), but with different regularisation-dependent terms, and  $\delta^A M_+^- \propto 1/M$  because the pseudovector coupling suppresses the  $Z$ -diagram. The leading nonanalytic contribution to the nucleon's mass is now unambiguous: it is given by the positive-energy nucleon Fock diagram, irrespective of the coupling's character. Implementing the

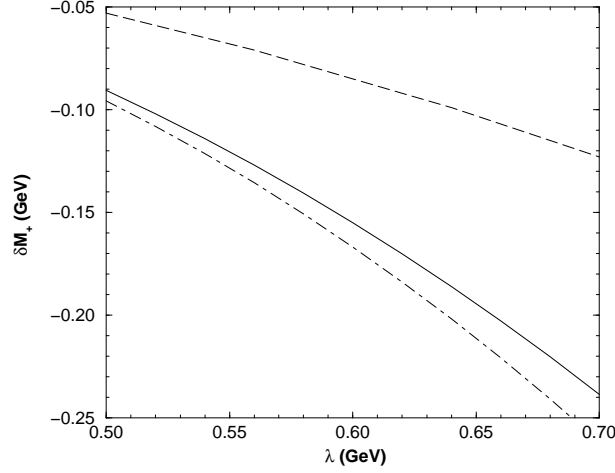


Fig. 5.1. Solid line: Shift in a positive-energy nucleon's mass due to the  $O(g^2)$   $\pi$ -contribution to the self energy. ( $M = 0.94$  GeV,  $m_\pi = 0.14$  GeV.)  $\delta M_+(\lambda = 0.6 \text{ GeV}) = -0.15$  GeV. Dashed line:  $\delta_F M_+$ , Eq. (5.21); dot-dashed line:  $\delta^A M_+$ , Eq. (5.24). (Adapted from Ref. [154].)

Pauli-Villars regularisation, a numerical evaluation of  $\delta^A M_+$  is straightforward with the result depicted in Fig. 5.1. It is evident that  $\delta^A M_+ \neq \delta_F M_+$ , which illustrates the difference between the regularisation-dependent terms in Eqs. (5.21) and (5.24). In addition, although it may not be immediately obvious,

$$\delta^A M_+ \equiv \delta M_+, \quad (5.25)$$

which is why there is only one solid curve in the figure. In this outcome one has a quantitative verification of the on-shell equivalence of the pseudoscalar and pseudovector interactions, in perturbation theory, as long as the interactions are treated in a manner consistent with chiral symmetry.<sup>160</sup>

### 5.2.2. Mass shift, nonperturbatively

The effect of infinitely many pion loops can be calculated using a DSE for the nucleon's self energy:

$$\Sigma(P) = 3 \int \frac{d^4 k}{(2\pi)^4} g_{PV}^2(P, k) \Delta_\pi((P-k)^2) \gamma \cdot (P-k) \gamma_5 G(k) \gamma \cdot (P-k) \gamma_5, \quad (5.26)$$

with  $G^{-1}(k) = i\gamma \cdot k + M + \Sigma(P) = i\gamma \cdot k \mathcal{A}(k^2) + M + \mathcal{B}(k^2)$ , where  $M$  is the nucleon's bare mass, which is obtained, e.g., by solving the Faddeev equation. In Eq. (5.26),  $\Delta_\pi(k^2) = 1/[k^2 + m_\pi^2]$  is the pion propagator, and  $g_{PV}(P, k)$  is a form factor that must describe the composite nature of *both* the pion and the nucleon. The self-consistent solution of Eq. (5.26) yields  $\mathcal{A}(k^2)$  and  $\mathcal{B}(k^2)$ , and therefrom the nonperturbative mass shift.

The  $\pi N$  vertex function can be calculated using a Poincaré covariant model of the nucleon, however, a calculation of the mass shift may again be expedited by

employing an algebraic parametrisation that is constrained by such studies; e.g.,<sup>154</sup>

$$g_{PV}(P, k) = \frac{g}{2M} g_\pi((P - k)^2) g_N(P^2) g_N(k^2), \quad (5.27)$$

$g_\pi(x) = e^{-x/\Lambda^2}$ ,  $g_N(x) = e^{-(x+M^2)/\Lambda_N^2}$ . This model provides for suppression of the coupling when either or both the nucleon and pion are off-shell, and in this it represents the compositeness of both. The exponential form facilitates an algebraic evaluation of many necessary integrals and each term in the product is phenomenologically equivalent to a monopole form factor  $1/[1 + x/\lambda^2]$  if the mass scales are related via  $\Lambda = \sqrt{2}\lambda$ . Another advantage of this algebraic form is that it enables an elucidation of the precise equivalence between the Minkowski and Euclidean space calculations of the mass shift.

A key aspect of a nonperturbative evaluation of  $\delta M_+$  is that the position of the pole in the nucleon's propagator is not known *a priori*: locating it is the goal, and this precludes an algebraic evaluation of the energy-integral that was straightforward in the one-loop calculation. In this case one must proceed by first evaluating the angular integrals in Eq. (5.26), which are independent of  $G(k)$ . That can be illustrated with the kernel of the equation for  $\mathcal{B}$

$$\mathcal{K}_{\mathcal{B}}(P^2, k^2) = \int d\Omega_k g_{PV}^2(P, k) \left[ 1 - \frac{2m_\pi^2}{(P - k)^2 + m_\pi^2} \right], \quad (5.28)$$

with  $d\Omega_k$  the usual angular measure. It is evident that  $\mathcal{K}_{\mathcal{B}}$  can be considered as a sum of two terms. The first is proportional to the angular average of  $g_{PV}^2(P, k)$ , and using Eq. (5.27) that integral can be evaluated exactly:

$$\begin{aligned} \bar{g}_{PV}^2(P^2, k^2) &:= \int d\Omega_k g_{PV}^2((P - k)^2) \\ &= \frac{g^2}{4M^2} e^{-\frac{2(P^2+k^2)}{\Lambda^2}} g_N^2(P^2) g_N^2(k^2) \frac{\Lambda^2}{2Pk} I_1\left(\frac{4Pk}{\Lambda^2}\right), \end{aligned} \quad (5.29)$$

where  $I_1(x)$  is a modified Bessel function and  $P = \sqrt{P^2}$ ,  $k = \sqrt{k^2}$ . The second term is proportional to

$$\omega_{g^2}(P^2, k^2) := \int d\Omega_k \frac{g_{PV}^2(P, k)}{(P - k)^2 + m_\pi^2}, \quad (5.30)$$

which, in general, cannot be expressed as a finite sum of known functions. However, if  $g_{PV}$  is regular at  $P = k$  and its analytic structure is not a key influence on the solution, then the approximation

$$\begin{aligned} \omega_{g^2}(P^2, k^2) &\approx \frac{g^2}{2M^2} g_\pi^2(|P^2 - k^2|) g_N^2(P^2) g_N^2(k^2) \int d\Omega_k \frac{1}{(P - k)^2 + m_\pi^2} \\ &= \frac{g^2}{2M^2} g_\pi^2(|P^2 - k^2|) g_N^2(P^2) g_N^2(k^2) \frac{1}{a + \sqrt{a^2 - b^2}} \end{aligned} \quad (5.31)$$

$$=: \tilde{g}_{PV}^2(P^2, k^2) \frac{1}{a + \sqrt{a^2 - b^2}}, \quad (5.32)$$

where  $a = P^2 + k^2 + m_\pi^2$ ,  $b = 2Pk$ , is a reliable tool.<sup>161</sup> These preconditions are obviously satisfied in this application because the dominant physical effect in  $\pi N$  physics is the pion pole and that appears at a mass-scale much lower than those present in  $g_{PV}$ . Qualitatively identical considerations apply to  $\mathcal{K}_A$ .

The nucleon's mass appears at  $P^2 < 0$  and hence to complete the specification of Eq. (5.26) one must define the continuation of the kernels into the timelike region. The kernels' primary nonanalyticity is a square-root branch point associated with the simple pole in the pion propagator, and in continuing to  $P^2 < 0$  it is necessary to include the discontinuity across the associated cut. That must not be forgotten and is readily accomplished<sup>162</sup> so that the nucleon's DSE is expressed by two coupled integral equations, which we illustrate with that for  $\mathcal{B}$

$$\begin{aligned} \mathcal{B}(x) = & -\frac{3}{16\pi^2} \int_{x_b}^0 dy y \tilde{g}^2(x, y) \Delta \tilde{\mathcal{K}}_{\mathcal{B}}(x, y) \frac{\mathcal{B}(y)}{y\mathcal{A}^2(y) + \mathcal{B}^2(y)} \\ & -\frac{3}{16\pi^2} \int_0^\infty dy y \tilde{\mathcal{K}}_{\mathcal{B}}(x, y) \frac{\mathcal{B}(y)}{y\mathcal{A}^2(y) + \mathcal{B}^2(y)}, \end{aligned} \quad (5.33)$$

where  $x_b = -(\sqrt{-x} - m_\pi)^2$  is the location of the branch point and

$$\Delta \tilde{\mathcal{K}}_{\mathcal{B}}(x, y) = m_\pi^2 \frac{\sqrt{(x+y+m_\pi^2)^2 - 4xy}}{xy}, \quad (5.34)$$

$$\tilde{\mathcal{K}}_{\mathcal{B}}(x, y) = \tilde{g}_{PV}^2(x, y) - \tilde{g}_{PV}^2(x, y) \frac{2m_\pi^2}{a + \sqrt{a^2 - b^2}}. \quad (5.35)$$

NB. The  $\Delta \tilde{\mathcal{K}}_{\mathcal{A}, \mathcal{B}}$  terms contribute only for  $P^2 + m_\pi^2 < 0$ .

With the solutions for  $\mathcal{A}$ ,  $\mathcal{B}$  in hand, the fully-dressed nucleon mass,  $M_D$ , is obtained by solving

$$M_D^2 \mathcal{A}^2(-M_D^2) = [M + \mathcal{B}(-M_D^2)]^2 \quad (5.36)$$

and the nonperturbative mass shift is  $\delta M_+ = M_D - M$ . The widths  $\Lambda$ ,  $\Lambda_N$  in Eq. (5.27) are constrained by model and phenomenological analyses:<sup>147,149,163,164</sup>

$$\Lambda \sim 0.9 \text{ GeV}, \quad \Lambda_N/\Lambda \sim 1.5 - 2.0 \quad (5.37)$$

and completing the calculation,<sup>9</sup> Ref. [154] reports a  $\pi N$ -loop induced mass shift

$$-\delta M_+ \approx (60 - 100) \text{ MeV}. \quad (5.38)$$

Allowing for model-dependence it is therefore safe to say that the  $\pi N$ -loop reduces the nucleon's mass by  $\sim 10$ -20%. Extant calculations<sup>13,151,165</sup> show that the contribution from the analogous  $\pi \Delta$ -loop is of the same sign and no greater in magnitude so that the total reduction is  $\lesssim 20$ -40%. These same calculations indicate that the  $\Delta$  mass is also reduced by  $\pi$  loops but by a smaller amount ( $\sim 50$ -100 MeV less).

<sup>9</sup>Three "pions in the air" are sufficient to yield a self-consistent solution and one pion alone provides 95% of the mass shift.

### 5.2.3. Pions, quarks and diquarks

The question now is does this contribution materially affect the quark-diquark picture of baryons? That may be addressed by solving the Faddeev equations again but this time requiring that the quark-diquark component yield higher masses for the  $N$  and  $\Delta$ :  $M_N = 0.94 + 0.2 = 1.14$  GeV,  $M_\Delta = 1.232 + 0.1 = 1.332$  GeV.

The results<sup>154</sup> of that exercise are presented in the third and fourth rows of Table 5.2 and establish that the effects are material but not disruptive. In this case omitting the axial-vector diquark yields  $M_N = 1.44$  GeV, which signals a 10% increase in the importance of the scalar-diquark component of the nucleon. (It is an *increase* because this component now requires less correction. The scalar diquark's charge radius was found to be  $r_{0+} = 0.63$  fm; i.e., 15% larger.) It also reveals a reduction in the role played by axial-vector diquark correlations in the nucleon, since now restoring them only reduces the nucleon's core mass by 21%, with  $\pi$  self-energy corrections providing the remaining 14%.

Requiring an exact fit to the  $N$  and  $\Delta$  masses using only quark and diquark degrees of freedom therefore leads to an overestimate of the role played by axial-vector diquark correlations: it forces the  $1^+$  diquark to mimic, in part, the effect of pions since they both act to reduce the mass cf. that of a quark+scalar-diquark baryon. An accurate picture would represent the nucleon as  $\sim 60\%$  quark+scalar-diquark,  $\sim 20\%$  quark+axial-vector-diquark and  $\sim 20\%$  pion cloud ( $\pi N + \pi\Delta$ ). This result can significantly impact upon the calculation of quantities such as the neutron's charge form factor and the ratio  $F_2^p(q^2)/F_1^p(q^2)$ , and consequently existing Faddeev-equation-based calculations of form factors should be revisited.

### 5.3. Nucleon form factors

The Faddeev equation also provides a bound state amplitude, which is a key element in the impulse approximation<sup>148,157</sup> used in many studies of the nucleon's electromagnetic and strong form factors.<sup>147,148,149,150</sup> However, those studies have all overlooked the pion cloud's contribution, which is certainly important at small  $q^2$  but may also implicitly affect results at larger  $q^2$  by causing some elements in the calculations to be overweighted in order to mimic the pion's effect. The studies must be updated. Nevertheless, with these remarks in mind, we briefly review a topical result.

References [148,149] employed a product *Ansatz* for the nucleon's Faddeev amplitude that retains only the scalar diquark component,  $\Psi_3^+$  in Eq. (5.3). This exploratory model involved three parameters, which were determined in a least-squares fit to  $G_E^p(q^2)$  on  $0 < q^2 < 3$  GeV<sup>2</sup>, and made predictions for a variety of other couplings and form factors. Its description of the neutron's charge form factor is poor, as it should be given the omission of the axial-vector diquark correlation and pion cloud. However, this is the only major quantitative defect; e.g.,  $G_M^{p,n}(q^2)$  are well described. In fact they are probably too well reproduced since  $\pi$ -loops are expected to contribute  $\sim 20\%$  to the nucleons' magnetic moments and charge

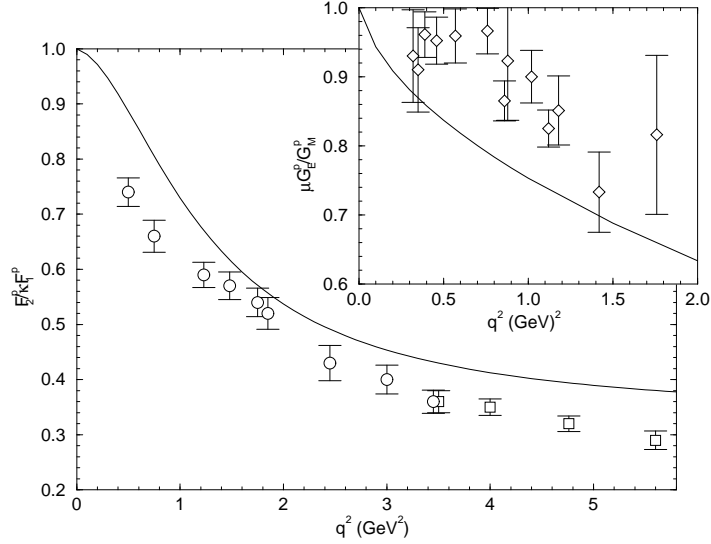


Fig. 5.2. Main Figure – Solid line:  $F_2^p(q^2)/[\kappa F_1^p(q^2)]$  calculated using a model Faddeev amplitude for the nucleon that retains only a scalar diquark.<sup>148,170</sup> Data: boxes, Ref. [166]; circles, Ref. [167]. Inset – Solid line  $\mu G_E^p/G_M^p$  calculated with the scalar-diquark model<sup>148</sup> cf. data from Ref. [168].

radii.<sup>169</sup> Hence, Refs. [148,149] provide a Poincaré covariant DSE model of the nucleon with a systematic error of  $\lesssim 30\%$ . The model has an important additional feature, absent in other approaches: calculated quantities evolve smoothly to their perturbative-QCD limit because the DSEs reproduce perturbation theory at weak coupling. We saw this explicitly for  $u_v^\pi(x)$  in Sec. 3.3 and  $F_\pi(q^2)$  in Sec. 4.1.

We plot results for  $F_2^p(q^2)/[\kappa F_1^p(q^2)]$ ,  $\kappa = F_2(0)$ , and  $\mu G_E^p(q^2)/G_M^p(q^2)$  in Fig. 5.2. It was remarked in Ref. [149] that the model agreed semiquantitatively with the then-current JLab data<sup>166</sup> but this is the first illustration.<sup>170</sup> The data has excited some interest<sup>171</sup> but we judge that here the situation is just as with  $F_\pi(q^2)$  [Fig. 4.2]. On the domain hitherto explored the form factors are evolving through the region on which infrared phenomena, such as the length-scales defined by bound state amplitudes and strongly-dressed quark propagators, are dominant. Thereupon a quantitative agreement with data is sensitive to model details. Eventually, the perturbative behaviour:<sup>108</sup>  $q^2 F_2^p(q^2)/F_1^p(q^2) = \text{constant}$ , will become evident but that is unlikely until significantly larger  $q^2$ . For instance, with  $F_\pi(q^2)$  the perturbative behaviour is not unambiguously evident until  $q^2 \gtrsim 15 \text{ GeV}^2$ . It is a challenge for quantum field theoretical DSE models of the nucleon, with their unique capacity for interpolating between the soft and hard domains, to locate the onset of perturbative behaviour in nucleon form factors. Given the experience with other elastic form factors it would have been a surprise to see that at  $q^2 < 10 \text{ GeV}^2$ .

## 6. Epilogue

We have provided a perspective on the contemporary application of Dyson-Schwinger equations (DSEs) to hadron physics. The keystone of this approach's success has always been an appreciation and expression of the momentum-dependence of dressed-parton propagators at infrared length-scales. That is responsible for the magnitude of constituent-quark and -gluon masses, and the length-scale characterising confinement in bound states. It is now recognised as a fact. Modern hadron physics experiments are probing a domain on which this phenomenon underpins observable behaviour. The next generation is likely to advance to a region wherein the transition to perturbative behaviour takes place. DSE methods, with their unique capacity to connect phenomena dominated by soft scales with their perturbative limits, will necessarily become increasingly valuable.

In recent years it has become clear why the simple rainbow-ladder DSE truncation has been successful for light vector and flavour nonsinglet pseudoscalar mesons. It is the first term in a systematic and nonperturbative scheme that preserves all the Ward-Takahashi identities that express conservation laws at an hadronic level. Studies in these channels showed that resumming subclasses of diagrams to infinite order provides a correction to bound state masses of  $\lesssim 10\%$ . Indeed, with just the first order correction to the rainbow-ladder kernel, the calculated masses are accurate to 99%. This analysis also explains why the truncation should, and does, fail for scalar mesons and points the way toward a systematically improved hadron phenomenology.

The existence of a systematic, nonperturbative, symmetry preserving truncation scheme has enabled the proof of exact results in QCD. It provides for a straightforward explanation of the dichotomy of the pion as both a Goldstone mode and a bound state of effectively very massive quarks. In arriving at that understanding, a mass formula for flavour nonsinglet pseudoscalar mesons was exposed which unifies the light- and heavy-quark regimes of QCD and provides a qualitative understanding of lattice simulations and their extrapolation to the chiral limit.

There have been numerous applications of well-constrained DSE models to hadronic phenomena. Among them, a calculation of the pion's valence-quark momentum-fraction probability distribution,  $u_v^\pi(x)$ , highlights the framework's ability to provide a description that unifies the soft and hard domains of a given phenomenon. In this case that has been crucial in exposing a serious discrepancy between theory and experiment. In agreement with perturbative QCD, the DSE study predicts  $u_v^\pi(x) \propto (1-x)^2$  in the valence-quark domain. However, extant experiments are consistent with  $u_v^\pi(x) \propto (1-x)$ . That is profoundly disturbing because a verification of the experimental result would even challenge the assumed vector-exchange nature of the force underlying the strong interaction.

The widespread success of a renormalisation-group-improved rainbow-ladder model is certainly one of the most significant achievements of the last five years.

The model is defined by one parameter, which is an analogue for light-quarks of the string tension. That parameter and the two light-quark masses  $m_u = m_d$ ,  $m_s$  are fitted to  $m_\pi$ ,  $f_\pi$ ,  $m_K$ ,  $f_K$  and everything calculated subsequently is a parameter-free prediction. These *ab initio* calculations have provided a unified description of many phenomena, among them: the spectrum of light-vector mesons;  $\pi$  and  $K$  electroweak form factors; vector meson transition form factors; and even  $\pi$ - $\pi$  scattering. And this has not merely been a quantitative success. The studies have provided important information on how and where the predictions of perturbative QCD become apparent in exclusive processes and, for the pion, tied that to features of low-energy  $\pi$ - $\pi$  scattering and current-algebra constraints. This body of work is unique in providing a systematically improvable, nonperturbative, Poincaré covariant, symmetry preserving approach to hadron physics.

A significant challenge is to emulate this success with baryons. Studies conducted hitherto, while preserving these important features, have been exploratory. They can and must be improved; e.g., by properly including  $\pi$ -cloud effects. To understand the data obtained at current and future hadron physics facilities a Poincaré covariant framework for baryons that naturally expresses the transition from the nonperturbative to perturbative domains will be necessary. The early studies suggest that a Faddeev equation built upon the DSE framework can fill that need.

### Acknowledgments

In preparing this article we benefited from conversations and correspondence with J.C.R. Bloch, S.J. Brodsky, F. Coester, M.B. Hecht, G.A. Miller and P.C. Tandy. This work was supported by the US Department of Energy (DOE), Nuclear Physics Division, under contract no. W-31-109-ENG-38, and DOE grant nos. DE-FG02-96-ER-40947, DE-FG02-97-ER-41048; and benefited from the resources of the US National Energy Research Scientific Computing Center.

### References

1. *Lattice 2001* — Proc. 19th Int. Symp. on Lattice Field Theory, eds. M. Mueller-Preussker, W. Bietenholz, K. Jansen, F. Jegerlehner, I. Montvay, G. Schierholz, R. Sommer and U. Wolff, *Nucl. Phys. Proc. Suppl.* **106-107** (2002); and also <http://www.ifh.de/~latt2001/>
2. P. Hasenfratz, *Nucl. Phys. Proc. Suppl.* **106**, 159 (2002).
3. *Light-Cone Physics: Particles and Strings* — Proc. Int. Wkshp. Trento 2001, eds. A. Bassetto, L. Griguolo, G. Nardelli and F. Vian, *Nucl. Phys. Proc. Suppl.* **108** (2002).
4. R.J. Perry, *Phys. Rept.* **348**, 33 (2001).
5. M. Burkardt and S. Dalley, *Prog. Part. Nucl. Phys.* **48**, 317 (2002).
6. J.R. Hiller, *Nucl. Phys. Proc. Suppl.* **90**, 170 (2000).
7. S.J. Brodsky, *Nucl. Phys. Proc. Suppl.* **108**, 327 (2002).
8. S. Capstick and W. Roberts, *Prog. Part. Nucl. Phys.* **45**, S241 (2000).
9. S. Boffi, L. Y. Glozman, W. Klink, W. Plessas, M. Radici and R. F. Wagenbrunn, *Eur. Phys. J.* **A 14**, 17 (2002); W. Plessas, *Nucl. Phys. Proc. Suppl.* **108**, 245 (2002).
10. E.S. Swanson and A.P. Szczepaniak, *Phys. Rev.* **D 59**, 014035 (1999).

11. P.R. Page, “Hybrid baryons,” nucl-th/0204031, to appear in *Baryons 2002 — Proc. 9th Int. Conf. on the Structure of Baryons*.
12. D.G. Robertson, E.S. Swanson, A.P. Szczepaniak, C.R. Ji and S.R. Cotanch, *Phys. Rev. D* **59**, 074019 (1999).
13. A.W. Thomas, S. Theberge and G.A. Miller, *Phys. Rev. D* **24**, 216 (1981); A.W. Thomas, *Adv. Nucl. Phys.* **13**, 1 (1984); G.A. Miller, *Int. Rev. Nucl. Phys.* **1**, 189 (1985).
14. M.C. Birse, *Prog. Part. Nucl. Phys.* **25**, 1 (1990).
15. R. Alkofer and H. Reinhardt, *Chiral quark dynamics* (Springer Verlag, 1995); J. Schechter and H. Weigel, in *Quantum Field Theory: a 20th Century Profile*, ed. A.N. Mitra (Hindustan Publ., 2000) p. 337.
16. A.W. Thomas and W. Weise, *The Structure Of The Nucleon* (Wiley-VCH, 2001).
17. B.D. Keister and W.N. Polyzou, *Adv. Nucl. Phys.* **20**, 225 (1991); F. Coester, *Prog. Part. Nucl. Phys.* **29**, 1 (1992).
18. R.D. Mattuck, *A Guide to Feynman Diagrams in the Many-Body Problem, 2nd Edition* (McGraw Hill, Inc., 1976).
19. P. Maris, C.D. Roberts and P.C. Tandy, *Phys. Lett. B* **420**, 267 (1998).
20. P. Maris and C.D. Roberts, *Phys. Rev. C* **56**, 3369 (1997).
21. C.D. Roberts and A.G. Williams, *Prog. Part. Nucl. Phys.* **33**, 477 (1994).
22. A. Bender, C.D. Roberts and L. v. Smekal, *Phys. Lett. B* **380**, 7 (1996).
23. A. Bender, W. Detmold, C.D. Roberts and A.W. Thomas, *Phys. Rev. C* **65**, 065203 (2002).
24. P. Maris and C.D. Roberts, in *Proc. of the Wkshp. on Nonperturbative Methods in Quantum Field Theory*, eds. A.W. Schreiber, A.G. Williams and A.W. Thomas (World Scientific, 1998) p. 132.
25. M.A. Ivanov, Yu.L. Kalinovsky and C.D. Roberts, *Phys. Rev. D* **60**, 034018 (1999).
26. H.J. Munczek and A.M. Nemirovsky, *Phys. Rev. D* **28**, 181 (1983).
27. P. Maris and P.C. Tandy, *Phys. Rev. C* **61**, 045202 (2000).
28. C.H. Llewellyn-Smith, *Annals Phys. (NY)* **53**, 521 (1969).
29. H.J. Munczek, *Phys. Rev. D* **52**, 4736 (1995).
30. D.C. Curtis and M.R. Pennington, *Phys. Rev. D* **42**, 4165 (1990).
31. P. Jain and H.J. Munczek, *Phys. Rev. D* **48**, 5403 (1993).
32. C.J. Burden, Lu Qian, C.D. Roberts, P.C. Tandy and M.J. Thomson, *Phys. Rev. C* **55**, 2649 (1997).
33. J.C.R. Bloch, M.A. Ivanov, T. Mizutani, C.D. Roberts and S.M. Schmidt, *Phys. Rev. C* **62**, 25206 (2000).
34. P. Maris, *Few Body Syst.* **32**, 41 (2002).
35. C.D. Roberts, in *Quark Confinement and the Hadron Spectrum II — Proc. of the 2nd Int. Conf.*, eds. N. Brambilla and G.M. Prosperi (World Scientific, 1997) p. 224.
36. S.R. Cotanch and P. Maris, hep-ph/0210151.
37. P. Maris and P.C. Tandy, *Phys. Rev. C* **62**, 055204 (2000).
38. A. Höll, P. Maris and C.D. Roberts, *Phys. Rev. C* **59**, 1751 (1999).
39. J.C.R. Bloch, C.D. Roberts and S.M. Schmidt, *Phys. Rev. C* **60**, 065208 (1999).
40. A. Bender, W. Detmold and A.W. Thomas, *Phys. Lett. B* **516**, 54 (2001).
41. K. Langfeld, R. Pullirsch, H. Markum, C.D. Roberts and S.M. Schmidt, “Concerning the quark condensate,” nucl-th/0301024.
42. M. Neubert, *Phys. Rep.* **245**, 259 (1994).
43. F.T. Hawes, P. Maris and C.D. Roberts, *Phys. Lett. B* **440**, 353 (1998).
44. C.D. Roberts, “Continuum strong QCD: Confinement and Dynamical Chiral Symmetry Breaking,” nucl-th/0007054.
45. F.D. Bonnet, P.O. Bowman, D.B. Leinweber, A.G. Williams and J.M. Zanotti, *Phys.*

- Rev. D* **64**, 034501 (2001).
46. J.C.R. Bloch, *Phys. Rev. D* **64**, 116011 (2001).
  47. R. Alkofer, C.S. Fischer and L. von Smekal, *Acta Phys. Slov.* **52**, 191 (2002).
  48. J. Skullerud and A. Kizilersu, *JHEP* **0209**, 013 (2002).
  49. P. Maris, A. Raya, C.D. Roberts and S.M. Schmidt, “Facets of confinement and dynamical chiral symmetry breaking,” nucl-th/0208071.
  50. J.C.R. Bloch, A. Cucchieri, K. Langfeld and T. Mendes, “Running coupling constant and propagators in SU(2) Landau gauge,” hep-lat/0209040.
  51. P. Maris and P.C. Tandy, *Phys. Rev. C* **60**, 055214 (1999).
  52. L. Montanet, *et al.* [Particle Data Group Collaboration], *Phys. Rev. D* **50**, 1173 (1994).
  53. K. Hagiwara, *et al.* [Particle Data Group Collaboration], *Phys. Rev. D* **66**, 010001 (2002).
  54. P.O. Bowman, U.M. Heller and A.G. Williams, *Phys. Rev. D* **66**, 014505 (2002).
  55. K. Johnson, M. Baker and R. Willey, *Phys. Rev.* **136**, B1111 (1964).
  56. C.D. Roberts, *Nucl. Phys. Proc. Suppl.* **108**, 227 (2002).
  57. P. Maris, in *Wien 2000, Quark Confinement and the Hadron Spectrum — Proc. of the 4th Int. Conf.*, eds. W. Lucha, K. Maung Maung (World Scientific, 2002) p. 163.
  58. P.C. Tandy, “Covariant QCD modeling of light meson physics,” nucl-th/0301040.
  59. A.W. Thomas, “Chiral extrapolation of hadronic observables,” hep-lat/0208023.
  60. M.B. Hecht, C.D. Roberts and S.M. Schmidt, in *Wien 2000, Quark Confinement and the Hadron Spectrum — Proc. of the 4th Int. Conf.*, eds. W. Lucha, K. Maung Maung (World Scientific, 2002) p. 27.
  61. K.C. Bowler, *et al.* [UKQCD Collaboration], *Phys. Rev. D* **62**, 054506 (2000).
  62. R.T. Cahill and C.D. Roberts, *Phys. Rev. D* **32**, 2419 (1985).
  63. P.C. Tandy, *Prog. Part. Nucl. Phys.* **39**, 117 (1997).
  64. R.T. Cahill and S.M. Gunner, *Fizika B* **7**, 171 (1998).
  65. C.D. Roberts, R.T. Cahill, M.E. Sevior and N. Iannella, *Phys. Rev. D* **49**, 125 (1994).
  66. C.D. Roberts, *Nucl. Phys. A* **605**, 475 (1996).
  67. R. Alkofer and C.D. Roberts, *Phys. Lett. B* **369**, 101 (1996).
  68. C.J. Burden, C.D. Roberts and M.J. Thomson, *Phys. Lett. B* **371**, 163 (1996).
  69. M.A. Pichowsky and T.-S.H. Lee, *Phys. Lett. B* **379**, 1 (1996); *Phys. Rev. D* **56**, 1644 (1997).
  70. Yu.L. Kalinovsky, K.L. Mitchell and C.D. Roberts, *Phys. Lett. B* **399**, 22 (1997).
  71. M.B. Hecht and B.H.J. McKellar, *Phys. Rev. C* **57**, 2638 (1998); *ibid.*, **C 60**, 065202 (1999).
  72. F.T. Hawes and M.A. Pichowsky, *Phys. Rev. C* **59**, 1743 (1999).
  73. P.C. Tandy, *Fizika B* **8**, 295 (1999).
  74. M.A. Pichowsky, S. Walawalkar and S. Capstick, *Phys. Rev. D* **60**, 054030 (1999).
  75. J.C.R. Bloch, Yu.L. Kalinovsky, C.D. Roberts and S.M. Schmidt, *Phys. Rev. D* **60**, 111502 (1999).
  76. M.B. Hecht, C.D. Roberts and S.M. Schmidt, *Phys. Rev. C* **63**, 025213 (2001).
  77. J.S. Conway, *et al.*, *Phys. Rev. D* **39**, 92 (1989).
  78. H.J. Munczek, *Phys. Lett. B* **175**, 215 (1986).
  79. C.J. Burden, C.D. Roberts and A.G. Williams, *Phys. Lett. B* **285** 347 (1992).
  80. G. Krein, C.D. Roberts and A.G. Williams, *Int. J. Mod. Phys. A* **7**, 5607 (1992).
  81. C.D. Roberts and S.M. Schmidt, *Prog. Part. Nucl. Phys.* **45**, S1 (2000).
  82. R. Alkofer and L. von Smekal, *Phys. Rept.* **353**, 281 (2001).
  83. M. Stingl, *Z. Phys. A* **353**, 423 (1996).
  84. P. Maris and C.D. Roberts, *Phys. Rev. C* **58**, 3659 (1998).
  85. A. Bashir, A. Kizilersu and M.R. Pennington, *Phys. Rev. D* **57**, 1242 (1998); and references therein.

86. J.S. Ball and T. Chiu, *Phys. Rev. D* **22**, 2542 (1980).
87. S.R. Amendolia, *et al.* [NA7 Collaboration], *Nucl. Phys. B* **277**, 168 (1986).
88. K. Kusaka, G. Piller, A.W. Thomas and A.G. Williams, *Phys. Rev. D* **55**, 5299 (1997).
89. M. Gluck, E. Reya and I. Schienbein, *Eur. Phys. J. C* **10**, 313 (1999).
90. P.J. Sutton, A.D. Martin, R.G. Roberts and W.J. Stirling, *Phys. Rev. D* **45**, 2349 (1992).
91. C. Best, *et al.*, *Phys. Rev. D* **56**, 2743 (1997).
92. S.J. Brodsky, M. Burkardt and I. Schmidt, *Nucl. Phys. B* **441**, 197 (1995).
93. R.M. Davidson and E. Ruiz Arriola, *Phys. Lett. B* **348**, 163 (1995); H. Weigel, E. Ruiz Arriola and L. Gamberg, *Nucl. Phys. B* **560**, 383 (1999); W. Bentz, T. Hama, T. Matsuki and K. Yazaki, *Nucl. Phys. A* **651**, 143 (1999).
94. A.E. Dorokhov and L. Tomio, *Phys. Rev. D* **62** (2000) 014016.
95. T. Frederico and G.A. Miller, *Phys. Rev. D* **50**, 210 (1994).
96. K. Wijesooriya, *et al.*, “The  $H(e, e'n)X$  Reaction and the Pion Structure Function,” proposal no. JLab PR01-110; and K. Wijesooriya, unpublished.
97. T. Shigetani, K. Suzuki and H. Toki, *Phys. Lett. B* **308**, 383 (1993); F. Bissey, J.R. Cudell, J. Cugnon, M. Jaminon, J.P. Lansberg and P. Stassart, *Phys. Lett. B* **547**, 210 (2002).
98. R.J. Holt and P.E. Reimer, in *Physics with an Electron Polarized Light-Ion Collider — Proc. of the 2nd Wkshp.*, ed. R.G. Milner, *AIP Conf. Proc.* **588**, 234 (2001).
99. P. Brauel, *et al.*, *Z. Phys. C* **3**, 101 (1979).
100. J. Volmer, *et al.* [JLab  $F_\pi$  Collaboration], *Phys. Rev. Lett.* **86**, 1713 (2001).
101. R. Alkofer, A. Bender and C.D. Roberts, *Int. J. Mod. Phys. A* **10**, 3319 (1995).
102. P. Maris,  *$\pi N$  Newslett.* **16**, 213 (2002).
103. S.R. Amendolia, *et al.*, *Phys. Lett. B* **178**, 435 (1986).
104. W.R. Molzon, *et al.*, *Phys. Rev. Lett.* **41**, 1213 (1978) [Erratum-ibid. **41**, 1523 (1978) ERRAT,41,1835.1978].
105. P. Maris and P.C. Tandy, *Phys. Rev. C* **65**, 045211 (2002).
106. H.J. Behrend, *et al.* [CELLO Collaboration], *Z. Phys. C* **49**, 401 (1991).
107. G.R. Farrar and D.R. Jackson, *Phys. Rev. Lett.* **43**, 246 (1979).
108. G.P. Lepage and S.J. Brodsky, *Phys. Rev. D* **22**, 2157 (1980).
109. M. Bhagwat, M.A. Pichowsky and P.C. Tandy, “Confinement phenomenology in the Bethe-Salpeter equation,” hep-ph/0212276.
110. C.-R. Ji and P. Maris, *Phys. Rev. D* **64**, 014032 (2001).
111. A. Apostolakis, *et al.* [CPLLEAR Collaboration], *Phys. Lett. B* **473**, 186 (2000).
112. C.G. Callan and S.B. Treiman, *Phys. Rev. Lett.* **16** (1966) 153.
113. J. Gasser and H. Leutwyler, *Nucl. Phys. B* **250**, 517 (1985).
114. M. Ademollo and R. Gatto, *Phys. Rev. Lett.* **13**, 264 (1964).
115. N. Isgur, *Phys. Rev. D* **12**, 3666 (1975).
116. L.C.L. Hollenberg, C.D. Roberts and B.H.J. McKellar, *Phys. Rev. C* **46**, 2057 (1992).
117. D.B. Leinweber and T.D. Cohen, *Phys. Rev. D* **49**, 3512 (1994).
118. K.L. Mitchell and P.C. Tandy, *Phys. Rev. C* **55**, 1477 (1997).
119. P. Maris and P.C. Tandy, “Mesons as bound states of confined quarks: Zero and finite temperature,” nucl-th/0109035.
120. D. Jarecke, P. Maris and P.C. Tandy, “Strong decays of light vector mesons,” nucl-th/0208019.
121. U.G. Meissner, *Comments Nucl. Part. Phys.* **20**, 119 (1991).
122. M.R. Pennington, “Riddle of the scalars: Where is the sigma?,” hep-ph/9905241.
123. D. Black, A.H. Fariborz and J. Schechter, “Exploring the structure of a possible light scalar nonet,” hep-ph/0008246.
124. M.B. Hecht, C.D. Roberts and S.M. Schmidt, in *Proc. of the Wkshp. on Lepton Scatter-*

- ing, Hadrons and QCD*, eds. W. Melnitchouk, A.W. Schreiber, P.C. Tandy and A.W. Thomas (World Scientific, 2001) p. 219; M.B. Hecht and C.D. Roberts,  *$\pi N$  Newslett.* **16**, 204 (2002).
125. R.I. Dzhelyadin, *et al.*, *Phys. Lett.* **B 102**, 296 (1981).
  126. P.C. Tandy, *Prog. Part. Nucl. Phys.* **36**, 97 (1996).
  127. S.J. Brodsky and G.P. Lepage, *Phys. Rev.* **D 24**, 2848 (1981).
  128. P. Maris, "Meson elastic and transition form factors," nucl-th/0209048.
  129. J. Praschifka, C.D. Roberts and R.T. Cahill, *Phys. Rev.* **D 36**, 209 (1987); C.D. Roberts, R.T. Cahill and J. Praschifka, *Annals Phys. (NY)* **188**, 20 (1988).
  130. J. Gronberg, *et al.* [CLEO Collaboration], *Phys. Rev.* **D 57**, 33 (1998).
  131. S.J. Brodsky and G.P. Lepage, *Phys. Rev.* **D 24**, 1808 (1981).
  132. A.V. Radyushkin and R.T. Ruskov, *Nucl. Phys.* **B 481**, 625 (1996).
  133. S.J. Brodsky, "Physics opportunities at a photon photon collider," hep-ph/0204197.
  134. D. Kekez and D. Klabucar, *Phys. Lett.* **B 457**, 359 (1999); *Fizika* **B 8**, 303 (1999).
  135. C.D. Roberts, *Fizika* **B 8**, 285 (1999).
  136. I.V. Anikin, A.E. Dorokhov and L. Tomio, *Phys. Lett.* **B 475**, 361 (2000).
  137. S. Weinberg, *Phys. Rev. Lett.* **17**, 616 (1966); *ibid.* **18**, 188 (1967).
  138. V. Bernard, U.G. Meissner, A. Blin and B. Hiller, *Phys. Lett.* **B 253**, 443 (1991); H.J. Schulze, *J. Phys.* **G 21**, 185 (1995).
  139. P. Bicudo, S. Cotanch, F. Llanes-Estrada, P. Maris, E. Ribeiro and A. Szczepaniak, *Phys. Rev.* **D 65**, 076008 (2002).
  140. J.F. Donoghue, C. Ramirez and G. Valencia, *Phys. Rev.* **D 38**, 2195 (1988).
  141. G. Colangelo, J. Gasser and H. Leutwyler, *Nucl. Phys.* **B 603**, 125 (2001).
  142. R.T. Cahill, J. Praschifka and C. Burden, *Austral. J. Phys.* **42**, 161 (1989).
  143. R.T. Cahill, C.D. Roberts and J. Praschifka, *Austral. J. Phys.* **42**, 129 (1989).
  144. C.J. Burden, R.T. Cahill and J. Praschifka, *Austral. J. Phys.* **42**, 147 (1989).
  145. H. Asami, N. Ishii, W. Bentz and K. Yazaki, *Phys. Rev.* **C 51**, 3388 (1995); H. Mineo, W. Bentz and K. Yazaki, *ibid.* **60**, 065201 (1999).
  146. M. Oettel, G. Hellstern, R. Alkofer and H. Reinhardt, *Phys. Rev.* **C 58**, 2459 (1998).
  147. M. Oettel, R. Alkofer and L. von Smekal, *Eur. Phys. J.* **A 8**, 553 (2000).
  148. J.C.R. Bloch, C.D. Roberts, S.M. Schmidt, A. Bender and M.R. Frank, *Phys. Rev.* **C 60**, 062201 (1999).
  149. J.C.R. Bloch, C.D. Roberts and S.M. Schmidt, *Phys. Rev.* **C 61**, 065207 (2000).
  150. M.B. Hecht, C.D. Roberts and S.M. Schmidt, *Phys. Rev.* **C 64**, 025204 (2001).
  151. A.W. Thomas and S.V. Wright, in *Frontiers in Nuclear Physics: From Quark-Gluon Plasma to Supernovae — Proc. of the 11th Physics Summer School*, ed. S. Kuyucak (World Scientific, Singapore, 1999) p. 171.
  152. B.C. Pearce and I.R. Afnan, *Phys. Rev.* **C 34**, 991 (1986).
  153. N. Ishii, *Phys. Lett.* **B 431**, 1 (1998).
  154. M.B. Hecht, M. Oettel, C.D. Roberts, S.M. Schmidt, P.C. Tandy and A.W. Thomas, *Phys. Rev.* **C 65**, 055204 (2002).
  155. R.T. Cahill and S.M. Gunner, *Phys. Lett.* **B 359**, 281 (1995).
  156. M. Hess, F. Karsch, E. Laermann and I. Wetzorke, *Phys. Rev.* **D 58**, 111502 (1998).
  157. M. Oettel, M.A. Pichowsky and L. von Smekal, *Eur. Phys. J.* **A 8**, 251 (2000); M.A. Pichowsky,  *$\pi N$  Newslett.* **16**, 219 (2002).
  158. R.T. Cahill, *Nucl. Phys.* **A 543**, 63C (1992).
  159. S. Weinberg, *Phys. Rev.* **166**, 1568 (1968).
  160. J.J. Sakurai, in *Pion-Nucleon Scattering*, eds. G.L. Shaw and D.Y. Wong (Wiley, New York, 1969) p. 209.
  161. C.D. Roberts and B.H.J. McKellar, *Phys. Rev.* **D 41**, 672 (1990); H.J. Munczek and D.W. McKay, *Phys. Rev.* **D 42**, 3548 (1990).

162. R. Fukuda and T. Kugo, *Nucl. Phys.* **B 117**, 250 (1976).
163. A.W. Thomas and K. Holinde, *Phys. Rev. Lett.* **63**, 2025 (1989).
164. B.C. Pearce and B.K. Jennings, *Nucl. Phys.* **A 528**, 655 (1991).
165. P.J. Bicudo, G. Krein and J.E. Ribeiro, *Phys. Rev.* **C 64**, 025202 (2001).
166. M.K. Jones, *et al.* [JLab Hall A Collaboration], *Phys. Rev. Lett.* **84**, 1398 (2000).
167. O. Gayou, *et al.* [JLab Hall A Collaboration], *Phys. Rev. Lett.* **88**, 092301 (2002).
168. O. Gayou, *et al.*, *Phys. Rev.* **C 64**, 038202 (2001).
169. E.J. Hackett-Jones, D.B. Leinweber and A.W. Thomas, *Phys. Lett.* **B 489**, 143 (2000); *ibid.* **494**, 89 (2000); D.B. Leinweber, A.W. Thomas and R.D. Young, *Phys. Rev. Lett.* **86**, 5011 (2001).
170. J.C.R. Bloch, private communication.
171. G.A. Miller, *Phys. Rev.* **C 66**, 032201 (2002).